Human serum albumin-stabilized gold nanoclusters and their applications for detection of bilirubin in serum samples

Thesis submitted by

SANTHOSH M

For the award of the degree

of

Doctor of Philosophy

DEPARTMENT OF BIOSCIENCES AND BIOENGINEERING

INDIAN INSTITUTE OF TECHNOLOGY GUWAHATI

GUWAHATI-781039, ASSAM, INDIA

JUNE 2016

Dedicated to my most precious possession-
My family

INDIAN INSTITUTE OF TECHNOLOGY GUWAHATI
Department of Biosciences and Bioengineering
Guwahati – 781039

STATEMENT

I do hereby declare that the matter embodied in this thesis is the result of investigations carried out by me in the Department of Biosciences and Bioengineering, Indian Institute of Technology Guwahati, Assam, India, under the guidance of Prof. Pranab Goswami.

In keeping with the general practice of reporting scientific observations, due acknowledgements have been made wherever the work described is based on the findings of other investigators.

June, 2016 **Santhosh M**

INDIAN INSTITUTE OF TECHNOLOGY GUWAHATI
Department of Biosciences and Bioengineering
Guwahati – 781039, Assam, INDIA

Dr. Pranab Goswami
Professor

Tel: +91-(0)361 2582202
Fax: +91-(0)361 2582249/2690762
Email: pgoswami@iitg.ernet.in

CERTIFICATE

It is certified that the work described in this thesis, entitled "**Human serum albumin-stabilized gold nanoclusters and their applications for detection of bilirubin in serum samples**", done by **Mr. Santhosh M (Roll No. 11610616)** for the award of degree of Doctor of Philosophy is an authentic record of the results obtained from the research work carried out under my supervision in the Department of Biosciences and Bioengineering, Indian Institute of Technology Guwahati, India.

The results embodied in this thesis have not been submitted to any other University or Institute for the award of any degree.

June, 2016

Prof. Pranab Goswami
(Research supervisor)

Acknowledgement

I take this opportunity with much pleasure to express my sincere gratitude to all those who have supported me through the course of my journey towards producing this thesis. First of all, I am thankful to Indian Institute of Technology Guwahati for giving me the opportunity to carry out Ph.D. in this esteemed Institute and providing me the financial support. I am deeply indebted to my supervisor, Prof. Pranab Goswami for his enthusiastic guidance, brainstorming discussions during my Ph.D. from its inception to its completion and most importantly, for the conviction he has shown in my abilities. He gave me many opportunities, which were helpful to build my research career. He was always supportive whenever I proposed new research topics or brought some problems of ongoing study.

I am thankful to my doctoral committee members, Prof. Aiyagari Ramesh, Dr. Bithiya G Jagnnathan and Prof. Biplab Mondal for their constructive criticism and helpful suggestions during my various progress seminars. I am gratified to Prof. Pranab Goswami, Dr, Biplab Bose, Prof. S. S. Ghosh, Prof. A. Ramesh and Prof. L. Sahoo for providing excellent lab facilities. I am also grateful to other faculty members, office staff and my colleagues from Department of Biosciences and Bioengineering for their inestimable support and help.

I would like to thank Central Instruments Facility, IIT Guwahati for providing the access to various instruments without which this study would not be feasible.

Thanks of appreciation to my former colleagues Dr. S.S Reddy, Dr. Urmila Saxena, Dr. Seraj Ahmed, Dr. Mitun Chakraborty and Dr. Madhuri Das for their inspired support at the time of my acclimatization in the lab and guidance in learning various experimental techniques. I would like to mention my special thanks to my amazing fellow lab members Ankana, Babina, Priyamvada, Mrinal, Naveen, Phurpa, Farhan, Priyanki, Sharbani, Vinay, Abdul and Roopam who have shared their struggles so intimately and trusted my assistance in their various endeavors. I am grateful to Pushpalatha (B-Tech project student) and Danish (M-Tech project student) for their contribution in completing my Ph.D. thesis work.

I am lucky to have friends like Dev, Binay, Seim, Thiyagarajan, Surjya, Basu, Raju, Sushant, Mohan, Himanshu, Deb, and Deepak. Special thanks to them for their unconditional support and all the help extended from time to time. Without numerous relaxing outings/parties with these people it wouldn't have been possible for me to finish. I am very much thankful to all of them for making my stay pleasant at IIT Guwahati.

The beauty of Assam, beauty of IITG campus never let me feel bored. Memories of this place and time spent together with friends (especially our numerous tea breaks) will always be remembered by me later in my life. I am also thankful to my seniors and friends Dr. Asim Bikas Das, Dr. Manab deb, Dr. Pojul Loying, Dr. Amit Jaiswal, Dr. Himangshu with whom I share tons of fond memories. My deep sense of gratitude to one and all who, directly or indirectly, have lent their helping hand in this endeavor.

Most of all, I would like to dedicate this work to my parents (Amma & Appa) my brother (Sandy) and my sister (Veda) whose love, teaching and unconditional support have brought me this far. Last but not the least I owe special thanks to Sowmya for her love and encouragement.

Santhosh M
June 2016

Abstract

The present investigation is focused on the utilization of human serum albumin-stabilized gold nanocluster (HSA-AuNC) as biorecognition element for detection of bilirubin in optical and electrochemical transducer platforms. The natural affinity of bilirubin to HSA and some unique optical and electrochemical features of gold nanoclusters (AuNCs) were exploited to develop the detection techniques. Following a simple microwave-based technique AuNCs were synthesized in the protein matrix of HSA. Using transmission electron microscopy (TEM) and matrix-assisted laser desorption ionization-mass spectrometry (MALDI-MS), the size and the number of gold atom in these NCs were determined to be ~ 2.5 nm and 18, respectively. The formation of AuNCs in the protein matrix though caused some perturbation in the secondary structure of the protein, the binding of bilirubin to the HSA-AuNC assembly was not much altered as evident from the reasonably good binding constant of 0.55 x 10^6 L $mole^{-1}$. Zeta potential studies revealed that the formation of nanoclusters caused to increase the surface charge density of the HSA protein. The HSA-stabilized AuNC, when excited at $\lambda_{380\ nm}$, produced an intense fluorescence at $\lambda_{640\ nm}$. Interestingly, the binding of bilirubin with HSA-AuNC quenched the fluorescence in a concentration dependent manner. The fluorescence quenching phenomena, which obeyed a simple static quenching mechanism, was utilized for interference-free detection of bilirubin with minimum detection limit (DL) of 248 ± 12 nM at a signal-to-noise (S/N) ratio of 3. Additionally, a peroxidase-like catalytic activity of these nanoclusters was observed and exploited for the detection of bilirubin following a colorimetric approach. The detection involves a decrease in absorbance of bilirubin at λ_{440nm} in the reaction solution upon addition of H_2O_2 due to peroxidative catalytic effect of the AuNCs. The minimum DL for bilirubin as discerned from the analysis was 200 ± 19 nM. The HSA-stabilized AuNC was also found to act as electron transfer bridge during

electrocatalytic oxidation of bilirubin on a fabricated electrode surface. The bioelectrode was fabricated by covalently immobilizing HSA-AuNC on silanized indium tin oxide (ITO) electrodes using N-ethyl-N'-(3-dimethylaminopropyl) carbodimide (EDC) and N-hydroxysuccinimide (NHS) ligand chemistry. The bioelectrode was characterized by using various advanced spectroscopic and electrochemical techniques. The AuNCs in the protein matrix acted as an electronic bridge by contacting a specific redox active moiety of the HSA-attached bilirubin molecule and the polarized electrode (0.27 V vs. Ag/AgCl). The HSA-AuNC based bioelectrode showed linear response range of 0.2 µM to 7 µM for bilirubin with a DL of 86.32 nM at an S/N ratio of 3. The bioelectrode showed efficient electron transfer rate constant *(K_s)* 1.38 s^{-1}. The fabricated bioelectrode was also found to exclude interference caused by the commonly co-existing electroactive species in blood serum such as ascorbic acid, uric acid, lactic acid and glucose thus, can be used as biosensors for highly selective analysis of bilirubin in serum samples. The bioelectrode retained ~75 % of its initial activity at the end of 15 measurements while it retained ~80 % of its original response after storing for 7 days at 4 °C. Finally, a microfluidic paper-based electrochemical device (μPED) was developed for the detection of bilirubin by using the HSA-AuNC as an electrochemical probe laying over an array of zinc oxide nanorods (ZnO-NRs) on a patterned paper surface. The μPED comprised of two layers of rectangular papers patterned with alkene ketene dimer (AKD) printing to produce circular detection zone with a loading capacity of 10 µl. A novel, stable conducting graphite ink was developed by using silk sericin as a binder. The counter electrode and reference electrode were placed on the top layer of paper while, working electrode was grafted on the bottom layer of the paper zone. The zinc oxide nanorods (ZnO-NRs) were grown *in-situ* over the working electrode *via* solvothermal method. Later, the HSA-AuNC was immobilized over ZnO-NRs following electrostatic interaction principle. The morphological characteristics of the working electrodes were analyzed by FESEM

technique. The μPED containing HSA-AuNC/ZnO-NRs showed linear response range of 0.5 µM to 35 µM (R^2 = 0.994) of bilirubin with a detection limit of 57.3 nM at an S/N of 3. The results embodied in this thesis have established the HSA-stabilized AuNC as suitable bio-recognition system for detection of free bilirubin in serum sample in optical (fluorescence and colorimetric) as well as electrochemical platforms.

Content

List of figures

List of tables

List of schemes

List of acronyms

AA	Ascorbic acid
ADP	Adenine dinucleotide phosphate
AFM	Atomic force microscopy
Ag	Silver
AgCl	Silver chloride
AKD	Alkyl ketene dimer
APTES	(3-aminopropyl) tetramethoxymethylsilane
AsOX	Ascorbic acid
ASSURED	Affordable, selective, sensitive, user-friendly, robust, equipment-free, and deliverable
Au	Gold
AuNCs	Gold nanoclusters
AuNPs	Gold nanoparticles
BOx	Bilirubin oxidase
BSA	Bovine serum albumin
CB	Conjugated bilirubin
CD	Circular dichroism
CHIT	Chitosan
CL	Chemiluminiscence
CNTs	Carbon nanotubes
CO	Carbon monoxide
CPs	Conducting polymers
CSA	(±)-10-camphorsulfonicacid
CV	Cyclic voltammetry
DB	Direct bilirubin
DET	Direct electron transfer
df	Dilution factor
DL	Detection limit
DMSO	Dimethyl sulphoxide
DPV	Differential pulse voltammetry
DSC	Differential scanning calorimetry

EDC	N-ethyl-N'-(3-dimethylaminopropyl) carbodimide
EIS	Electrochemical impedance spectroscopy
Eu^{3+}	Europium ion
FAB	Fatty acid binding protein
Fc	Ferrocene
FDA	Food and drug administration
FESEM	Field emission scanning electron microscopy
FIA	Flow injection analysis
FTIR	Fourier transform infrared spectroscopy
GCE	Glassy carbon electrode
GT	Glucuronyl transferase
GO	Graphene oxide
h	Hour
HAP	Hydroxyapatite
HMT	Hexamethyl tetraamine
H_2O_2	Hydrogen peroxide
HPLC	High performance liquid chromatography
HRP	Horse radish peroxidase
HSA	Human serum albumin
ITO	Indium tin oxide
kDa	Kilo Dalton
MIP	Molecularly imprinted polymer
MPTS	(3-mercaptopropyl)-trimethoxysilane
μPADs	Microfluidic paper based analytical devices
μPEDs	Microfluidic paper based electroanalytical devices
MW	Microwave radiation
Mw	Molecular weight
MWCNT	Multiwalled carbon nanotubes
$NADP^+$	Nicotinamide adenine dinucleotide phosphate
NADPH	Nicotinamide adenine dinucleotide phosphate(reduced)
NaH_2PO_4	Sodium dihydrogen phosphate
Na_2HPO_4	Di sodium hydrogen phosphate
NBS	N-hydroxysuccinimide

NF	Nafion
NHS	N-hydroxysuccinimide
NPs	Nanoparticles
NR	Nanorod
OATP	Organic anion transporter protein
O_2	Oxygen
OD	Optical density
Os	Osmium
PBS	Phosphate buffer solution
PEI	Polyethylene imine
pI	Iso electric point
Pt	Platinum
QC	Quantum cluster
QCM	Quartz crystal microbalance
RSD	Relative standard deviation
RT	Room temperature
Ru	Ruthenium
s	Second
SAM	Self- assembled monolayer
SB	Serum bilirubin
SD	Standard deviation
SDS	Sodium dodecylsulfate
SPR	Surface plasmon resonance
SWV	Square wave voltammetry
TcB	Transcutaneous bilirubin
TEM	Transmission electron microscopy
TEOS	Tetraethylorthosilicate
TGA	Thermo-gravimetric analysis
Trp	Tryptophan
UB	Unconjugated bilirubin
UDP	Uridine diphosphate
UV-Vis	UV-Visible
WHO	World health organization

XRD	X-ray diffractometer
ZnO	Zinc oxide

List of symbols

A	Electrode surface area
cP	Centipoise
df	Dilution factor
$E^{o'}$	Apparent standard potential
E_p	Peak potential
E_{pa}	Anodic peak potential
E_{pc}	Cathodic peak potential
F	Faraday constant
GHz	Gigahertz
I_{pa}	Anodic peak current
I_{pc}	Cathodic peak current
K_{cat}	Turnover number
k_m	Michaelis-Menten constant
k_s	Electron transfer constant
R	Thermodynamic rate constant
R^2	Regression coefficient
Rct	Charge transfer resistance
$t_{1/2}$	Half life
W	Watt
Z	Impedance
α	Charge transfer coefficient
ΔE_p	Potential Peak separation
ε	Extinction coefficient
ζ	Zeta potential
ν	Potential scan rate
MΩ	Megaohm
Γ	Surface concentration of ionic species

Introduction

Introduction

Bilirubin is a tetrapyrrole compound produced from the breakdown of heme moiety in hemoglobin and other hemoproteins, such as cytochromes, catalases, and peroxidases (Roy-Chowdhury et al., 2004). This linear tetrapyrrole compound exists in the serum in different forms: unconjugated (free), albumin-bound and conjugated bilirubin. Increased bilirubin level in blood is known as hyperbilirubinemia. The incidence of hyperbilirubinemia is higher in the neonates than adults and is generally treated by phototherapy or by exchange transfusion. This requires frequent monitoring of serum bilirubin. The current guidelines of the American academy of pediatrics for the "monitoring and treatment of hyperbilirubinemia", clearly state the need for routine measurement of bilirubin levels (American academy of pediatrics subcommittee on hyperbilirubinemia, 2004). The guidelines for intervention depend principally on total bilirubin levels. However, fundamental biochemical and increasing clinical evidences predict that the free bilirubin rather than total bilirubin correlates more with the bilirubin mediated neurotoxicity (Wennberg et al., 2009; Oh et al., 2010). Free bilirubin is sparingly soluble in water and is associated with all known toxic effects of

bilirubin. On the other hand, a low free bilirubin concentration is associated with iron deficiency and coronary artery disease (Stocker et al., 1987). Free bilirubin determination in serum is therefore useful in assessing the risk involved in cardiovascular diseases. Hence, there is a strong demand to develop an inexpensive, rapid and reliable analytical method for the determination of free bilirubin in serum samples (Slusher et al., 2011).

The landscape of rapid bioanalytical detection has been fundamentally changed by the emergence of the concept of biosensors. According to International Union of Pure and Applied Chemistry (IUPAC) definition, "A biosensor is a self-contained integrated device which is capable of providing specific quantitative or semi-quantitative analytical information using a biological recognition element (biochemical receptor) which is in direct spatial contact with a transducer element" (Thévenot et al., 2001). The basic concept of a biosensor's operation can be illustrated with the help of Scheme A. Biosensor research holds promise for developing stable portable devices for rapid, sensitive, selective, reproducible, and economical detection of analytes of different chemical natures. It has the advantage of being used by semi-skilled operators and by patients themselves.

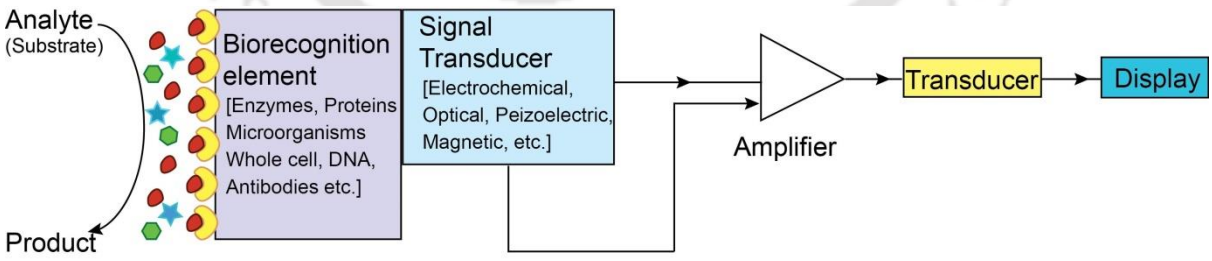

Scheme A: Schematic representation of the general configuration of biosensor.

Over the past few decades, a variety of bilirubin biosensors have been developed, which generally employ bilirubin oxidase (BOx) or molecularly imprinted polymer (MIP) as

the biorecognition element. Among various kinds of biosensors which employ BOx, a majority of them were focused on amperometric and optical techniques. However, utilization of BOx for the detection of bilirubin has severe drawbacks such as poor stability, high K_m, high cost of the enzymes and high sensitivity to environmental conditions (Sheldon, 2007). The molecular imprint-based biomimetic sensors, which usually employ quartz crystal microbalance (QCM) as the transducer are yet to attain acceptable sensitivity in most cases (Vasapollo et al., 2011). The focus of the current bilirubin detection research is to develop non-enzymatic method to overcome the instability and other hurdles being encountered by the enzyme-based detection approaches. Most of these alternative methods increasingly utilize the properties of advanced nanomaterials. The unique and attractive properties of nanomaterials have paved the way for the development of nanomaterial-biomolecule hybrid systems that exhibit attractive and promising analytical behaviors. Varieties of nanomaterials such as multi-walled carbon nanotubes (MWCNTs), gold nanoparticles (AuNPs), and graphene were used to construct electrochemical bilirubin sensors. These strategies exploit the unique properties of the nanomaterials suitable for sensitive detection of electroactive bilirubin on the electrode surface. However, these methods though provide stable and sensitive detection of bilirubin, suffer from interference in the signal due to poor selectivity of the recognition systems. Therefore, introduction of specific selective barrier that allows only free bilirubin to get oxidized at the nanomaterial interface may be a more rational approach in developing successful bilirubin sensor.

In view of the importance of bilirubin detection in the serum and the above mentioned challenges, the present investigation aims to develop HSA-stabilized gold nanocluster as biorecognition element for developing bilirubin detection in different tranducing platforms. Here we propose to exploit the naturally evolved strong binding affinity between HSA and

bilirubin for the sequestration of free bilirubin from the solution phase of the serum sample to the HSA protein matrix containing *in-situ* synthesized gold-nanoclusters (AuNCs). Here, the protein-stabilized AuNCs expected to initiate signal on the binding of bilirubin to the HSA protein surface due to possible perturbation of its unique electronic properties caused by the binding.

The specific objectives of the work are:

- HSA-stabilized gold nanoclusters: Synthesis, characterization and studies on their interaction with free bilirubin.
- HSA-stabilized gold nanocluster as optical probe for detection of bilirubin.
- HSA-stabilized gold nanocluster as electrochemical probe for detection of bilirubin.
- HSA-stabilized gold nanocluster in microfluidic paper based platform for electrochemical detection of bilirubin.

The studies embodied in this thesis are categorized into the following chapters:

Chapter 1: Literature Review

The objective of this chapter is to summarize the current status and progress in the area of bilirubin detection. This chapter also includes a brief overview on protein-nanoparticle conjugation and its importance in the development of biosensors. Additionally, the special features of gold nanocluster and their importance in designing the concept for developing sensors have been included in this chapter.

Chapter 2: HSA-stabilized gold nanoclusters: Synthesis, characterization and studies on their interaction with bilirubin

In this chapter, synthesis and preliminary characterization of the HSA-stabilized gold nanocluster relevant to our subsequent studies on their utilization for bilirubin detection have

been described. Analyses of molecular weight, size, *pI* and secondary structure of the prepared HSA-AuNC are performed. The effect of these stabilized gold nanoclusters on the binding of HSA with its natural ligand bilirubin has been investigated. Where spectroscopic techniques such as, fluorescence, UV-Visible, and circular dichroic spectroscopy are utilized to retrieve the information on the interaction.

Chapter 3: HSA-stabilized gold nanocluster as optical probe for the detection of bilirubin

In this chapter a non-enzymatic interference free, reagent-less dual fluorometric and colorimetric bilirubin detection method with high sensitivity has been described. The interaction of the substrate bilirubin with HSA-AuNC resulted in fluorescence quenching of the AuNC in a concentration dependent manner. This observation was thus utilized for the quantitative detection of bilirubin in blood serum sample. Additionally, the peroxidase-like catalytic property of these HSA-stabilized AuNCs was utilized for sensitive colorimetric detection of bilirubin in the human serum sample. A detailed account of the findings has been presented in this chapter.

Chapter 4: HSA-stabilized gold nanocluster as electrochemical probe for the detection of bilirubin

The studies in this chapter include the fabrication of an amperometric bioelectrode based on HSA-AuNC immobilized on silanized ITO electrode. Detailed electrochemical and morphological characterization of the fabrication process is presented here. The responses of the bioelectrode towards bilirubin with various response parameters were investigated. The results pertaining to the application of the biosensor for real sample analysis is also presented in this chapter.

Chapter 5: HSA-stabilized gold nanocluster in microfluidic paper based platform for electrochemical detection of bilirubin.

The chapter describes an effort to develop a simple microfluidic paper-based electrochemical device (μPED) for the detection of bilirubin by using the HSA-AuNC as an electrochemical recognition probe. For device fabrication, a new conductive ink based electrode has been prepared. Morphological and electrochemical characterizations of the fabricated bioelectrode are discussed in detail. The results pertaining to optimization of different parameters of the μPED are also presented here.

Chapter I

Literature Review

CHAPTER 1

Literature Review

1.1. Overview

Bilirubin is a yellow pigment belonging to the class of 'tetrapyrroles' (chemical compounds with four pyrrole rings). This compound is formed as a result of the degradation of heme in the blood of mammals. The first step in the process of the degradation involves the cleavage of the heme ring at α carbon bridge resulting in the liberation of iron, formation of carbon monoxide and biliverdin. This cleavage is catalysed by the enzyme heme oxygenase (HO). In the second step, biliverdin is reduced to bilirubin by the catalytic activity of a cytosolic enzyme biliverdin reductase (Scheme 1.1) (Sticova and Jirsa, 2013; Tenhunen et al., 1969). Bilirubin (IUPAC name: 3-[2-[[3-(2-carboxyethyl)-5-[(Z)-(3-ethenyl-4-methyl-5-oxopyrrol-2-ylidene)methyl]-4-methyl-1H-pyrrol-2-yl]methyl]-5-[(Z)-(4-ethenyl-3-methyl-5-oxopyrrol-2-ylidene) methyl] -4-methyl-1H-pyrrol-3-yl]propanoic acid) has a peculiar stereo-chemical structure in which all hydrophilic groups are involved in the intra molecular hydrogen bond which turns the molecule into a ridge tile conformation and hydrophobic

(Bonnett et al., 1976). This compound has poor aqueous solubility, present as a bound form with serum albumin. The dissociation constant of the bilirubin and albumin interaction is in the range of 10^8-10^7 M^{-1} (Jacobsen and Brodersen, 1983; Petersen et al., 2000). Once bound to albumin, it is transported in to liver. The entry of the bilirubin into the hepatocyte is partly passive and partly involves organic anion transporter proteins (OATP 1B1). In hepatocytic micrsome bilirubin is conjugated into sugar through ester linkage catalysed by uridine diphosphate- glucuronyltransferase (UDP-GT) (Tenhunen et al., 1970). In this conjugation through the ester link, one or two sugar moieties are coupled to the COOH of the propionic acid side chain(s) of unconjugated bilirubin, resulting in the formation of corresponding monoconjugated or diconjugated bilirubin (Scheme 1.1). The esterification disrupts the intramolecular hydrogen bonds, thereby opening the molecule and rendering the conjugated bilirubins more water soluble or amphipathic, allowing transportation through serum and excretion in the bile.

1.1.1. Disorder in bilirubin metabolism

Hyperbilirubinemia is a condition in which bilirubin concentration in the blood is increased due to an abnormally high peripheral breakdown of hemoglobin, termed as hemolysis which is far more frequent cause of unconjugated hyperbilirubinemia. Neonates are more prone to develop hyperbilirubinemia. In fact, 80 % of new-born develops hyperbilirubinemia in the early stage of their birth (Holtrop and Maisels, 1996). The reason might be attributed to the fact that in neonates red cells have shorter life span than the adult which leads to a greater bilirubin burden for hepatic metabolism. High bilirubin level in body is eliminated efficiently following the conjugation process as discussed above. The enzyme responsible for the conjugation of bilirubin UDP-GT, is immature at birth is also another reason for high concentration of bilirubin in serum and the condition status is termed as

neonatal jaundice. Mutations in exons coding for UDP-GT lead to Crigler–Najjar disease which is characterized by complete absence of enzyme activity resulting in very high level of unconjugated bilirubin. The blockage or infection of biliary tract or congenital disorders of the bile duct (biliary atresia) also resulted in the hyperbilirubinemia.

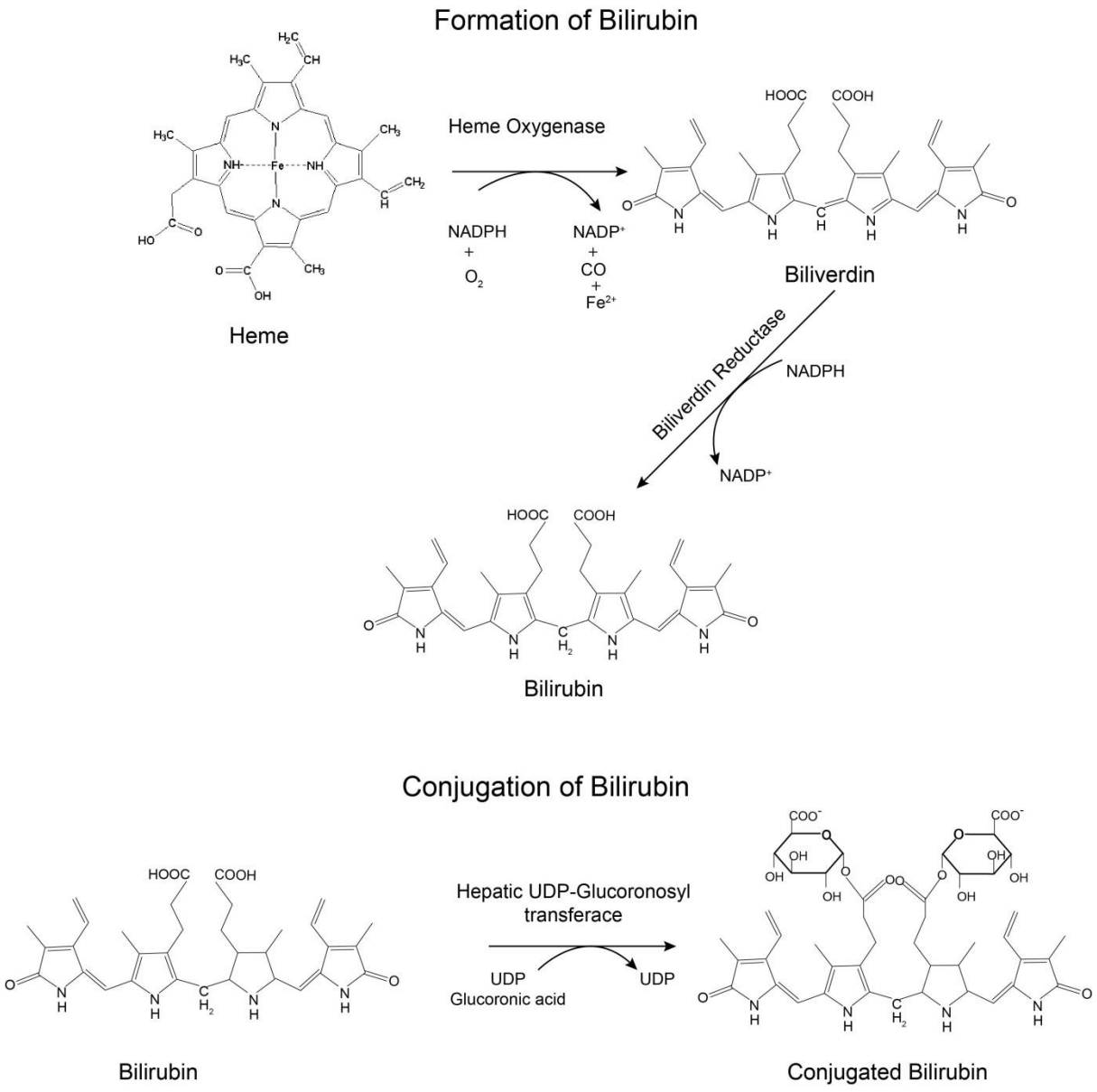

Scheme 1.1: Mechanism of formation and conjugation of bilirubin.

1.1.2. Importance of bilirubin detection

As mentioned in the previous section, jaundice is common in the neonates. In some severe cases, it requires timely treatment for which frequent monitoring of serum bilirubin is important. The American academy of pediatrics suggests the need for routine analysis of bilirubin levels for cases of neonatal hyperbilirubinemia (American Academy of Pediatrics Subcommittee on Hyperbilirubinemia., 2004). Moreover, the assay of serum bilirubin is widely used to test liver function, which may be impaired due to inflammatory or obstructive lesions. On the other hand, a low level of serum bilirubin concentration is associated with iron deficiency and coronary artery disease (Stocker et al., 1987). As an antioxidant, bilirubin is known to suppress the oxidation of lipids and lipoproteins, especially LDL cholesterol, and hence its level may be directly co-related to the serum antioxidant capacity in humans (Lin et al., 2010). Thus, free bilirubin determination may be useful in assessing the risk involved in cardiovascular diseases. Bhutani et al., (2013) conducted an systematic review and meta-analyses to estimates the national prevalence, mortality, and kernicterus due to extreme hyperbilirubinemia (EHB) and Rhesus (Rh) sensitivity. This study estimates the number of neonatal survivor and impairment cases for the year 2010. Twenty-four million (18 % of 134 million live births ≥32 week gestational age from 184 countries) were at risk for neonatal hyperbilirubinemia-related adverse outcomes. The global burden of EHB and Rh disease is disproportionately heavy for the poorest countries (11 fold more). Hence, there is a strong demand to develop an inexpensive analytical method for rapid and reliable determination of bilirubin in blood serum (Slusher et al., 2011).

1.2. Current methods for detection of bilirubin in serum

During the last century, many analytical methods were developed for measuring bilirubin in the serum sample. Bilirubin can be quantified as native or derivatized tetrapyrroles or after its conversion to azo-derivatives. Various methods were used to determine bilirubin in serum as discussed below.

1.2.1. Optical based methods

1.2.1.1. Direct spectroscopy

The total bilirubin concentration in serum can be estimated by measuring the absorbance in the range of $\lambda_{450\ nm}$ to $\lambda_{460\ nm}$ using a calibration equation (Hertz et al., 1974; Watson, 1961). This procedure is simple, rapid, and requires no dilution of the sample. However, this direct spectrophotometry based assay has several disadvantages. Among which, spectral and matrix interferences caused by hemoglobin, which absorbs at both $\lambda_{454\ nm}$ and $\lambda_{528\ nm}$ equally are widely known. Subtraction of the absorbance at $\lambda_{528\ nm}$ from that at $\lambda_{454\ nm}$ eliminates the effect of hemolysis and yields a value that can be attributed primarily to bilirubin. Unfortunately, other pigments, such as carotenoids, also absorb at $\lambda_{454\ nm}$. The absorption measurement at multiple wavelengths and/or use of differential spectra were employed to overcome the interference caused by hemoglobin (Amazon et al., 1981; Bijster et al., 1981).

1.2.1.2. Diazo based method

The majority of the methods developed for bilirubin detection make use of diazo reaction, which involves reactions of bilirubin with diazo dye to form an intense colored product called azobilirubin. This diazo reaction discovered by Ehrlich (1880) was first utilized for the detection of bilirubin in serum by Van den Bergh and Snapper (Fowweather,

1932). The diazo reaction is shown in scheme 1.2. In this reaction of bilirubin two isomeric azopigments with absorbance maxima at $\lambda_{530\ nm}$ are formed. The conjugated bilirubin reacts directly with diazo reagents due to their greater solubility and less affinity for albumin, hence termed it 'direct bilirubin' (DB). The unconjugated bilirubin, on the other hand needs accelerator for its solubilization and hence, it is termed 'indirect bilirubin'. A small organic molecule is used as an accelerator to solubilize unconjugated bilirubin and/or displace it from albumin. Many publications report bilirubin detection with minor and insignificant modification of diazo reaction based procedures. Among these, Malloy and Evelyn method (1936), utilized 50 % methanol as an accelerator and the absorbance of azodipyrrole was measured at $\lambda_{540\ nm}$ to determine the total bilirubin. Jendrassik and Grop (1938) used a mixture of caffeine and benzoate in acetate as an accelerator in the diazo reaction for the determination of total bilirubin level. The method involves the addition of alkaline tartrate at the end of the reaction, which shifted the absorbance maxima of the azodipyrrole products from $\lambda_{530\ nm}$ to $\lambda_{600\ nm}$ resulting in the reduction of interference caused by hemoglobin. This method was recommended as a procedure of choice for total bilirubin estimation by the U.S. National Committee for Clinical Laboratory Standards (Doumas et al., 1985). Some modifications of this method involve the substitution of caffeine by dyphylline, dimethyl sulfoxide, N,N-dimethyl formamide, acetamide and sodium dodecyl sulfate. In other methods, ascorbic acid or potassium iodide were added to destroy excess diazo reagent which otherwise causes product decomposition (Doumas, 1986; Homsher and Chu, 1983; Lauff et al., 1983).

1.2.1.3. Enzymatic oxidation based methods

Bilirubin oxidase (BOx) (EC 1.3.3.5) isolated from *Myrothecium verrucaria* (Murao and Tanaka, 1981) and different fungal sources were used for the estimation of direct

bilirubin concentration in blood serum. The determination was based on measuring the decrease in absorbance at $\lambda_{450\ nm}$ caused by the enzymatic oxidation of bilirubin as reported by Doumas et al., (1987) (Scheme 1.3A). The method employs pH 3.7 and pH 7.2 for the detection of direct and total bilirubin concentration, respectively (Kosaka et al., 1987; Otsuji et al., 1988). The use of BOx to measure the apparent unbound bilirubin concentration in human plasma was investigated (Goldfinch and Maguire, 1988). However, the method was not recommended for the assay due to poor precision (Heinemann and Vogt, 1988; Mullon and Langer, 1987). For direct bilirubin measurement, the enzymatic oxidation method using BOx was found to be not suitable due to its light sensitivity as compared to the diazo method (Ihara et al., 1990). Differences between enzymatic and diazo methods for measuring

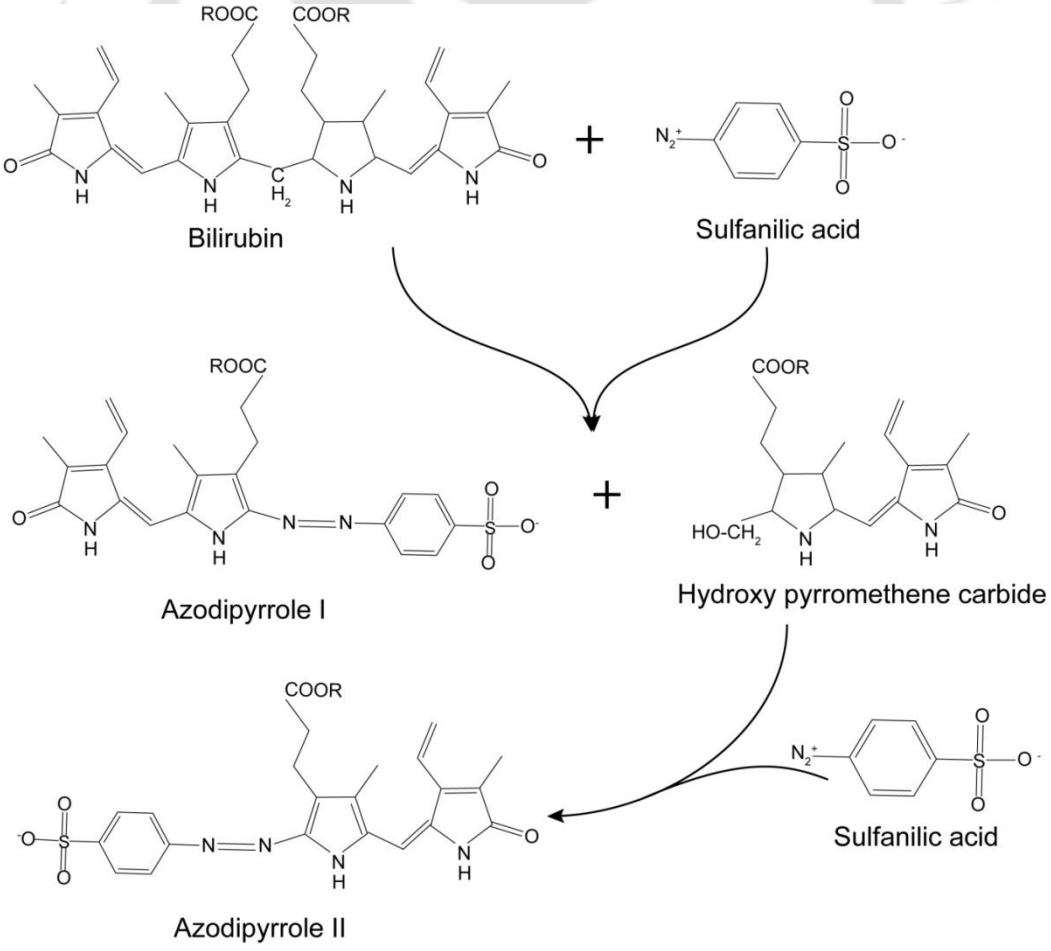

Scheme 1.2: Scheme of diazo reaction involves in bilirubin detection.

direct bilirubin were also studied by Nakayama and his group and reported that BOx catalyzes the oxidation of direct bilirubin at ~ pH 4, total bilirubin at ~ pH 8 and a small portion of unconjugated bilirubin at pH 10 (Nakayama, 1995). The enzyme's dependency on pH for the oxidation of different fraction of bilirubin makes it unsuitable for routine laboratory measurements. An immobilized tri-enzyme system containing glucose oxidase, BOx and horseradish peroxidase (HRP) was also investigated for the enhanced oxidation of bilirubin (Daka et al., 1989).

HRP (EC 1.11.1.7) based assay was commonly employed for determination of only the non-albumin bound fraction of bilirubin (free bilirubin) in the serum of newborn infants (Jacobsen and Wennberg, 1974). The enzyme in the presence of peroxide oxidizes free bilirubin into a colorless compound while albumin-bound bilirubin was protected from the oxidation. Since the equilibrium between albumin and bilirubin occurs rapidly, the oxidation step was rate limiting, and the initial oxidation velocity of total bilirubin was proportional to the unbound bilirubin concentration (scheme 1.3B). This method is currently used for the detection of unbound fraction of bilirubin. An FDA approved semi-automatic analytical instrument, UB analyzer (Arrow co Ltd. Osaka, Japan) has been dedicated for the purpose of determining unbound fraction of bilirubin based on the principle stated above. This approach, however, suffers from some of the technical pitfalls including the need of sample dilution before analysis, which may alter intrinsic bilirubin binding properties to albumin (Ahlfors, 2000). Influence of conjugated bilirubin on the determination of serum unbound bilirubin was also investigated and reported that the peroxidase method overestimates the unbound bilirubin concentration in the presence of excess conjugated bilirubin (Itoh et al., 2002). Further, effects of sample dilution, peroxidase concentration, and chloride ion on the measurement of unbound bilirubin in premature newborns were studied and reported that the

accurate free bilirubin measurements can be made only in minimally diluted serum or plasma (Ahlfors et al., 2007). Even though the peroxidase-based method is the only method approved by FDA for free bilirubin measurement, the method is not routinely used due to some complexity involved in the measurement.

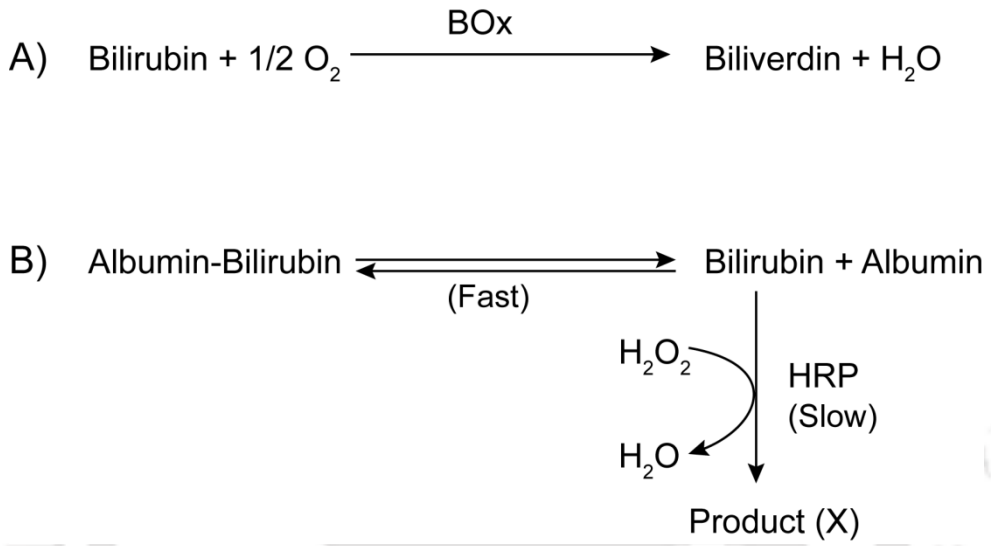

Scheme 1.3: Enzymatic oxidation of bilirubin by BOx and HRP.

1.2.1.4. Spectro fluorometric based method

The fluorescence quantum yield of bilirubin in aqueous solution is very low. When bound to albumin, the quantum efficiency of bilirubin in aqueous solution increased that makes fluorescence measurements useful for the measurement of bound fraction of bilirubin. The bilirubin-albumin complex emits fluorescence at $\lambda_{520\ nm}$ (Athar et al., 1999; Lamola et al., 1979; Plavskii et al., 2007; Zietz et al., 2004). Based on this fluorometric measurement of albumin- bound bilirubin, the technique for determining the binding capacity was developed. The custom designed hemato-fluorometer was constructed that makes use of automated front face fluorescence measurements on whole blood for rapid micro-assay of bilirubin. Measurement of unconjugated serum bilirubin concentrations using a novel and sensitive

method based on static fluorescence quenching of dansylated BSA was also developed, which requires very low sample volume and can detect bilirubin over a wide range of 17- 343 µM (Nagaoka and Cowger, 1979).

An enzyme-based fiber-optic fluorescence biosensor was developed for the determination of bilirubin (Li et al., 1996). Later on, a miniaturized fiber optic biosensor was developed for rapid detection of bilirubin through an indirect approach exploiting fluorescence quenching of tris(4,7-diphenyl-l,l0-phenanthroline) ruthenium chloride [$Ru(dpp)_3$] caused by the dissolved molecular oxygen. In the reaction oxygen is consumed in the oxidation of bilirubin to biliverdin, catalyzed by the enzyme BOx (Li and Rosenzweig, 1997). This sensor offered a detection limit of 0.1 µM and a linear range of 0.1 to 300 µM. In another approach, fluorescent reaction of bilirubin with Zn^{2+} in dimethyl sulfoxide was successfully employed for the detection of bilirubin in serum. The method offers linear range of 1.7 to 85 µM with a detection limit of 85 nM (Kohashi et al., 1998). The measurement of changes in fluorescence caused by BOx catalyzed reaction was also employed for the determination of all the fractions of bilirubin following a multivariate analysis approach. The method offers a linear range upto 20 µM (Andreu et al., 2002, 2000). A chemiluminescence (CL) based method for detection of bilirubin was developed by Lee et al., (2007). The method exploits bilirubin led inhibition of CL produced by of lucinigen- H_2O_2 system. The decrease in CL intensity was proportional to the concentration of bilirubin in the range 0.1-100 µM. The detection limit discerned from the developed calibration plot was ~13.5 nM. Furthermore, a fluorescent imprinted polymer that binds bilirubin selectively was developed. The imprinted polymer was synthesized by using functional monomer- methacrylic acid and fluorescent zinc(II) protoporphyrin (Chou and Syu, 2009). Many fluorescence-based techniques for determination of bilirubin have been reported during last five years. Bian et

al., (2011 and 2010) reported bilirubin led fluorescence quenching of tetracyclin- europium (Eu^{3+}) complex and oxytetracyclin for quantification of bilirubin. In another example, fluorescent yttrium–norfloxacin complex was utilized for spectrofluorimetric quantification of bilirubin. The method showed a good linear relationship in the range of 0.05- 3.9 mM (Kamruzzaman et al., 2012). Huber et al, (2012) developed a fluorescence-based sensor utilizing mutated fatty acid binding protein tagged with fluorescence dye acrylodan that specifically binds to unconjugated bilirubin. Detection assay was based on the quenching of fluorescence of the dye when the bilirubin specifically binds to a mutated fatty acid binding protein. For spectrofluorimetric determination of bilirubin enoxacin-terbium probe was utilized by Bian, (2014). In the recent past, water soluble polyfluorene with glucuronic acid appendages was utilized for sensitive detection of free bilirubin. The role of glucuronic acid was to inhibit the adherence of the serum protein which otherwise interfere with the detection of bilirubin (Senthilkumar and Asha, 2015). The effect of serum proteins could also be neutralized by layering a polymer film contains an optimized amount of HSA over silver nano-island. The polymer layer impedes serum proteins, allows only free bilirubin to diffuse through it, which later binds with the HSA in the film. Silver layer present below enhances the fluorescence of the HSA bound bilirubin complex up to 10^3 times through the mechanism of metal-enhanced fluorescence signal. The metal-enhanced fluorescence technique was applied for the specific assay of free bilirubin in neonatal serum (Geddes, 2014). Table 1.1 summarizes few of the prominent fluorometric method employed for the detection of bilirubin.

1.2.2. Electrochemical based methods

Electrochemical methods, especially amperometric methods have been widely utilized in bilirubin sensing. Mainly three approaches are used in the electrochemical detection of

Table 1.1: Fluorometry based methods for the detection of bilirubin.

Detection type	Detection probe	Detection Limit (µM)	Linear Range (µM)	Reference
Fluorescence quenching	Dansylated BSA	NA	17-342	Nagaoka and Cowger, (1979)
CL	N-bromosuccimide/ Hypochloriire	0.085	0.34-34	Palilis et al., (1996)
Fluorescent intensity changes	Perylene and BOx immobilized membrane	0.44	0.44 – 300	Li et al., (1996)
Fluorescent intensity changes	$[Ru(dpp)_3]$ and BOx immobilized membrane	0.1	0.1 - 300	Li and Rosenzweig, (1997)
CL	Zn^{2+} in DMSO	0.085	1.7- 80	Kohashi et al., (1998)
Fluorescent intensity changes	BOx-Fs	0.2	NA	Andreu et al., (2002)
CL	Lucigenin	0.015	NA	Lee et al., (2007)
Fluorescence quenching	Fluorescent imprinted polymer	0.04	0.1-50	Chou and Syu, (2009)
Fluorescence quenching	Tetracyclin –Eu^{3+}	NA	0.2-25	Bian et al., (2010)
Fluorescence quenching	Oxy teteracyclin- Eu^{3+}	0.77	0.5-30	Bian et al., (2011)
Fluorescence quenching	Mutated FAB labelled with acylodan	NA	NA	Huber et al., (2012)
Fluorescence quenching	Polyfluorene	0.15	25- 50	Senthilkumar and Asha, (2015, 2013)

* Few values were normalized for making the units uniform for better comparison. BOx: Bilirubin oxidase, HRP: Horse radish peroxidase, BSA: Bovine serum albumin, Fs: Fluorescein, CL: chemiluminiscence, $Ru(dpp)_3$:tris(4,7-diphenyl-1,10-phenanthroline) ruthenium chloride, Eu^{3+}: Europium, FAB: Fatty acid binding protein.

bilirubin. Two of them are non-enzymatic methods, which include direct oxidation of bilirubin at the electrode surface and the use of molecular imprinting polymer for the

bilirubin detection. Other is an enzymatic biosensing method which employs enzyme BOx for the electrochemical detection of bilirubin.

1.2.2.1. Enzymatic electrochemical detection of bilirubin

Electrochemical detection of bilirubin using BOx as biorecognition element was reported by Matui et al. (1985). Later on Wang and Ozsoz (1990) reported an amperometric dual-enzyme electrode for bilirubin which was based on co-immobilizing of BOx and HRP within a graphite-epoxy matrix. The resulting bi-enzyme electrodes were renewable (by polishing) and offered low-potential for the detection of bilirubin. The sensor offered a limit of detection of 4 µM and a linear detection range upto 10 mM. An amperometric bilirubin biosensor constituting self-assembled multilayer network of BOx over gold electrode was also developed. The sensor had a self-life of more than three months when stored at 4 ºC (Shoham et al., 1995). Fortuney and colleagues described a platinum electrode modified with a crosslinked adduct of BOx, BSA, and glutaraldehyde. The concentration of bilirubin was determined by monitoring the increase in H_2O_2 concentration resulting from the enzymatic reaction (Fortuney and Guilhault, 1996). The bilirubin biosensors displayed a linear range up to 300 mM and a detection limit of 0.7 mM. Indirect detection of bilirubin by monitoring depletion in O_2 concentration upon enzymatic oxidation of bilirubin was also reported (Klemm et al., 2000). In their system, BOx was chemically bonded using BSA and glutaraldehyde to a pre-activated membrane. The O_2 depletion was recorded using an oxygen electrode. This method was free from interference, fast and the modified electrode retained 80 % of its initial activity after 30 successive measurements. A biosensor array system consisting of cholesterol, bilirubin, and glutamate sensors was developed by Song et al. (2007). In this array sensor, bilirubin was detected by using BOx immobilized over nanoporous silicon electrode. Kannan et al. (2011) developed a 2nd generation amperometric

biosensor using $[Fe(CN)_6]^{-3/-4}$ as mediator. The sensor was constructed by immobilizing BOx on gold nanoparticles (AuNPs) embedded in a sol-gel network over a gold electrode. A detection limit of 1.4 nM bilirubin was achieved through this biosensor. Although very sensitive, the biosensor was stable only for two days. Feng et al. (2013) developed a nanocomposite electrode made of MWCNT, graphene and *in-situ* synthesized gold nanoparticles over which BOx was immobilized by adsorption. This device exhibited a linear range of 1.33 mM to 71.56 mM and a bilirubin detection limit of 0.34 mM. Subsequently, Batra et al. (2013) elaborated a composite electrode comprising BOx covalently immobilized onto zirconia coated silica nanoparticles with a detection limit of 0.1 nM. Poor stability, high K_m and weak activity of the enzyme BOx prompted to explore other enzymes as biorecognition element for developing bilirubin biosensor. Rahman et al, (2008) reported the use of Ascorbic acid oxidase instead of BOx as biorecognition element for the electrochemical detection of bilirubin. Table 1.2 summarizes few of the prominent enzyme based electrochemical methods employed for the detection of bilirubin.

1.2.2.2. Non-Enzymatic electrochemical detection of bilirubin

Several electrochemical studies were performed both in aqueous (Longhi et al., 1987) as well as in non-aqueous media (van Norman and Szentirmay, 1974) which confirmed the electroactive nature of bilirubin. The studies further confirmed that the electrochemical oxidation of bilirubin was a multistep process in which, it was electrochemically oxidized to biliverdin, purpurin or choletelin depending on the magnitude of the applied potential. Electrochemical measurement of bilirubin is a promising method for assessing unbound or free bilirubin in blood serum as albumin-bound fraction of bilirubin is inert for oxidation at the electrode surface (Balamurugan and Berchmans, 2015). Non-enzymatic electrochemical

detection involving oxidation of bilirubin mostly studied at the nanomaterial interface and molecular imprint platform. Feasibility of utilizing electrochemical properties of bilirubin for its detection in serum was initially investigated by Koch and Aklngbe (1981) using a hanging

Table 1.2: Enzyme based electrochemical methods for the detection of bilirubin.

Detection platform	Detection Limit (µM)	Linear Range (µM)	Sensitivity* µA μM^{-1}	Reference
BOx-HRP/ epoxy graphite electrode; mediator based; Amperometric	4	4-100	NA	Wang and Ozsoz, (1990)
SAM of BOx/gold electrode; Mediator Fc; Chronoamperometry	NA	10-100	NA	Shoham et al., (1995)
BOx-BSA/Pt electrode; Amperometric	0.7	1-300	NA	(Fortuney and Guilhault, 1996)
BOx-BSA preactivated membrane; O_2 electrode; Amperometric	8	10-250	NA	Klemm et al., (2000)
BOx/ Nano porous Silica electrode; Amperometric	NA	2- 20	0.153	Song et al., (2007)
BOx/AuNP/MPTS/Au electrode; Mediator Fc; Chronoamperometry	0.002	1- 500	NA	Kannan et al., (2011)
BOx/MWCNT/Graphene /AuNP's/GCE; Amperometry	0.001	0.02-250	0.327	Feng et al., (2013)
BOx/ SiO_2@ZrO Np /Au electrode; Amperometry	0.84	2-20	NA	Batra et al., (2013)
Poly –TTCA-MnII/ PEI-AsOx/GCE Chronoamperometry	0.04	0.1-50	NA	Rahman et al., (2008)

* Few values are normalized for making the units uniform for better comparison. BOx: Bilirubin oxidase, HRP: Horse radish peroxidase, SAM: Self assembled monolayer, Fc: Ferrocene, BSA: Bovine serum albumin, Pt: Platinum, AuNP: Gold nanoparticle, Au: Gold, MPTS: (3-mercaptopropyl)-trimethoxysilane, MWCNT: Multi walled carbon nanotube, SiO_2@ZrO Np: Silica oxide coated zironica oxide nanoparticles, Poly –TTCA: Poly terthiopene-3-(carboxylic acid), PEI: Poly ethylene imine, AsOx: Ascorbic oxidase, GCE: Glassy carbon electrode.

mercury drop electrode for the reduction of bilirubin. A voltammetric stripping method for the determination of bilirubin at the sub- nanomolar concentration levels was also reported

(Wang et al., 1985). The method was based on controlled adsorptive accumulation of bilirubin at the static mercury drop electrode followed by differential pulse measurement of the surface species that led to a detection limit of 5 nM. The electrochemical behavior of bilirubin on mercury electrode in aqueous solution and at physiological pH was investigated using differential pulse polarography technique (Longhi et al., 1987). The hanging mercury drop electrode was also further investigated to detect bilirubin in Tris-HCl solution and reported a detection limit of 0.2 nM and a linear range of 1 nM to 0.4 µM using differential pulse voltammetry (DPV) technique (Jin et al., 1992). However, the progress of research in this direction for detection of bilirubin on the electrode surface was halted for some time because of the rapid surface passivation associated with the adsorption of bilirubin and/or biliverdin and lack of solubility of bilirubin in aqueous solutions. Moreover, the potential employed for gaining the oxidation/ reduction signal for bilirubin species is significantly high resulting in high interference susceptibility caused by the electroactive compounds present in the blood serum.

Nanotechnology has opened new frontiers by offering unique enabling technologies and raw materials for electrochemical techniques. Nanomaterials modified electrodes provide a larger electroactive surface area for higher biomolecule loading (Asefa et al. 2009; Kerman et al. 2008) and increased flow of electrons between the electrode and the biomolecules due to their high surface area, favorable electronic properties and electro- catalytic effect. This probably helps in decreasing the over potential, amplifying biorecognition signal and increasing overall sensitivity of the biosensor. Among the various nanomaterials, gold and graphene-based nanoparticles have received increasing attention for developing bilirubin sensor. A glassy carbon electrode (GCE) modified with ferrocene carboxamide, gold nanoparticles (AuNPs) and multiwall carbon nanotubes (MWCNT) were constructed by

Wang et al. (2009). The nanoparticle modified electrode exhibits an excellent electrocatalytic response to bilirubin with a response time of less than 5 s, a broad linear range of 1 to 100 μmol L^{-1}. Taurino et al. (2013) investigated the direct electrochemical behavior of bilirubin on a nanostructured electrode with a thin film of MWCNT and observed that the nano-fabricated electrode exhibited a higher sensing performance than bare electrodes. The authors further reported the use of nanographite modified screen printed electrode with a free bilirubin detection limit of 56 ± 33 μM. Moreover, the performance of the constructed sensor in terms of sensitivity and detection limit towards bilirubin was not affected even in the presence of potential interferents, ascorbic acid and uric acid (Taurino et al., 2014). A non-enzymatic sensor specific for bilirubin was developed by Noh et al. (2014) using Nafion/Mn–Cu electrode. At the optimized condition, the sensor offered a dynamic range between 1.2 μM and 0.42 mM, and a detection limit of 25 ± 1.8 nM. A sensitive square wave voltammetric sensor for the quantification of bilirubin at the GCE modified with Nafion-electrochemically reduced graphene oxide (NF/ER-GO) hybrid composite was reported by Avan et al. (2015). The modified electrode offered a detection limit of 0.84 μM and dynamic range of 2 μM and 20 mM for bilirubin. In addition to that many other non-enzymatic bilirubin sensors have been reported during recent past. An NF/MWCNT hybrid film modified electrode was reported by Filik et al. (2015). The linear detection range for bilirubin furnished by the sensor was 0.8 μM to 10 μM. Balamurugan and Berchmans, (2015) reported a graphene–polystyrene sulfonate composite modified GC to detect free bilirubin at nanomaterial interface. Table 1.2 summarizes few of the prominent non-enzyme based electrochemical methods for the detection of bilirubin.

The molecularly imprinted polymer (MIP) approach uses target molecules or their molecular analogs as templates which direct the formation of recognition sites within a

polymer. During polymerization, target template molecules were mixed with functional monomers. After formation of the polymer, template molecules are washed out which leave specific cavities into which the original template can be rebound. By using this approach, some bilirubin detection methods were developed. Firstly, Syu et al. (2005) developed Poly (methacrylic acid-co-ethylene glycol dimethyl acrylate) (poly(MAA-co-EGDMA)) imprinted with bilirubin which binds specifically to α-bilirubin. They studied different parameters which affect the binding of bilirubin to MIP. Later the same MIP was immobilized over micro-sensing electrode for amperometric detection of bilirubin. At the potential 0.55 V a detection limit of 1 mg dL^{-1} was obtained (Syu et al., 2006). Huang et al. (2007) developed a portable potentiostat for the specific detection of bilirubin by using the same MIP. Molecularly imprinted polymer using β-cyclodextrin as a functional monomer for the efficient recognition of bilirubin was prepared by Yang et al (2008). Bilirubin imprinted super macroporous cryogels which can be used for the adsorption of bilirubin from human plasma was also developed (Baydemir et al., 2009). Titania film imprinted by bilirubin molecule on the surface of quartz crystal was prepared using molecular imprinting and surface sol–gel process. Based on this bilirubin imprinted titania polymer a novel quartz crystal microbalance (QCM) sensor with a high selectivity and sensitivity was developed for bilirubin determination (Yang et al., 2012, 2011). Another piezoelectric sensor was developed for bilirubin detection, which uses molecularly imprinted hydroxyapatite (HAP) film developed onto a quartz crystal surface using sol–gel technique. This biosensor presents high- selectivity with better linear range (0.05–80 µM) and lower detection limit (0.01 µM) (Yang and Zhang, 2011).

1.2.3. Separation based techniques for bilirubin detection

One of the most useful tools in the separation and identification of organic chemical components is the high-performance liquid chromatography (HPLC). Using sephadex column Wells et al. (1981) separated free bilirubin and albumin through a competitive binding

Table 1.3: Non-enzyme based electrochemical methods for the detection of bilirubin.

Technique	Electrode configuration	Detection Limit (µM)	Linear Range (µM)	Sensitivity* (µM μA^{-1})	Reference
ASV	Hanging mercury drop electrode	0.005	NA	NA	Wang et al., (1985)
DPV	Hanging mercury drop electrode	NA	NA	NA	Longhi et al., (1987)
DPV	Hanging mercury drop electrode	0.2×10^{-3}	1 nM-0.4 µM	NA	Jin et al., (1992)
Amperometric	Ferrocenecarboximide modified MWCNT/GNP/GCE	0.12	1-100	0.1336	Wang et al., (2009)
Amperometric	MWCNT based Screen printed electrode	4.2	200-500	0.0862	Taurino et al., (2013)
Amperometric	Nafion/Mn–Cu electrode	0.025	1.2-0.42	0.457	Noh et al., (2014)
Amperometric	Nanographite based micro electrode	56	100-500	15.47	Taurino et al., (2014)
SWV	NF/ER-GO/GCE	0.84	2-20	NA	Avan et al., (2015)
SWV	NF/MWCNT/GCE	0.014	0.8-10	NA	Filik et al., (2015)
Amperometric	GO/Polystyrene sulfonate composite/GCE	2	Up to 450	0.16	Balamurugan and Berchmans, (2015)

* Few values were normalized for making the units uniform for better comparison. GNP: Gold nanoparticle, GCE: Glassy carbon electrode, MWCNT: Multi walled carbon nanotube, NF: Nafion, ER-GO: Electrochemically reduced graphene oxide, Mn-Cu: Manganese copper bimetallic surface, ASV: Adsorptive stripping voltammetry, DPV: Differential pulse voltammetry, SWV: Square wave voltammetry.

approach. The bilirubin fraction retained in the column was later eluted with sodium hydroxide. Similarly, HPLC was employed for the separation of unconjugated bilirubin and its mono and di-glucuronide conjugates from the bile. Unconjugated bilirubin was separated by using reverse phase column while its derivatives were separated by μ-Bondapak carbohydrate column (Lim, 1979). Reverse-phase chromatography was also used for the separation of bilirubin using short-chain alkyl silica (C2) or octadecyl silica (C18) as stationary phase (Lauff et al., 1981; Lim et al., 1981; Singh and Bowers, 1985; Spivak and Careyt, 1985; Uesugi et al., 1983; Yamashita et al., 1986). A technique, alkaline methanolysis HPLC was developed for quantitative conversion of all conjugated bilirubin to their corresponding mono-and di methyl ester derivatives. These derivatives, which are poorly soluble in water as unconjugated bilirubin, were separated from serum by solvent extraction and later quantified by HPLC (Gordon and Goresky, 1982; Li et al., 1986; Muraca and Blanckaert, 1983; Scharschmidt et al., 1982). Quantitative liquid-chromatographic estimation of bilirubin species in pathological serum was also carried out (Lauff et al., 1983). Effect of pH and molarity on the chromatographic elution of unconjugated bilirubin was studied (Goresky and Gordon, 1990). Osawa et al. (2006) developed an assay for separating and quantifying four bilirubin fractions in untreated human serum using isocratic HPLC. A sensitive method for the detection of unconjugated bilirubin in biological fluids and tissue was developed based on the reverse phase HPLC (Zelenka et al., 2008). Later on, a highly sensitive HPLC method which detects unconjugated bilirubin in sub-nanomolar concentration was developed by using reverse-phase C18 support coupled with thermal lens spectrometric detection (TLS) (Martelanc et al., 2014). The HPLC methods are highly specific, and can quantitatively determine the individual fraction of bilirubin more accurately. However, the

methods suffer from major drawback among which these are labor intensive and not practical for routine use.

1.2.4. Non-invasive techniques for bilirubin detection

The correlation between ‘‘yellowness’’ of the skin and serum bilirubin concentration led to the development of transcutaneous bilirubinometer (Jaundice meter: JM), through a joint venture work of Yamanouchi et al. and the Minolta Camera Co. (1980). This noninvasive approach was based on measurement of reflectance of yellow intensity from the skin, thus providing the information on the concentration of transcutaneous bilirubin (TcB) in the jaundiced neonates. A product developed later on called Jaundice Meter JM-102 (Minolta/Hill-Rom Air-Shields, Hatboro, PA) that relies on two-wavelength analysis, was used to measure hemoglobin-corrected yellow color for TcB. This meter was evaluated in a couple of studies carried out in different racial groups (Kitsommart et al., 2013). All the studies showed that TcB is highly correlated with serum bilirubin (SB). Effects of melanin and oxyhemoglobin on TcB measurement by transcutaneous bilirubinometry was also conducted (Onks et al., 1993) and found variability on the reading. Efforts to overcome the variability in reading due to different pigments present in the skin were made in a device BiliCheck (SpectR, Inc, Norcross, GA) using reflectance data at multiple wavelengths (Bhutani et al., 2000; Robertson et al., 2002). A comparative study with the traditional laboratory invasive method demonstrated that transcutaneous bilirubinometry results significantly overestimated total serum bilirubin measurements (Grohmann et al., 2006). Although transcutaneous bilirubinometers exist for over 30 years, the clinical utility of the technique is limited to a screening method for hyperbilirubinemia, rather than a replacement

for invasive blood sampling. TcB cannot be used directly to make decisions about transfusions or phototherapy in neonates.

1.3. Nanoparticle-protein conjugation: Application in developing biosensors

Nanoparticles were routinely defined as particles with sizes between about 1 and 100 nm that show some properties not found in bulk samples of the same material. Nanoparticles show unique physicochemical properties such as high surface-to-volume ratio, unique spectral and optical properties, which encouraged the development of a plethora of biosensing platforms. Nanoparticles in conjugation with a suitable biological entity can be used as recognition elements in fabricating biological sensors. Protein is one such biological entity, whose size is comparable to that of nanoparticles, making them excellent scaffolds for use as biosensors. The assembly of proteins and nanoparticles provides the resultant hybrid system with unique optical and electrical properties. These functional hybrid nanosystems have found application in many fields, prominently in biotechnology, biosensing and bioimaging field (Rana et al., 2010).

One of the important challenges faced in the creation of effective conjugates is the difficults in long term retention of biological activity of the protein. The conjugation of nanoparticles with biomolecules such as proteins and DNA usually involves two approaches, direct covalent linkage (with linker molecules that form a bridge between nanoparticle and biomolecule) and non-covalent interactions (incubating biomolecules with nanoparticles that are densely passivated by protective molecules) between the particle and biomolecules (De et al., 2008). The main drawbacks of these strategy include a sizable percentage of nanoparticles are lost during the conjugation process, and the product often must be stored at low

temperatures to maintain stability. Such nanoparticles conjugates have a strong tendency to aggregate with even mild processing, and since they were densely passivated by protective molecules, they possess minimal free surface area for interaction with external species (Dickerson et al., 2008).

Relatively gentle approaches for the production of bioconjugated metal nanoparticles, nanorods, and nanowires make use biomimetic or biomolecule-enabled synthesis (Dickerson et al., 2008; Rahman et al., 2013; Rana et al., 2010). The "green" aspects of bio-enabled syntheses are particularly relevant for certain applications in which the surfactants and stabilizers being used in the chemical synthesis of metal nanoparticles may persist as contaminants in the final product, which are often toxic. The biomimetic synthesis of metal nanoparticles utilize relatively mild conditions that are difficult to achive in chemically driven synthesis processes. Biomolecules can be used to control the shape, size, size distribution, and solution stability of metal nanoparticles. Moreover, biomolecules impart new functional groups onto the material surface. This idea was thought to be a more straight-forward, direct, eliminates the need for intermediate stabilizing agents and potentially less deleterious route for the production of biomolecule-conjugated metal nanoparticles. The reducing and stabilizing ability of some amino acids for the syntheses of AuNPs were investigated (Bhargava et al., 2005; Shao et al., 2004). Aspartic acid, lysine, arginine, tyrosine, and tryptophan were found to initiate and control the syntheses of AuNPs at room temperature. The thiol side group of cysteine was suggested to be a source of electrons for the reduction of gold and was well known to bind with gold and other noble metals (Daniel and Astruc, 2004).

Because of its popularity among biomimetic mineralization in producing stable bioconjugated nanoparticles, the phenomena of protein-mediated synthesis of nanoparticles

are also investigated widely. One of the commonly studied protein for the synthesis of gold nanoparticles is bovine serum albumin (BSA), as it is readily available and inexpensive. The first study on the synthesis of BSA-assisted AuNPs was reported in 2004 (Burt et al., 2004). Later on, several research groups reported different size, shaped gold nanoparticle using BSA as stabilizing agent and different reducing agents (Au et al., 2010). In addition to BSA, several other commercially available proteins, as well as enzymes, were utilized in the bioenabled syntheses of AuNPs. Silk fibroin purified from *Bombyx mori* (silk worm) silk was also utilized to produce highly stable AuNPs dispersions. The enzymes α-amylase, alkaline phosphatase, HRP, lysozyme, RNAase, alcohol oxidase were also found to exhibit gold reducing capabilities (Chinnadayyala et al., 2015; Rangnekar et al., 2007; Zhou et al., 2001).

Recent advances in nanotechnology have given rise to a new class of nanomaterials called fluorescent metal nanoclusters also known as nanodots (NDs) or quantum clusters (QCs). Gold nanoclusters (AuNCs) typically consist of less than one hundred gold atoms, with sizes within the range of 0.3 to 3 nm. Unlike the most popular and well-known spherical, large Au NPs, AuNCs do not exhibit surface plasmon resonance (SPR) absorption in the visible region but emit fluorescence in the visible to near-infrared region. The detailed mechanism for the fluorescence of AuNCs is not yet completely understood, but a basic model has been proposed. The 'free electron' theory is of particular importance to understand the fundamental optical and electrical properties of AuNCs (Chen et al., 2015). The free electrons on the nanoparticle surface give rise to the polarization in an electronic field. The electron number determines the size dependent plasmonic optics. However, when the free electron number decreases to a critical value where the nanoparticle size approaches the Fermi wavelength, the continuous band breaks up into discrete energy levels. The numeric

size of the energy level spacing (E_δ) is a determining factor for the fluorescence of AuNCs (Zheng et al., 2007). The relation between E_δ, the number of gold atom (N) and Fermi energy (E_f) is given by the following equation

$$E_\delta = \frac{E_f}{N^{1/3}}$$

When the fluorescence of AuNCs is solely attributed to the metal centered electron transition, the fluorescence of AuNCs undergoes a red shift upon increasing their size and no emission in the visible region can be observed when cluster becomes larger.

The stability of AuNCs is an important issue that must be resolved for their practical utility. In the past decade, many strategies for the preparation of stable, water dispersible, highly fluorescent and biocompatible AuNCs have been reported. The procedure for AuNCs synthesis can be categorized into two groups, one which utilizes etching of larger AuNPs by thiol compounds such as, mercaptopropionic acid to yield smaller AuNCs (Chaudhari et al., 2011). The second category is from the reduction of Au^{3+} in the presence of a ligand or template mostly biomolecules such as protein or DNA (Lan et al., 2011; Xie et al., 2009). The later strategy involves biomimetic mineralization and hence requires fewer chemicals. Some proteins can act as reducing as well as capping agents, and thus, no additional reducing agent is needed. The first biomimetic synthesis protein stabilized AuNCs was reported by Xie and colleagues (Xie et al., 2009). The method makes use of BSAs capability to sequester and reduce Au precursor's *in-situ* for the preparation of AuNCs with red emission. Inspired by this finding, many researchers reported other proteins and enzymes such as HSA, lysozyme, HRP, glucose oxidase (GOx), urease, chymotrypsin, lactoferrin etc. as scaffold for the synthesis of AuNCs (Jin et al., 2011; Wen et al., 2011; Xavier et al., 2010; Yan et al., 2012). The production of AuNCs directed by enzymatic activity can integrate the catalysis function

of enzymes and the luminescence of metal NCs in a single conjugate, thus leading to the possibility of constructing multifunctional nanoprobes.

The analytical application of AuNCs had gained great attention recently due to their excellent properties, such as large Stokes shift, biocompatibility, ease of conjugation, as well as size and ligand dependent fluorescence properties. The fluorescence properties of AuNCs have been utilized successfully in sensing heavy metal ions (Hg^{2+}, Cd^{2+}, Pb^{2+} and Cu^{2+}), inorganic anions (S^{2-} and CN^{-}), small biomolecules (glucose, heparin, urea, dopamine,folic acid, ATP etc.) and some proteins (Interleukin, trypsin, proteinase K) (Chen et al., 2013; Cui et al., 2013; Hu et al., 2012; Li et al., 2012; Lu et al., 2014; Shang et al., 2012; Wang et al., 2014; Yang et al., 2013a; Yang et al., 2013b).

AuNCs were also employed for electrochemical sensing. Unlike the bigger nanoparticles which were extensively used for electrochemical sensing due to their high conductivity, these small AuNCs however, shown to possess redox properties as well. They behave as tiny conductors. Some electrochemical and computational studies revealed that the redox properties of nanocluster can be tuned effectively by controlling their core size. However, the electrochemical properties of the AuNCs are yet to be adequately investigated though these properties are well suited for designing the concept of developing commercial biosensors. (Lee et al., 2004; Lopez-Acevedo et al., 2010). Recently, redox active Au_{25} clusters were reported in electrochemical sensing of ascorbic acid, uric acid, dopamine (Kumar et al., 2011) and glucose (Kwak et al., 2014). Nanocluster in conjugation with redox mediator Azure A was reported in sensing H_2O_2 non-enzymatically (Priya et al., 2012).

Chapter II

HSA-stabilized gold nanoclusters: Synthesis, characterization and studies on their interaction with bilirubin

CHAPTER II

HSA-stabilized gold nanoclusters: Synthesis, characterization and studies on their interaction with bilirubin

2.1. Overview

Human serum albumin (HSA) is the most abundant protein in human plasma (~ 600 mM). It is a monomeric protein of 66 kDa containing three homologous helical domains (I–III), each divided into A and B subdomains. The main role of HSA is to transport various endogenous compounds including bilirubin in serum through the reversible binding process. HSA solubilizes bilirubin through the binding and acts as a buffer preventing the transfer of bilirubin from blood to tissue and thereby alleviate the toxic effect of bilirubin on the tissue. Due to this, the interaction of HSA with bilirubin has attracted much attention (Blaha et al., 1997; Goncharova et al., 2013; Moosavi-Movahedi et al., 2007) and the phenomena has been exploited to develop methods for determining free bilirubin in blood serum (Lamola et al., 1979). The previous studies suggest that two types of binding site are present on albumin protein surface. One is the primary binding site of high affinity, whereas the second site binds

bilirubin with 2-3 order lower affinity. Studies indicated that the HSA acts as a chiral matrix that can selectively recognize the P-form of bilirubin enantiomer. However, binding of bilirubin with native HSA does not produce any strong signal for analytical application of the phenomena to detect bilirubin. We propose the incorporation of AuNCs in the HSA- protein matrix likely to create some change on the property of this protein due to the intense electronic property of these NCs as discussed elsewhere. In this regard, first, we direct our investigation on synthesis and characterization of the HSA stabilized nanocluster. We then focus our studies on the effect of binding of HSA containing stabilized AuNC with its natural ligand bilirubin. This study utilizes some spectroscopic techniques such as fluorescence, UV-visible, and circular dichroic spectroscopy.

2.2. Experimental approaches

2.2.1. Reagents and stock solutions

HSA, auryl chloride ($HAuCl_4$), sinapinic acid and (±)-10-camphorsulfonic acid, bilirubin (98 %) were purchased from Sigma-Aldrich (USA). Spectroscopic grade potassium bromide (KBr), ethanol, sodium hydroxide (NaOH), sodium dihydrogen phosphate (NaH_2PO_4) and disodium hydrogen phosphate (Na_2HPO_4) were purchased from Merck (India). All other reagents were of analytical reagent grade and used without further purification. Nanopure water (18.2 MΩ: Millipore Co., USA) was used throughout the experiment.

A stock solution of bilirubin (0.1 mM) was freshly prepared in 10 mM NaOH solution. The HSA and HSA-AuNC stock solution each of 150 µM was prepared in sodium phosphate buffer (pH 7.4, 50 mM). The stock solutions were protected from light. Concentration of bilirubin, HSA and HSA-AuNC were determined by using extinction coefficients ε_{450} = 64500 $M^{-1}cm^{-1}$, ε_{278} = 36500 $M^{-1}cm^{-1}$ (Charbonneau et al., 2009) and ε_{278} =

57700 $M^{-1}cm^{-1}$ for bilirubin, HSA and HSA-AuNC, respectively.

2.2.2. Synthesis of HSA-stabilized nanocluster

All glassware were washed with aqua regia (HCl: HNO_3, volume ratio 1:3) and then rinsed with ultrapure water. HSA stabilized nanocluster were synthesized following a reported method with a minor modification (Yan et al., 2012). Briefly, 31 mg of HSA dissolved in 500 µl of ultrapure water was transferred to 500 µl of $HAuCl_4$ (10 mM) with constant stirring and mixed with 50 µL of 1M NaOH solution after 2 min. The solution when irradiated with microwave (300 W, 2.45 GHz) for 6 min, HSA-AuNC were formed, as indicated by the change in color to deep brown with the emission of red fluorescence under an UV lamp ($\lambda_{365\ nm}$). The scheme of microwave mediated synthesis of HSA stabilized nanocluster is shown in scheme 2.1A.

2.2.3. Purification of HSA-stabilized nanocluster

The HSA- stabilized nanoclusters were separated from free protein using the Zn^{2+}-assisted co-precipitation method (Guan et al., 2014), which preferentially precipitates HSA-AuNC (Scheme 2.1B). Briefly, 500 µl of freshly synthesized HSA stabilized nanocluster was mixed with 500 µl of 10 mM zinc acetate. The reaction mixture was allowed to stand for 2 min. Later it was centrifuged at 9160 xg for 10 min. Supernatant containing unreacted HSA was discarded and the pellets were washed with a copious amount of water and dispersed in PBS (pH 7.4). The dispersed HSA nanocluster was dialyzed against distilled water for 24 h to remove the Zn^{2+} ions. The dialyzed HSA nanoclusters were lyophilized and stored at 4 °C for further use. The purification process was monitored by MALDI-MS.

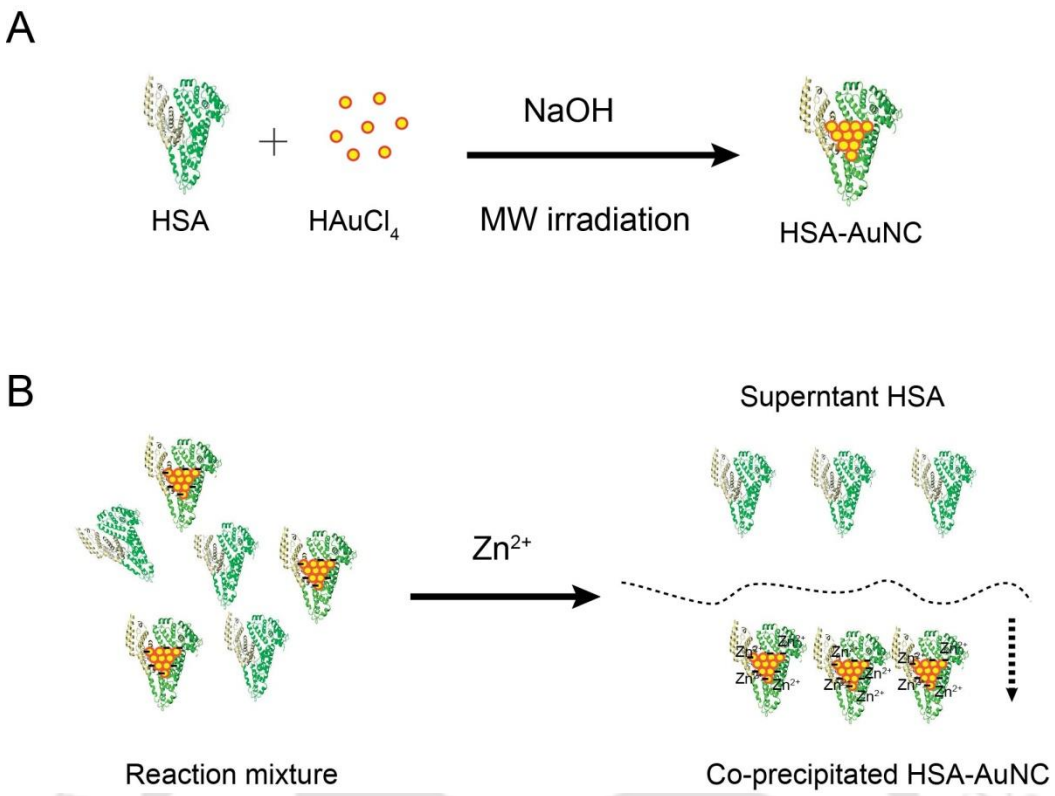

Scheme.2.1: A) Preparation of AuNCs within HSA protein matrix *via* microwave irradiation method. **B):** Scheme of purification of HSA-AuNC *via* zinc-assisted co-precipitation method.

2.2.4. Spectroscopic characterization of HSA-stabilized nanocluster

Spectrophotometric analyses were done on a Cary UV-100 UV-visible spectrophotometer (Varian, USA) using 1 cm path length quartz cuvette at scan rate 100 nm min^{-1}. The concentration of both HSA and HSA-AuNC were kept at 1 mg ml^{-1}. Fluorescence measurements were recorded using LS-55 spectrofluorometer (Perkin Elmer, USA) at 25 °C. Emission spectra for HSA-AuNC were recorded by exciting at $\lambda_{380\ nm}$. Both emission and excitation slit width were kept at 5 nm. The scan rate of 50 nm min^{-1} was used throughout the fluorescence measurement.

2.2.5. Circular dichroism and Fourier transform infrared spectroscopic study

Circular dichroism (CD) spectra of HSA and HSA-AuNC were performed using a spectropolarimeter (J-815, Jasco, Japan.) calibrated with 0.06 % (w/v) aqueous solution of (±)–10–camphorsulfonic acid. The spectra were recorded in the range of $\lambda_{240\ nm}$–$\lambda_{190\ nm}$, in 0.1 cm path length suprasil quartz cuvette, at a scan rate of 50 nm min^{-1}, 1 nm bandwidth, with a time constant of 2 s, and an average of 4 scans. The temperature of the cell was maintained at 25 °C by using a peltier temperature control unit. The spectrum was corrected for baseline and smoothed by Savitsky–Golay filter using Jasco spectral analysis software. The secondary structure analysis was performed using online server DICROWEB structure estimation program which utilizes CONTIN program to evaluate the structure (Greenfield., 2007).

Fourier transform infrared (FTIR) spectra of HSA and HSA-AuNC were performed on UNICAM Mattson 1000 model Fourier transform spectrophotometer (England) using spectroscopic grade KBr pressed disc.

2.2.6. Matrix- assisted laser desorption ionization- mass spectroscopy and transmission electron microscopic study

Intact mass of HSA and HSA-AuNC were determined by performing matrix- assisted laser desorption ionization-Mass Spectrometry (MALDI-MS) (4800 plus MALDI TOF/TOF Analyzer, AB SCIEX, USA). Sinapinic acid was used as a matrix for MALDI and the spectra were collected in a positive mode and averaged for 100 shots. Transmission electron microscopy (TEM) images were obtained from a JEOL 2100 (Japan) electron microscope operated at an accelerating voltage of 200 kV. For TEM analysis samples were prepared by evaporating a drop of dilute solution of HSA-AuNC on a carbon coated copper TEM grid.

2.2.7. Zeta potential study

Isoelectric point (*pI*) of the HSA and HSA-AuNC was determined using Zetasizer Nano Instrument system (Malvern Instruments Limited, UK). HSA and HSA-AuNC each with a concentration of 1 mg ml^{-1} was incubated in buffers of different pH from 4.0 to 7.5 with a pH increment of 0.5. All solutions were filtered through 0.22-micron syringe filter. The filtered HSA and HSA-AuNC in different pH buffer were charged into specially designed folded capillary cell with gold plated copper electrode (Malvern Instruments Limited, UK). Data were acquired at 20 °C, repeated 20 times and averaged. The viscosity was set to 1 cP at a scattering angle of 90° and resulting autocorrelation function was analyzed by the integrated control software to obtain the *pI* value of both HSA and HSA-AuNC.

2.2.8. Interaction studies of HSA-AuNC with bilirubin through fluorescence and circular dichroism spectroscopic study

Fluorescence spectra were recorded using LS-55 spectrofluorometer (Perkin Elmer, USA). Tryptophan fluorescence was monitored for studying the interaction of HSA-AuNC and native HSA with bilirubin. A series of solutions containing a fixed concentration of HSA-AuNC (5 μM) and HSA (5 μM) with different concentrations of bilirubin (0-7 μM) were prepared in 50 mM PBS pH 7.4. Tryptophan fluorescence spectra, each with an average of four scans, were recorded in the scan range of $\lambda_{304\ nm}$ to $\lambda_{450\ nm}$ with an excitation at λ_{295nm} using a slit width of 5 nm and a scan rate of 50 nm min^{-1}. Background fluorescence was subtracted from the sample spectra and the fluorescence spectra of HSA-AuNC (5 μM) and HSA (5 μM) in the absence of bilirubin served as control. The binding process is described by the following equilibrium,

$$Protein + n\ (Bilirubin) \rightarrow [Protein - Bilirubin_n]$$

where the protein binds with *n* equivalents of bilirubin to form a protein-bilirubin complex [protein-bilirubin$_n$]. The fluorescence intensity at $\lambda_{348\ nm}$ was used to calculate the binding constants (K_a) and *n* by using the well established Scatchard equation (Liang et al., 2008 and Min et al., 2004),

$$\log_{10}\frac{F_0 - F}{F} = \log_{10} K_a + n\ \log_{10}[Bilirubin]$$

In this equation, F_0 is the initial fluorescence intensity prior to addition of bilirubin, and *F* is the fluorescence intensity at a specific bilirubin concentration [*Bilirubin*]. By titration of bilirubin and plotting log (F_0-*F*)/*F* against log [*Bilirubin*], a linear curve was obtained with a slope of *n*. The y-intercept of log K_a provides the value of K_a (Min et.al, 2004 and Kang et.al, 2004).

The CD spectra were recorded at 25 °C using a quartz cell with a path length of 1 and 0.1 cm for visible- region of 300–550 nm and far- UV region of 190–240 nm, respectively. For far-UV CD measurement the concentration of HSA, HSA-AuNC and bilirubin were kept at 2 µM. The spectra were analyzed as mentioned in the section 2.2.5. For CD measurement in the visible region, the concentration of HSA and HSA-AuNC and bilirubin were fixed at 12 µM. The obtained spectra were corrected for baseline and smoothed for noise elimination.

2.3. Results and discussion

2.3.1. Spectroscopic characterization of HSA-AuNC

UV-visible absorption spectra of HSA and HSA-AuNC are shown in the Fig. 2.1A. The HSA-AuNC spectrum is featureless in the visible region, indicating absence of any bigger sized plasmon inducing nanoparticles. However, the intense red emission of the reaction mixture generated by UV irradiation indicates the formation of ultra-small fluorescent nanocluster (Fig. 2.1A inset). Fig. 2.1B depicts the fluorescence excitation and

emission spectrum of the HSA-AuNC conjugate. Although the excitation of HSA-AuNC had produced two peaks corresponding to λ_{370nm} and $\lambda_{500\ nm}$, the emission showed a single peak at $\lambda_{645\ nm}$ which agrees with a previous report (Yan et al., 2012). The fluorescence is considered to arise from the quantum confinement effect caused by the very small size of the AuNC. The formation of nanocluster within the protein matrix is proposed to be formed by the process of bioreduction, where protein HSA acts as both reducing and stabilizing agent. It is suggested that initially the gold (Au^{3+}) ions are sequestered into the HSA protein cage, once entrapped the reductive ability of some amino acids present in the HSA molecules assist the conversion of the Au^{3+} ions to AuNC (Xie et al., 2009). The whole process of progressive reduction of Au^{3+} ions can be activated by microwave irradiation. Selective dielectric heating by microwave may provide more efficient energy transfer between HSA and $HAuCl_4$, leading to the formation of AuNC rapidly (Shang et al., 2012). The HSA-AuNC synthesized by microwave irradiation in an alkaline solution was separated from the reaction mixture of $AuCl_4$ and HSA by co-precipitation with Zn^{2+} ion. HSA- protected AuNC precipitated out immediately upon the addition of Zn^{2+} solution at pH 11. It has been reported that OH^- ions can stably bind to Au^{3+} on the cluster surface. Zn^{2+} ions consequently interact with OH^- ion on the surface of AuNC to form zinc hydroxide (Guan et al., 2014). At the experiment pH, $Zn(OH)_2$ (pK_a ~10.5) co-precipitated with the HSA-AuNC, whereas unreacted HSA molecules are retained in the solution. Well dispersed nanoclusters with average diameters of ~ 2.5 nm correspond to dark spots are visible in the TEM image (Fig 2.2 and inset). MALDI-MS spectra of the reaction mixture (Fig. 2.2B) show two peaks, one at 66.9 kDa which corresponds to HSA and the other peak at 70.5 kDa which corresponds to HSA-AuNC. After purification through Zn^{2+} co-precipitation, only the peak at 70.5 kDa was observed indicating the successful purification of HSA-AuNC. The number of gold atoms formed within HSA protein matrix was 18 as discerned from the following equation.

$$Number\ of\ Au\ atom = \frac{\frac{m}{z} of\ HSA, AuNC - \frac{m}{z} of\ HSA}{Atomic\ weight\ of\ Au}$$

Microwave-mediated method generally yields small core sized nanocluster as compared to the incubation method which commonly yields 25 atom cluster in the protein matrix (Yue et al., 2012). Molar extinction coefficient of HSA-AuNC at $\lambda_{278\ nm}$ was determined as 55770 ± 500 cm^{-1} M^{-1}.

2.3.2. Secondary structure of HSA-AuNC

CD measurements were performed with free HSA and HSA-AuNC systems to understand any transition of secondary structure of HSA after formation of the NCs in the protein. The CD spectra (Fig. 2.3A) of HSA and HSA-AuNC exhibited two negative bands in the UV region at 208 nm and 222 nm which is a characteristic feature of α-helical structure of protein. The reasonable explanation is that the negative peaks near 208 nm and 222 nm are the results of $n \rightarrow \pi^*$ transition in the α-helical bands. The percentages of various conformations were calculated for both pure HSA and HSA-AuNC (Fig.2.3A Inset). Free HSA comprises 48 % α-helix content, 34 % β-sheets turns content and 18 % random coil content, which is in agreement with the previous reports (Monacelli et al., 2013). A noticeable change in the secondary structure of HSA was observed when AuNC formed within it. The α-helix content was decreased to 32 %, and β-sheets and turns and random coil contents were increased to 41.5 % and 26.1 %, respectively, indicating a partial destabilization of the α-helix of the protein as a result of its complexation with the nanocluster. In the FTIR spectra, the frequencies of bands due to the amide I, II, and III vibrations are sensitive to the secondary structure of proteins. Particularly, the amide I in the region 1600-1700 cm^{-1} (mainly CO stretch) band is useful for the secondary structure studies. FTIR spectra of HSA and HSA-AuNC are shown in Fig. 2.3B. The slight shift in the peak

position of amide I from 1650.7 cm^{-1} to 1656.5 cm^{-1} and decrease in transmission intensity at this region were noticed when nanocluster was formed within the HSA. This further infers secondary structural perturbation due to the formation of nanoclusters in the protein matrices.

2.3.3. Isoelectric point (*pI*) of HSA-AuNC

The Zeta (ζ) potential values of HSA and HSA-AuNC solutions were measured at different pH buffers (4.0 to 7.0). The plot of ζ- potential of HSA and HSA-AuNC vs. pH was represented in the Fig. 2.4A and 2.4B. The point where the plot of ζ- potential vs. pH gradient passes through zero is the isoelectric point (*pI*). The calculated *pI* value of HSA was found to be ~5, which is in agreement with a previous report (Taboada et al., 2004). The p*I* of HSA-AuNC was ~5.7, which is a shift of more than half a pH unit towards basic pH as compared to *pI* of the native HSA. This is due to the presence higher surface charge density caused by the formation of AuNC within HSA protein matrix (Hladilkova et al., 2016).

2.3.4. Interaction study of HSA-AuNC with bilirubin

2.3.4.1. Fluorescence spectroscopic studies

Tryptophan fluorescence is highly sensitive to the local environment, and a change in the emission spectra of tryptophan is an indicative of changes in protein conformational changes and substrate binding. When molecules interact with HSA, the magnitude of tryptophan fluorescence changes depend upon the impact of the interaction (Eftink and Ghiron, 1976). HSA binds to bilirubin with K_d value of 10^{-7}-10^{-8} M at high affinity site and acts as a buffer preventing the toxic effect caused by bilirubin (Levine, 1977; Sato et al., 1988). To investigate the impact of embedded gold nanocluster on binding of bilirubin to HSA-AuNC, an interaction study with bilirubin was performed. The HSA contains a single polypeptide of 585 amino acids with one tryptophan (Trp 214) residue. We considered the

tryptophan fluorescence at the excitation wavelength of 295 nm to nullify the possible interference from tyrosine fluorescence. The HSA solutions, exhibited an intense fluorescence emission with peak centered on $\lambda_{348\ nm}$ when excited at $\lambda_{295\ nm}$. Fig. 2.5 shows the tryptophan fluorescence quenching of HSA and HSA-AuNC by bilirubin. The tryptophan fluorescence of HSA (Fig. 2.5A) was reduced by 3 times in HSA-AuNC solution (Fig. 2.5B). This might be due to the changes in the micro environment within HSA protein matrix by the *in-situ* formed gold nanocluster and due to the fact that the reductive nature of tryptophan is involved in the formation of AuNCs (Yan et al., 2012). The fluorescence intensities of HSA and HSA-AuNC solution were then studied in presence of bilirubin in the solution. The plot of log [$(F_0\text{-}F)/F$] vs. log [*bilirubin*] (Fig. 2.5C and 2.5D) yield a linear response with log K_a as the intercept and n as the slope. The binding constants obtained were 2.45×10^8 and 0.55×10^6 L mole^{-1} for HSA and HSA-AuNC, respectively. The numbers of binding sites (n) discerned from the slopes were 1.51 and 1.12 for HSA and HSA-AuNC, respectively.

2.3.4.2. Far- UV CD spectroscopic studies

The effect of bilirubin binding on the secondary structure of HSA and HSA-AuNC was investigated through far-UV CD measurements. Fig. 2.6A and 2.6B represent the far-UV CD spectra HSA and HSA-AuNC in absence and presence of bilirubin, respectively. Both HSA and HSA-AuNC exhibited two negative bands in the UV region at 208 and 222 nm which are characteristic of a α-helical structure of protein. The negative peak at around 208 nm and 222 nm were increased in presence of bilirubin in both the cases and the intensity at 195 nm was oppositely changed i.e, decreased for HSA and increase for HSA-AuNC upon interaction with bilirubin. The α-helical content of the HSA and HSA-AuNC were decreased from 48% and 32 % to 45 % and 30 % respectively, upon formation of complex with bilirubin. Whereas β- sheet content was increased both in case of HSA-bilirubin complex and

HSA-AuNC-bilirubin complex, while the content of random coils were remain unchanged.

2.3.4.3. UV-visible and Induced CD spectroscopic studies

Free bilirubin (unbound) solution produced an absorption spectrum with a maximum intensity (λ_{max}) at 440 nm (Fig. 2.7B dotted line). Addition of HSA to bilirubin solution shifted the λ_{max} to 460 nm (red shift) and the absorbance increased significantly (Fig. 2.7B solid line). A significant red shift and increase in absorbance were indicative of the binding of bilirubin to HSA (Khan et al., 2002). The absorption spectra of bilirubin and HSA-AuNC are qualitatively similar, with a λ_{max} at 450 nm (Fig. 2.7D solid line). The increase in absorbance at λ_{max} was, however, lesser in HSA-AuNC- bilirubin complex as compared to HSA-bilirubin complex. These differences in the absorption characteristics can be ascribed to the differences in the binding affinity as well as the conformation of bilirubin binding site in the HSA and HSA-AuNC as described elsewhere.

In solution, bilirubin adopts a ridge-tile structure existing as two isoenergetic M (left handed) and P (right handed) helical conformers where the angle between two dypyrrione groups is about 100^0, which is stabilized by the presence of intramolecular hydrogen bonds. Bilirubin easily racemizes to an optically inactive state in an isotropic solution. However, interactions with appropriate chiral matrices known to support chiral resolution of compounds. Receimic bilirubin, when subjected to such matrix exhibits optical activity by one of the fractions. Typically for HSA- bilirubin complex, two bands of opposite signs are observed in CD. Such a bisignate nature of the CD spectra of HSA- bilirubin complex has been described by the exciton mechanism (i.e. exciton coupling) (Lightner, 2013; Zsila, 2011). Fig. 2.7A and 2.7C represent the induced circular dichroic spectra of bilirubin in presence HSA and HSA-AuNC. It is interesting to note that both CD spectra of HSA and HSA-AuNC with bilirubin show bisignate characteristics, indicating the formation of the

ridge tile conformation of the bound bilirubin with both the proteins. For HSA and bilirubin, the appearance of negative peak around 410 nm and positive peak around 455 nm imply that P-form bilirubin binds to primary binding site in the HSA protein matrix which corroborates to the previous reports (Minomo et al., 2011; Peterson et al., 2000). For HSA-AuNC and bilirubin interaction, the CD spectrum resumes similar bisignate form with negative peak around 420 nm and positive peak around 475 nm which indicates that HSA-AuNC binds to P-form of bilirubin. However, the red shift in the peak position with decrease in intensities implies a change in the binding site for bilirubin in HSA-AuNC. Similar changes in the induced CD peaks and absorption maxima (λ_{max}) upon bilirubin complexation with secondary binding site of HSA were previously reported (Goncharova et al., 2013; Orlov et al., 2014).

2.4. Conclusions

Gold nanoclusters were synthesized successfully in the HSA protein matrix following a simple microwave-based technique. The nanoclusters had exhibited bright red fluorescent at 640 nm at an excitation of 380 nm. The TEM and MALDI studies revealed that the *in-situ* formed nanocluster had a size of ~ 2.5 nm comprising of Au_{18} atoms. Zeta potential studies showed that the formation of nanoclusters increases the surface charge density of the conjugate that resulted in the shifting *pI* value of the native HSA after the conjugation. The binding constant for HSA-AuNC and bilirubin interaction was found to be $0.55x10^6$ L $mole^{-1}$. The formation of nanocluster within the protein matrix causes a change in the secondary structure of the protein. The bilirubin is attached to the secondary binding site at HSA and adopts P-conformation following its complexation with HSA-AuNC.

Figures

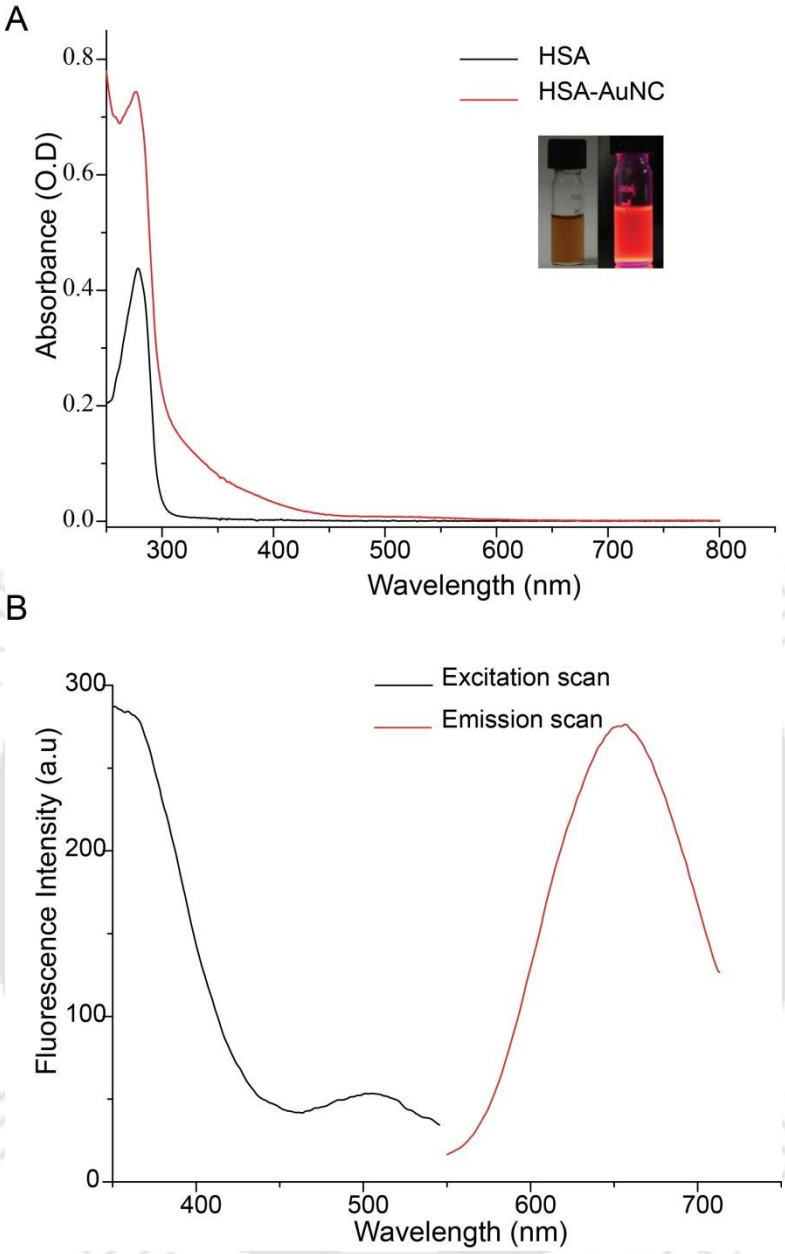

Fig. 2.1: A) UV–visible absorption spectra of the HSA-AuNC and HSA. Inset: photographs under visible light (left) and ultraviolet light (right) of the HSA-AuNC solution. B) Fluorescence excitation (left) and emission spectra (right) of HSA-AuNC.

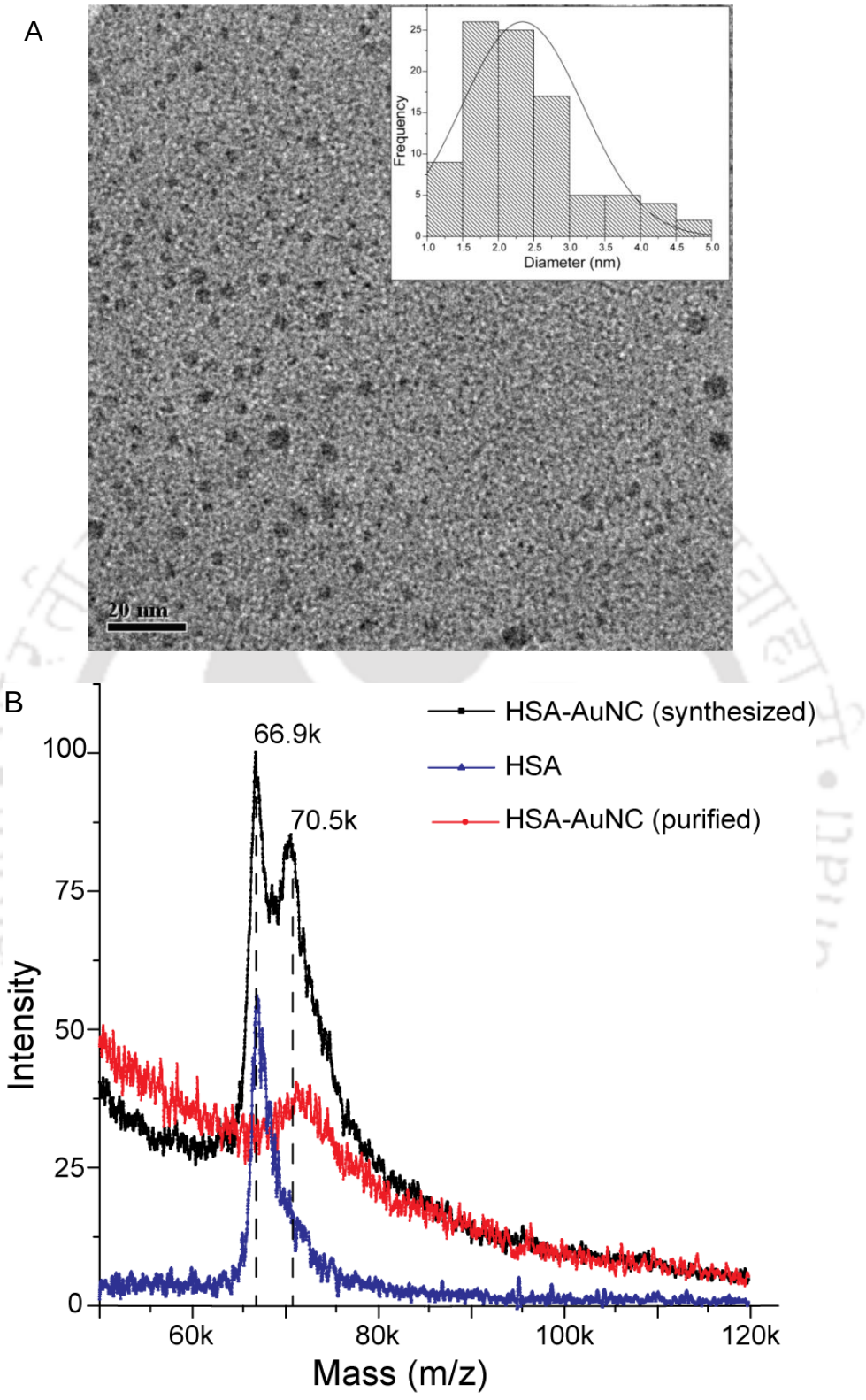

Fig. 2.2: A) TEM images of HSA-AuNC (Inset: size distribution histogram). B)) MALDI-MS spectra of HSA (blue trace), HSA-AuNC (black trace) and HSA-AuNC purified (red trace).

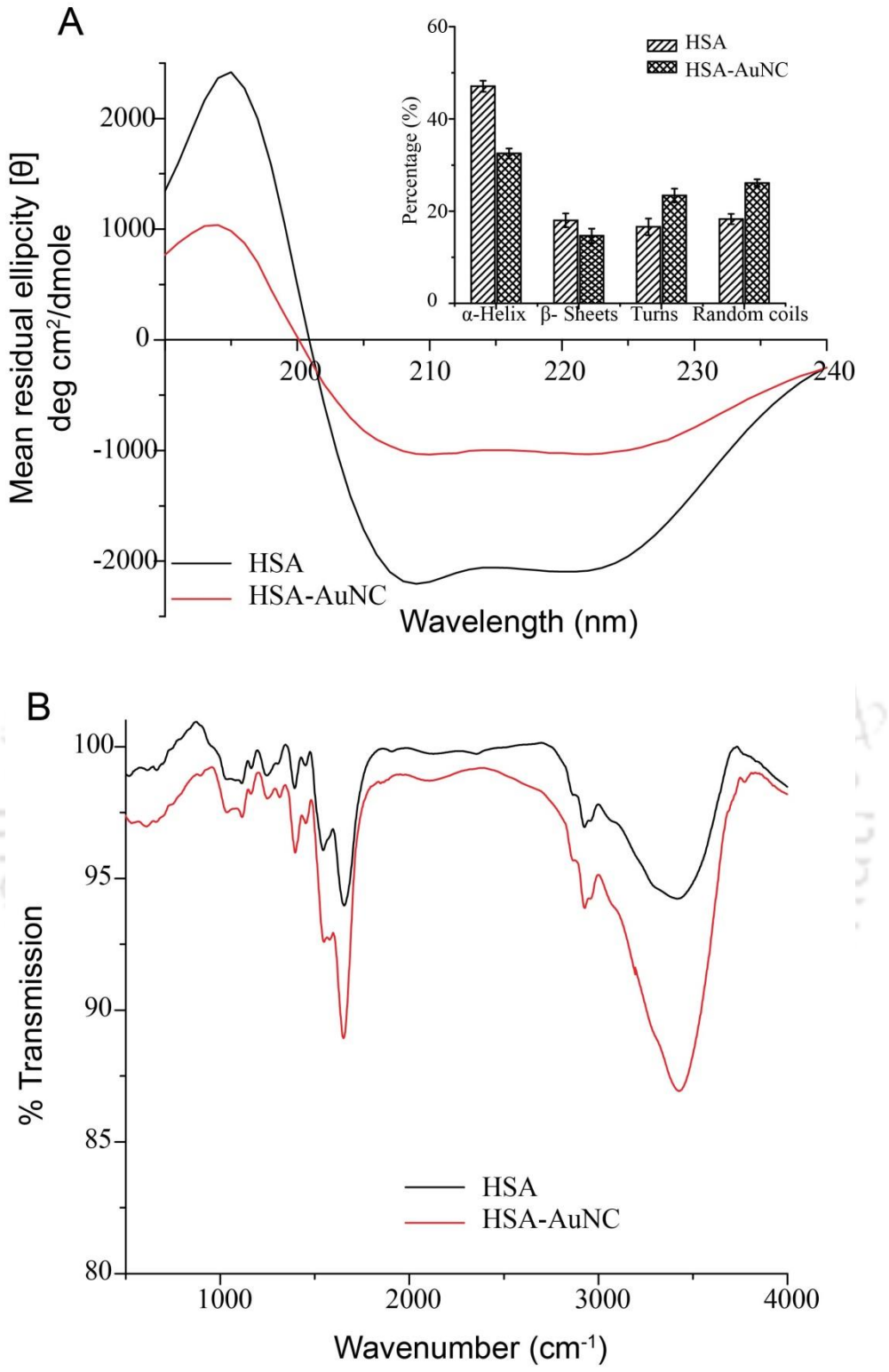

Fig. 2.3: (A) CD spectra of HSA and HSA-AuNC in 50 mM PBS buffer, pH 7.5. Inset showing the percentage of secondary structure motifs of the proteins HSA and HSA-AuNC. B) FTIR spectra of HSA and HSA-AuNC.

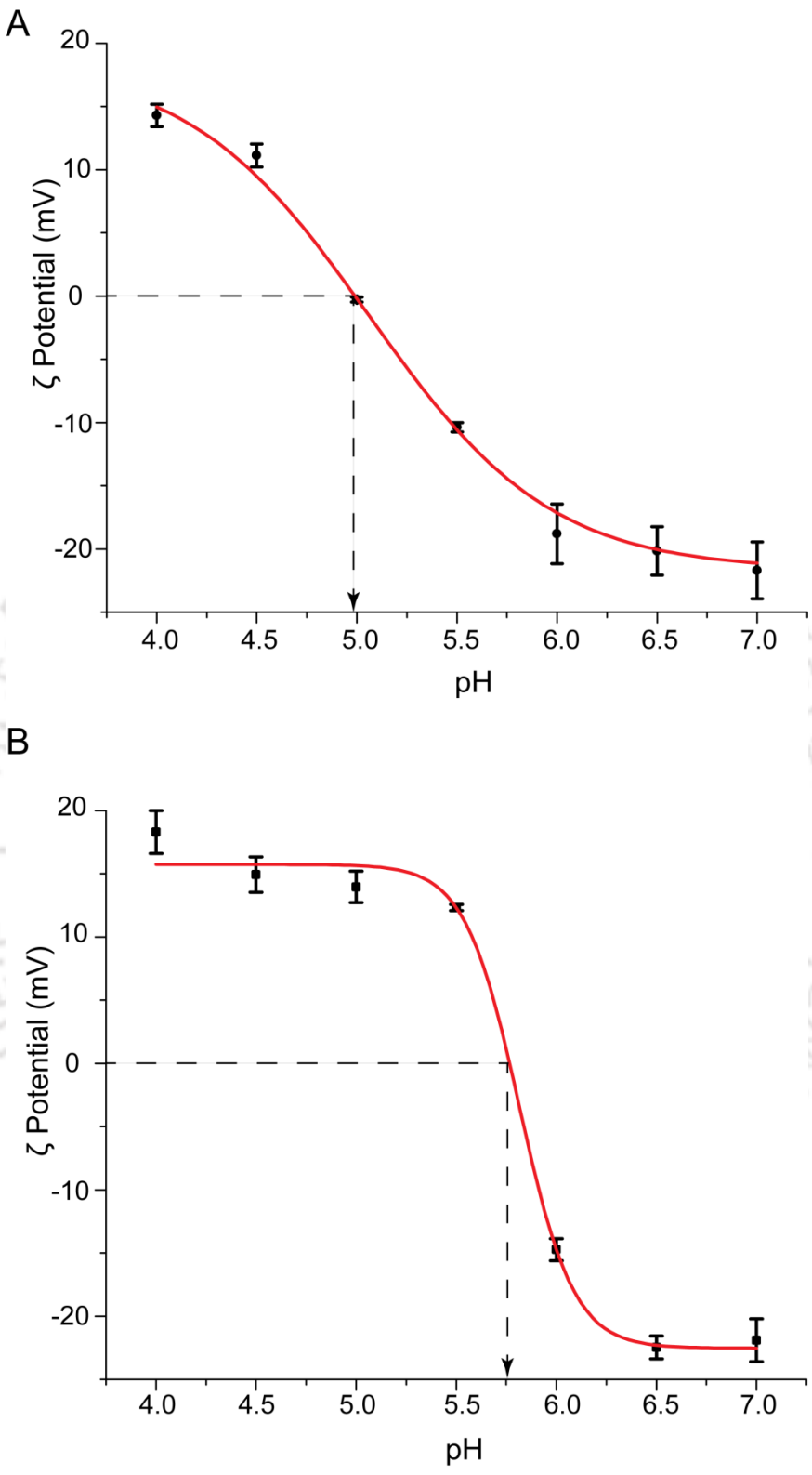

Fig. 2.4: Zeta potential vs. pH of HSA (A) and HSA-AuNC (B). The different pH buffers each at a concentration of 50 mM were sodium acetate (pH 4.0 to 5.5), potassium phosphate (pH 6.0 to 7.0).

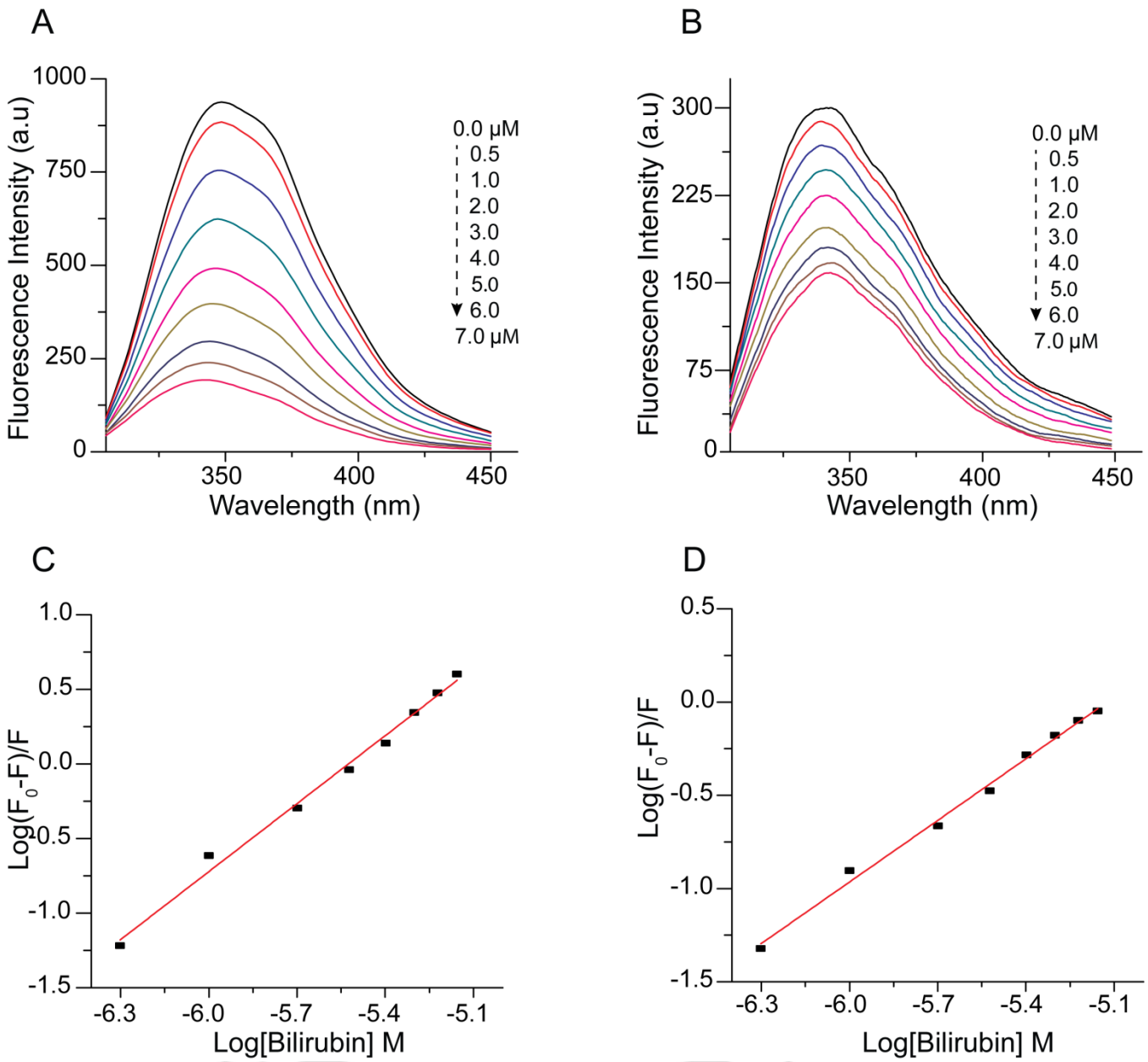

Fig. 2.5: Tryptophan fluorescence emission spectra of HSA (A) and HSA-AuNC (B) when excited with 295 nm in the presence of varying concentration of bilirubin (0 to 7 μM). The plot of Log (F_0-F)/F vs. log (bilirubin) for HSA (C) and HSA-AuNC (D).

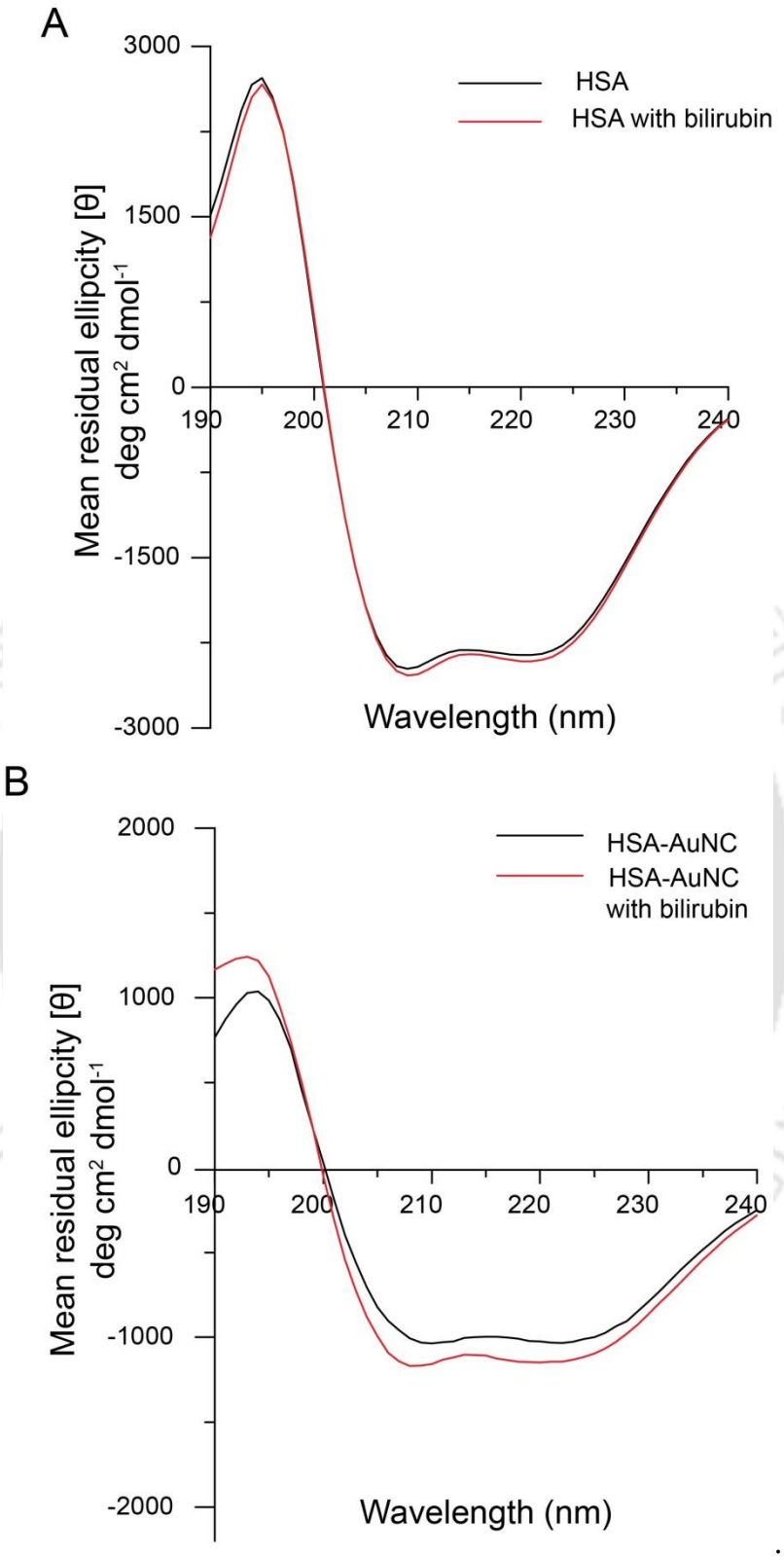

Fig. 2.6: Far-UV CD spectra of HSA (A) and HSA-AuNC (B) in presence and absence of bilirubin.

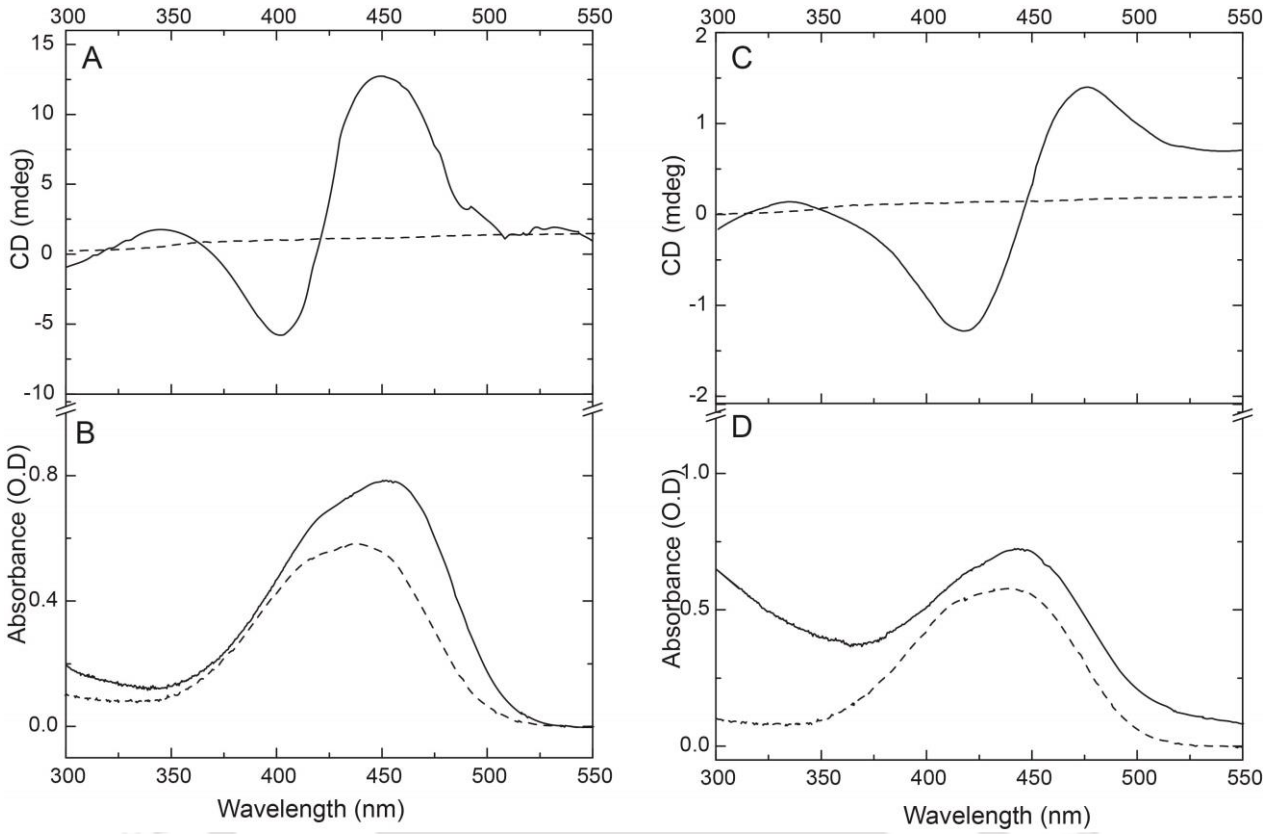

Fig. 2.7: Induced visible range CD (A) and UV–vis absorption spectra (B) of bilirubin (dotted line) and HSA- bilirubin (1:1) (Solid line). Induced visible range CD (C) and UV–vis absorption spectra (D) of bilirubin (dotted line) and HSA-AuNC- bilirubin (1:1) (Solid line) complex. All studies were carried out in a PBS, pH 7.4. The concentration of HSA, HSA-AuNC, and bilirubin were 12 μM.

Chapter III

HSA-stabilized gold nanocluster as optical probe for detection of bilirubin

CHAPTER III

HSA-stabilized gold nanocluster as optical probe for detection of bilirubin

3.1. Overview

Quantitative detection of free bilirubin has enormous importance in probing hyper bilirubinemic conditions such as, bilirubin encephalopathy. Many analytical methods have been developed for measuring bilirubin in serum sample. These include diazo method with a number of modifications, peroxidase and bilirubin oxidase (BOx) based oxidation methods, fibre optic sensors, fluorometric methods and some separation based methods as described in chapter II. Among the above mentioned methods, diazo method requires to compromise the accuracy as the reaction is pH dependent (Li and Rosenzweig, 1997), while the peroxidase-based method is indirect, complex and requires multiple measurements (Ahlfors, 2000; Huber et al., 2012). During last five years several enzyme-based biosensors for detection of bilirubin using mainly BOx as the biorecognition element in conjunction with various nanomaterials / nanocomposites were reported (Batra et al., 2013; Feng et al., 2013; Kannan

et al., 2011). However, the enzyme-based analytical methods and biosensor devices in general, are known to suffer from the major snags of low stability and high cost. Moreover, the enzyme-based catalytic and electrocatalytic reactions are highly sensitive to changes in physical and chemical environment such as temperature and pH and to chemical inhibitors surrounding them. The stability of BOx is reported to be significantly low as 50 % of its activity was lost within 17 h at 37 °C (Sung et al., 1986) thus, restraining its application in analytical techniques from both technical and commercial perspectives. Hence, there is an urge to explore an alternative non-enzymatic method for rapid and reliable detection of free bilirubin that could help proper diagnosis and risk assessment of bilirubin encephalopathy.

In this chapter a non-enzymatic interference free, reagent-less dual fluorometric and colorimetric bilirubin detection method with high sensitivity has been described. Here we exploit the naturally evolved strong binding affinity between HSA and bilirubin and excellent properties of gold nanocluster formed within HSA protein matrix as discussed in the chapter II for the interference-free detection of free bilirubin. Additionally, the peroxidase-like catalytic property of these HSA stabilized AuNC was observed and the phenomena was utilized for sensitive colorimetric detection of bilirubin in human serum sample. Detailed accounts of the findings are presented in this chapter.

3.2 Experimental Approaches

3.2.1. Reagents and stock solutions

Horse radish peroxidase (HRP), bilirubin and cholesterol were purchased from Sigma-Aldrich (USA). Peroxide (H_2O_2), galactose, glucose, fructose, urea, uric acid, glutathione and all other chemicals were procured from Merck (India). The stock solutions of HSA-AuNC and HRP were freshly prepared in sodium phosphate buffer solution (50 mM, pH 7.4) prior to being used. The stock solution of bilirubin was freshly prepared in 10 mM

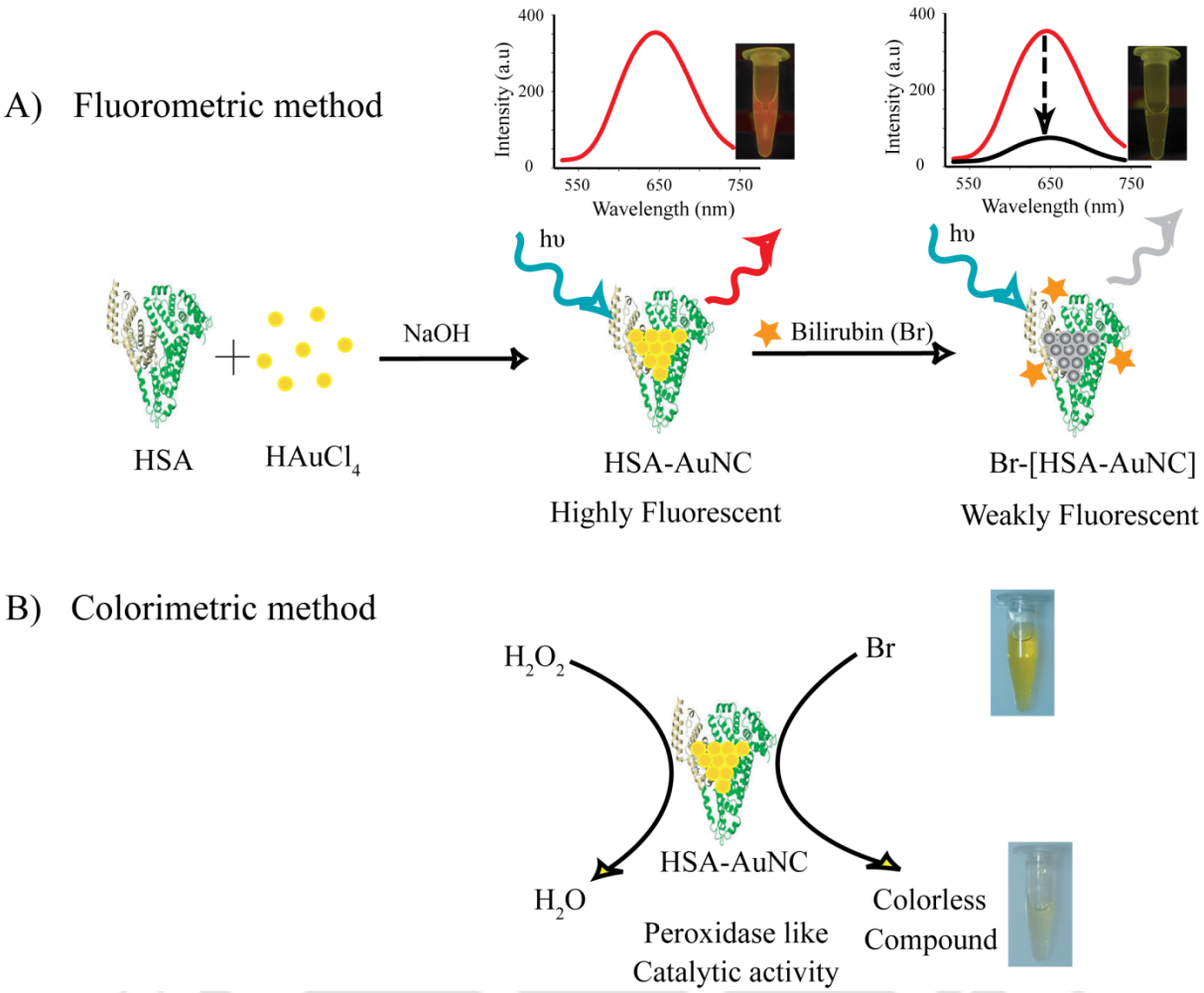

Scheme 3.1: Detection of free bilirubin by using HSA-AuNC as fluorometric probe (A) and as colorimetric probe (B).

NaOH solution and protected from light. All solutions were prepared with deionized water (15 MΩ.cm) from Millipore water purification system (Millipore, USA).

3.2.2. Synthesis and purification of HSA- stabilized nanocluster

The HSA-stabilized nanoclusters were synthesized by microwave-assisted method which is described under the section 2.2.2. Purification of synthesized HSA-AuNC was done by following Zn^{2+} assisted precipitation method as described under the section 2.2.3.

3.2.3. Fluorescence-based detection of bilirubin

Fluorescence spectra were recorded by an LS-55 spectrofluorometer (Perkin-Elmer, USA) equipped with a quartz cuvette (1.0 cm × 1.0 cm) using 5 nm slit widths for excitation and emission and at scan rate of 50 nm min^{-1}. Aliquots (1 mL) containing 50 mM PBS (pH 7.4) with HSA-AuNC (10 μM) as fluorescence probe and different concentration of bilirubin (0-75 μM) were equilibrated at room temperature (RT) and fluorescence intensities were monitored by exciting HSA-AuNC at $\lambda_{380\ nm}$. The fluorescence response towards different bilirubin concentration was independently tested. The linear response curve was generated by plotting $(F_0\text{-}F)/F$ vs. [bilirubin], where F_0 and F are fluorescence intensity at $\lambda_{645\ nm}$ in absence (control) and presence of bilirubin, respectively. The selectivity of the assay was evaluated by measuring the fluorescence intensity of HSA-AuNC in presence of various other relevant substances normally present in blood serum such as albumin, galactose, glucose, fructose, urea, uric acid, glutathione and cholesterol (100 μM each). Plot of relative fluorescence intensity (F_0/F) vs. interfering substances each at a fixed concentration was generated. Effect of solution pH and temperature on the response of HSA-AuNC towards 50 μM bilirubin was studied at PBS (50 mM) with different pH values (6 to 9) and temperatures (25 ºC to 50 ºC). All the above fluorescence measurement was done thrice and the average was considered.

3.2.4. Zeta-potential and time resolved fluorescence studies

Zeta potential of HSA-AuNC with or without bilirubin in PBS buffer (pH 7.4) was determined by using Zetasizer Nano Instrument system (Malvern Instruments Limited, UK). All solutions were filtered through 0.22-micron syringe filter prior to their analysis. The filtered solutions were charged into specially designed folded capillary cell with gold plated copper electrode (Malvern Instruments Limited, UK). Data were acquired at a scattering angle of 90° at 20 °C, repeated 20 times and averaged. The viscosity was set to 1 cP and

resulting autocorrelation function was analyzed by the integrated control software to obtain the zeta potential of the solutions.

Fluorescence lifetime was measured using the time correlated single-photon counting (TCSPC) method on an Edinburgh Instrument Life-Spec II instrument (UK). A 375 nm laser diode was used as the excitation source. The fluorescence decays of HSA-AuNC with and without bilirubin were analyzed by reconvolution method using the FAST software provided by Edinburgh Instruments. The goodness of fit was determined by the reduced chi-square ($\chi 2$) values and weighted residuals which were between the ranges of ± 4.

3.2.5. Catalytic activity of HSA-AuNC against bilirubin

HSA-AuNC (7 mg mL^{-1}) and H_2O_2 (1% v/v) stock solutions were prepared in 50 mM PBS (pH 7.4). Unbound bilirubin was oxidized by the peroxidase-like activity of HSA-AuNC in the presence of peroxide to a colorless compound. The rate constant for oxidation of bilirubin by HSA-AuNC (K_p) was determined by measuring the decrease in A_{440nm} (ΔA) following addition of HSA-AuNC (10 µL) and H_2O_2 (5 µL) to dilute solutions of bilirubin (1, 2 and 3 µM) (volume made up to 1 mL with PBS buffer). The above reaction mixture without HSA-AuNC served as control ($\Delta A_{control}$). K_p was calculated by using the equation (1)

$$K_p = \frac{\Delta A - \Delta A_{control}}{(A_0 \times [HSA-AuNC] \times \Delta t)} \text{ ---------- (1)}$$

where ΔA is the change in absorbance ($A_0 - A_t$) at λ_{440nm}, A_0 and A_t are the initial and final absorbance, [HSA-AuNC] is the concentration of AuNC in µg mL^{-1} and Δt is the difference between final and initial time in min. The steady state free bilirubin (B_f) in solutions was determined by measuring the decrease in A_{440nm} over 1 min in the presence of H_2O_2 and [HSA-AuNC] following the equation (2) (Roca et al., 2006).

$$B_f = \frac{\Delta A}{(\varepsilon_{440} \times K_p \times [HSA-AuNC] \times \Delta t)} \text{ ---------- (2)}$$

where, ε_{440} is the extinction coefficient of bilirubin at $\lambda_{440\ nm}$ (47500 M^{-1} cm^{-1}).

3.2.6. Kinetic studies of HSA-AuNC catalyzed reaction

Steady state kinetic assay was carried out at 1ml of 50 mM PBS buffer (pH7.4) containing 70 ng of HSA-AuNC or 1 ng of HRP in the presence of varying concentration of bilirubin and H_2O_2. To investigate the mechanism, assays were carried out under standard reaction conditions as described above by varying concentrations of bilirubin at a fixed concentration of H_2O_2 or vice versa. The apparent kinetic parameters such as Michaelis-Menten constants were calculated from using Lineweaver–Burk plot

$$1/v = K_m/V_{max} \left(1/[S] + 1/K_m \right) \text{.....(3)}$$

where 'v' is the initial velocity, 'V_{max}' is the maximal reaction velocity, '[S]' is the concentration of substrate and 'K_m' is the Michaelis constant.

3.2.7. Preparation of human serum samples

Fresh human blood samples collected from healthy volunteers were allowed to clot at RT and later centrifuged at 1123 xg for 15 min to isolate the serum. The serum sample (1000 µL) was mixed with acetonitrile (1000 µL) to precipitate proteins and then centrifuged at 1466 xg for 40 min (Chen et al., 2012). The supernatant was collected and acetonitrile was removed under reduced pressure in vacuum evaporator at 60 ºC for 15 min and later stored at 4 ºC for further use. For fluorescence measurements, solutions containing 10 µM of HSA-AuNC and 100 µL of serum sample spiked with different concentrations of bilirubin was used with a final volume made up to 1 mL by using PBS (pH 7.4). The above solution without bilirubin served as control. The fluorescence intensities of this solution were

measured at RT by exciting at $\lambda_{380\ nm}$. The slit widths for both the excitation and the emission were 5 nm. For colorimetric detection, a solution containing serum sample (100 µL) with bilirubin, 10 µL of HSA-AuNC (10 mg mL^{-1}) and 5 µL H_2O_2 (1 %) were used with a final volume made up to 1 mL by using PBS (pH 7.4). The change in absorbance at $\lambda_{440\ nm}$ was recorded for 1 min at RT.

3.3. Results and discussion

3.3.1. Fluorescence response of HSA-AuNC with bilirubin

Fluorescence responses of the HSA-AuNC in the presence of different concentrations of bilirubin were studied by exciting HSA-AuNC at $\lambda_{380\ nm}$ and monitoring fluorescence from $\lambda_{530\ nm}$ to $\lambda_{745\ nm}$. The fluorescence emission at $\lambda_{645\ nm}$ of HSA-AuNC decreased gradually with increasing concentrations of bilirubin (Fig. 3.1A) (Scheme 3.1). The decrease in fluorescence intensity of HSA-AuNC after adding bilirubin was represented as $(F_0 - F)/F$, where F and F_0 are the fluorescence intensities of AuNC with and without bilirubin, respectively. The plot of decrease in fluorescence intensity $(F_0 - F)/F$ vs. the bilirubin concentrations (Fig. 3.1B) was linear over a concentration range of 1 µM to 50 µM with a limit of detection of 248 ± 12 nM at a signal to noise ratio of 3. Moreover, it was found that a lower concentration of HSA-AuNC provides better sensitivity, whereas, higher concentration of it offers a broader detection range. To investigate the specificity of this method for detection of bilirubin, we performed interference study in presence of foreign substances such as albumin, galactose, glucose, fructose, urea, uric acid, glutathione and cholesterol (100 µM each) commonly present in the blood serum. Only bilirubin (50 µM) induces a dramatic decrease in fluorescence intensity, whereas no obvious fluorescence changes were observed in the presence of other compounds (Fig. 3.1C).

Effect of pH and temperature on the fluorescence response of HSA-AuNC against bilirubin was studied at different PBS (50 mM) with pH values ranging from 6 to 9 and at different temperature from 25 ºC to 50 ºC. It was assumed that the maximum possible variation of sample pH may be ± 1.5 from the physiological pH (7.4). The temperature of 50 ^{o}C was taken as the upper limit for the analysis considering the temperature of hot climatic conditions. There was no significant change in the fluorescence response of HSA-AuNC towards bilirubin at the studied pH and the temperature ranges (Fig. 3.2A and 3.2B). The results showed acceptable reproducibility with a relative standard deviation (RSD) of ~ 2.5 % for pH studies and ~ 3.5 % for temperature studies.

The mechanism of the sensitive fluorescence response of HSA-AuNC towards bilirubin was investigated. The excited lifetimes of HSA-AuNC in the absence and presence of bilirubin were found to be 1.881 μs and 1.857 μs, respectively (Fig. 3.3A). The results showed that the lifetime of HSA-AuNC did not change much in presence of bilirubin, indicating that bilirubin is not interacting with the excited state of AuNC and hence no dynamic process is involved. The zeta potential of HSA-AuNC before and after addition of bilirubin was also measured. A significant reduction of the zeta potential from -22.8 mV of free HSA-AuNC to -12.8 mV in the presence of bilirubin at pH 7.4 (Fig. 3.3B and 3.3C) was observed indicating strong electrostatic interaction between HSA-AuNC and bilirubin. This confirmed the formation of non fluorescent bilirubin-HSA-AuNC complex at ground state. The results further confirmed that the fluorescence quenching obeyed a simple static quenching mechanism which is accorded with the fact that the minor structural changes in the HSA-AuNC lead to the quenching of their fluorescence (Valeur, 2001).

3.3.2. Catalytic activity of HSA-AuNC

The peroxidase-based oxidation is the most widely used method to determine free bilirubin (Roca et al., 2006). It has been demonstrated that the BSA-stabilized AuNC exhibit highly intrinsic peroxidase-like activity (Wang et al., 2015, 2011). Here, we tested the possibility of using HSA-AuNC to oxidize free bilirubin by taking the advantage of its peroxidase-like activity (Scheme 3.1). As shown in Fig. 3.4A unbound bilirubin is oxidized to mostly colorless compounds by peroxide (H_2O_2) in the presence of HSA-AuNC with first-order kinetics; while HSA bound bilirubin i.e, bilirubin-HSA (1:10) is prevented from oxidation. So HSA-AuNC can be used instead of enzyme peroxidase to measure free bilirubin in the sample because of their ability to oxidize only free bilirubin and their excellent stability. The rate constant ($K_{p)}$ for oxidation of bilirubin by HSA-AuNC was found to be 2.57 ± 0.63 mL μg^{-1} min^{-1}. Free bilirubin in the sample was determined by measuring the decrease in A_{440} over 1 min (ΔA) in the presence of HSA-AuNC and H_2O_2. There is a minor under estimation of free bilirubin content in the sample caused by its pre-adsorption on the HSA-AuNC due to their inherent high binding affinity thus preventing the oxidation of that fraction of bilirubin. The fraction of bilirubin concentration which binds to HSA-AuNC (100 nM, n = 1.51) in the assay was ~ 150 nM. This additional amount needs to be added to the calculated amount of free bilirubin obtained from the equation 2. The sensitivity of this assay as discerned from the plot of the change in absorbance at λ_{440nm} (Fig. 3.4B) was found to be 0.033 ΔA min^{-1} μM^{-1} of bilirubin. The limit of detection was found to be 200 ± 19 nM. The results demonstrated that the proposed HSA-AuNC based colorimetric method can be suitably employed for the detection of free bilirubin.

3.3.4. Kinetic parameters of HSA-AuNC towards bilirubin oxidation

To investigate the mechanism of the peroxidase activity of the HSA-AuNC, we determined apparent steady-state kinetic parameters for the reaction. As noted from Fig. 3.5A the HSA-AuNC catalyzed reaction was inhibited by high bilirubin concentrations, similar to the peroxidase enzyme-catalyzed reaction. However, within the dynamic range of bilirubin concentrations, the typical Michaelis–Menten plot could be built for both HSA-AuNC (Fig. 3.5A and 3.5B) and HRP (Fig. 3.6A and 3.6B). The data were fitted to the Michaelis–Menten model to obtain the parameters which are shown in Table 3.1. The apparent K_m value of the HSA-AuNC with bilirubin as the substrate is 4.18 ± 0.21 μM which is ~ 7 times lower than that for HRP (Table 3.1), thus supporting the observation that in case of HRP a higher concentration of bilirubin was required to observe a maximal activity. The apparent K_m value of the HSA-AuNC with H_2O_2 as the substrate was higher than HRP.

Table 3.1: Comparison of kinetic parameters of HSA-AuNC and HRP against bilirubin and H_2O_2 as substrate

Reaction System	Substrate	[a]K_m	[a]V_{max}
HSA-AuNC	Bilirubin	4.18 ± 0.21 μM	0.722 μM min^{-1}
	H_2O_2	55.65 ± 1.05 mM	2.01 mM min^{-1}
HRP	Bilirubin	30.28 ± 0.58 μM	10.38 μM min^{-1}
	H_2O_2	11.26 ± 0.32 mM	2.98 mM min^{-1}

[a] The values represent mean ± SD (n = 3) ; K_m is the Michaelis constant; V_{max} is the maximal reaction velocity .

3.3.5. Detection of bilirubin in human serum

The developed assays were applied to the analysis of free bilirubin in human serum samples. A suitable volume of serum solution appropriately spiked with the standard bilirubin solution was taken and the concentrations of bilirubin were measured by the proposed

fluorometric, colorimetric and standard peroxidase methods. The results were summarized in Table 3.2. The proposed methods offered good recoveries and acceptable RSD values as compared to the peroxidase method suggesting acceptable accuracy and reliability of the present methods for bilirubin determination in real samples. The repeatability of the developed assays was analyzed by conducting fifteen different experiments under identical conditions at a fixed bilirubin concentration (10 μM). The results show acceptable repeatability with RSD of 6.3 % and 4.8 % for the fluorometric method and colorimetric method, respectively. These results show that the proposed methods have great potential for quantitative determination of bilirubin in human serum samples.

Table 3.2: Performance evaluation of the proposed fluorometric and colorimetric methods for determination of free bilirubin in serum samples by comparing with standard peroxidase method.

Method	Sample	Spiked amount (μM)	Detected amount [a] (μM)	RSD (%, n=5)[b]	Recovery (%)
Fluorometric	Sample 1	5	4.9±0.3	6.1	98
	Sample 2	10	10.6±0.6	5.6	106
	Sample 3	25	24.8±0.4	1.7	99.2
Colorimetric	Sample 1	5	5.1±0.2	2.9	102.2
	Sample 2	10	9.7±0.3	3.1	97.8
	Sample 3	25	24.5±1.2	4.8	98.9
Peroxidase	Sample 1	5	4.8±0.2	4.1	96.8
	Sample 2	10	10.1±0.6	5.9	101.3
	Sample 3	25	24.7±1.1	4.5	98.8

[a] Value = mean ± S.D. (n=5); [b] RSD = Relative standard deviation.

3.4. Conclusions

In this work we have demonstrated for the first time a highly sensitive fluorometric and a colorimetric method for the selective detection of free bilirubin in human serum using HSA stabilized gold nanoclusters as the detection probe. The fluorescence-based method relies on the fluorescence quenching through static interaction between HSA-AuNC and

bilirubin. This method relies on the natural carrier (HSA) of bilirubin in the blood serum as biorecognition element where bilirubin binds specifically and avidly. Further, the response obtained from the fluorometric method was practically unaltered in a wide pH and temperature ranges, thus, the method offers to analyze samples under considerably compromised physiological conditions. Additionally, in the colorimetric method, since the free bilirubin is oxidized to a colorless compound as a result of the peroxidatic action of HSA-AuNC, the progress of the assay may also be visually monitored. The HSA-AuNC acts as a highly effective receptor, with a higher binding affinity for the substrate bilirubin than HRP.

Figures

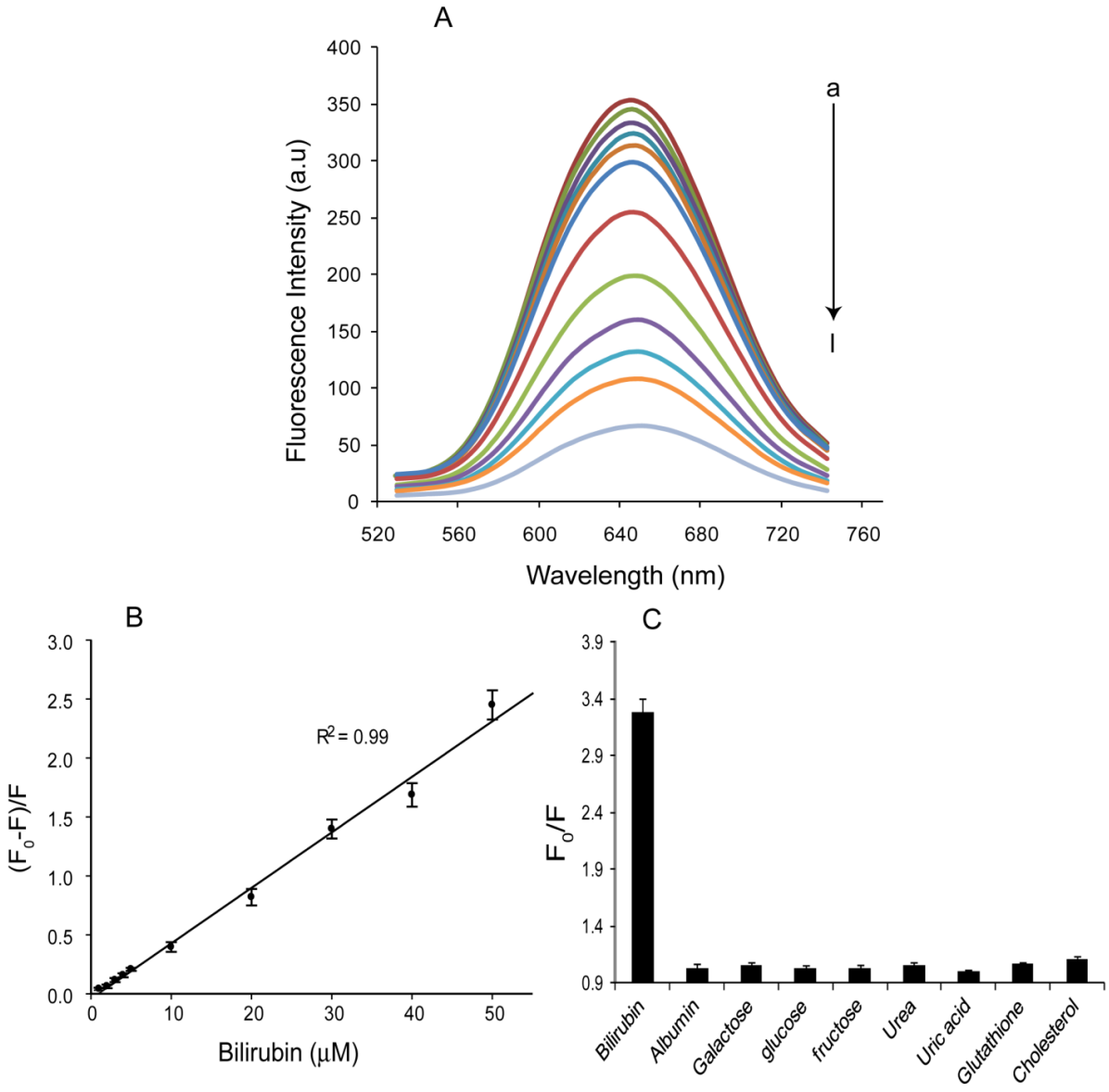

Fig. 3.1: A) Fluorescence emission spectra of HSA–AuNC in the presence of different concentration of bilirubin a) 0 μM, b) 1 μM, c) 2 μM, d) 3 μM, e) 4 μM, f) 5 μM, g) 10 μM, h) 20 μM, i) 30 μM, j) 40 μM. k) 50 μM and l) 75 μM. B) The plot of quenching efficiency $(F_0-F)/F$ at $\lambda_{645\ nm}$ vs. various concentration of bilirubin. C) Influence of various potential interferents (100 μM) and bilirubin (50 μM) on relative fluorescence (F_0/F) of HSA-AuNC.

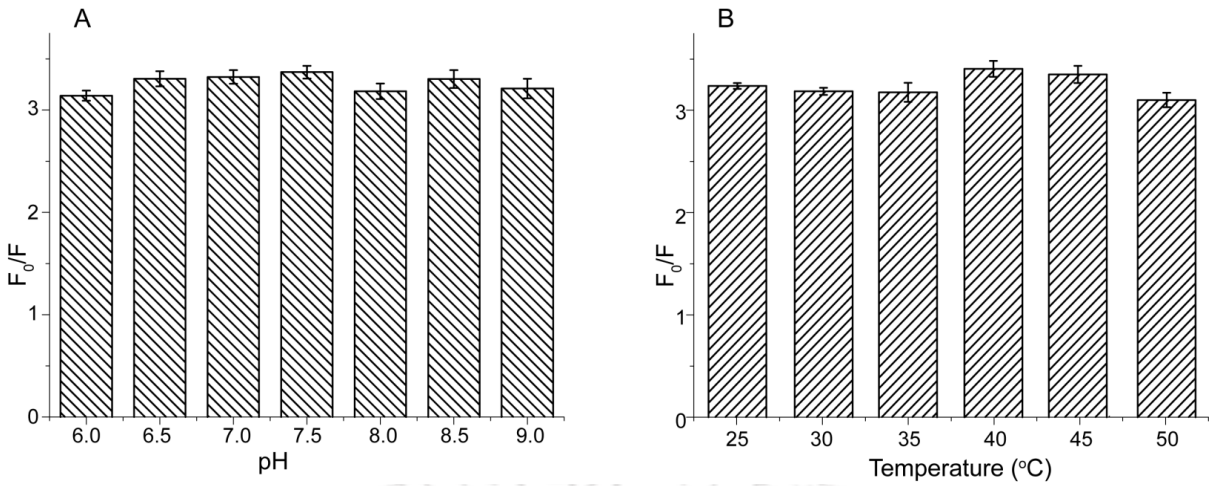

Fig. 3.2: Relative fluorescence (F_0/F) of HSA-AuNC in presence of bilirubin (50 µM) at various pH conditions (A) and temperature (B).

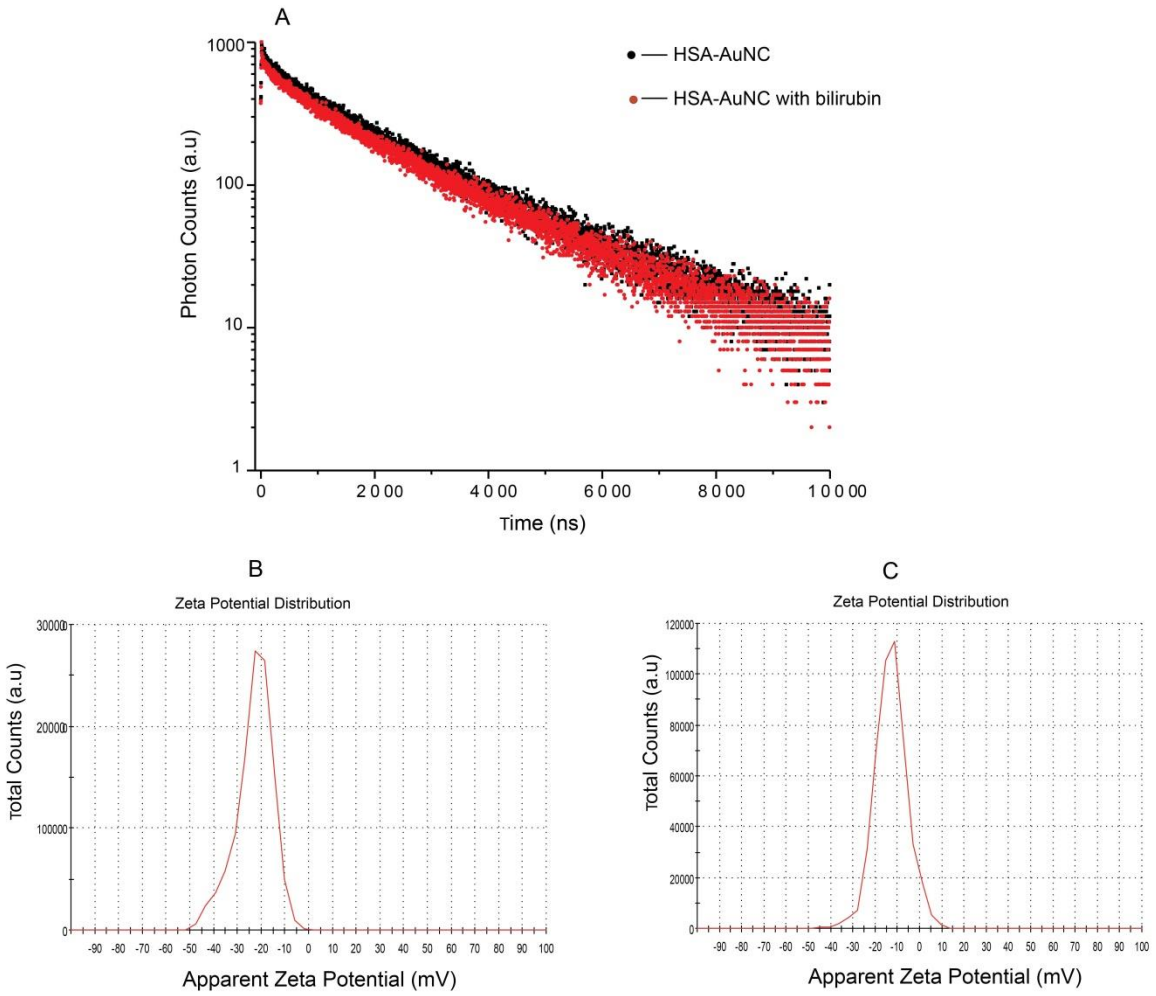

Fig. 3.3: A) Fluorescence decay of the HSA-AuNC as a function of time in the absence (black) and presence (red) bilirubin. Zeta potential distribution of HSA-AuNC at pH 7.4, in the absence (B) and presence (C) of bilirubin.

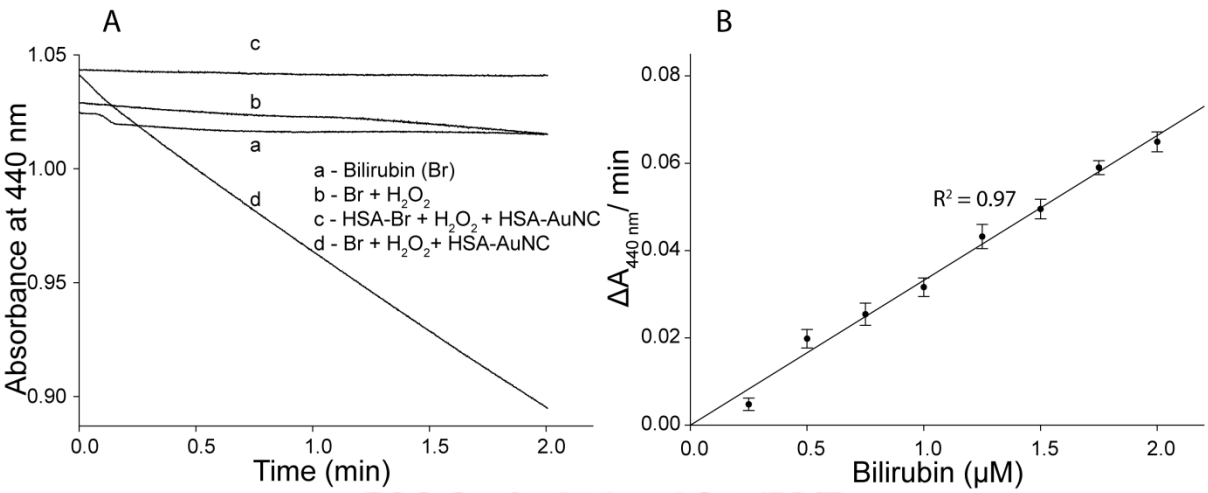

Fig. 3.4: A) Time-dependent absorbance changes at $\lambda_{440\ nm}$ of bilirubin (Br) in different reaction systems. B) The plot of change in absorbance per min vs. bilirubin concentration. The experiment was repeated thrice and the average values were shown. Error bar indicates the SD.

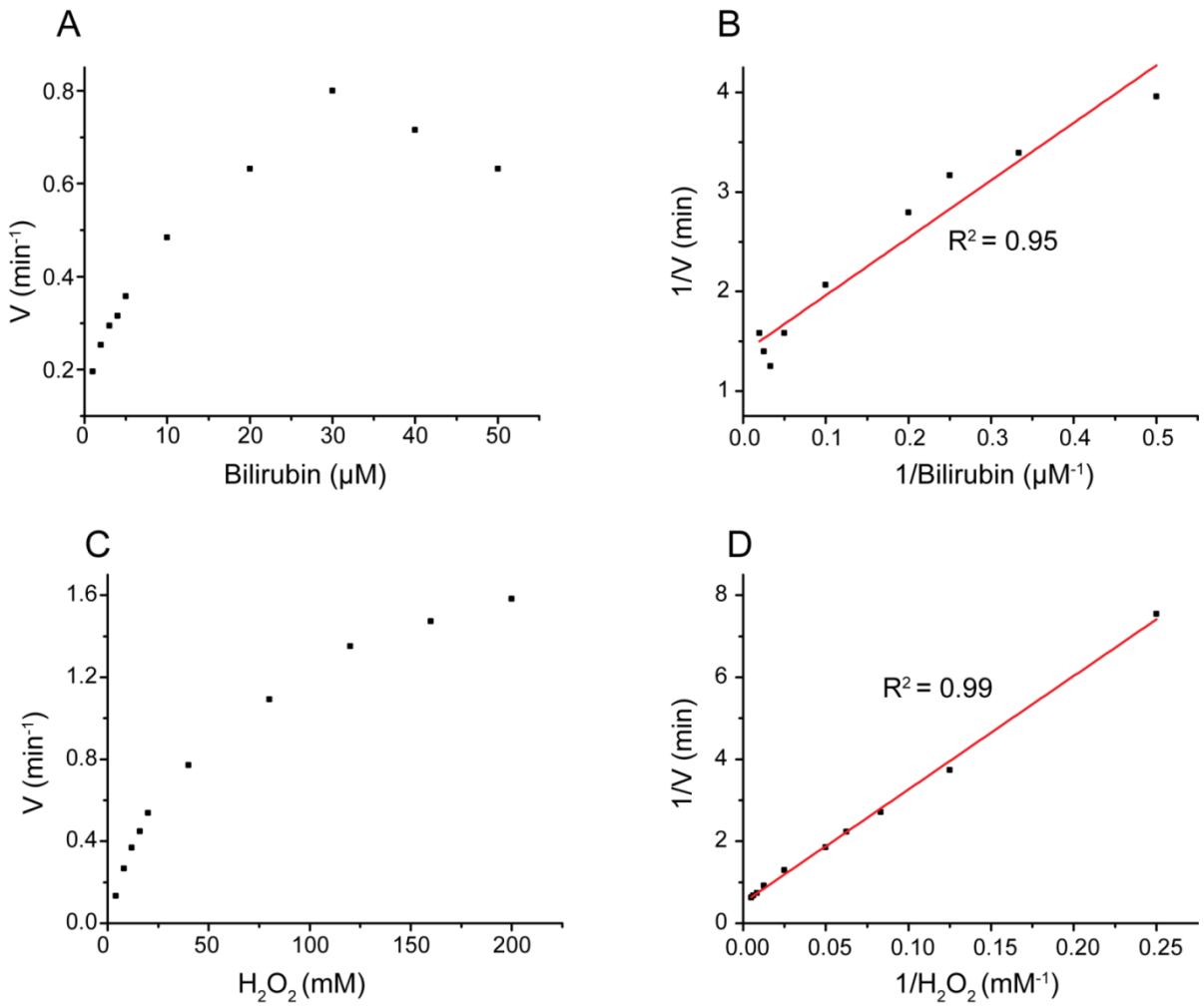

Fig. 3.5: Initial reaction velocity of the reactions measured using 50 nM of HSA-AuNC at varying concentration of bilirubin (A) and H_2O_2 (C) while concentration of the other substrate was kept constant. (B) and (D) are double reciprocal plots corresponding to plot (A) and (C).

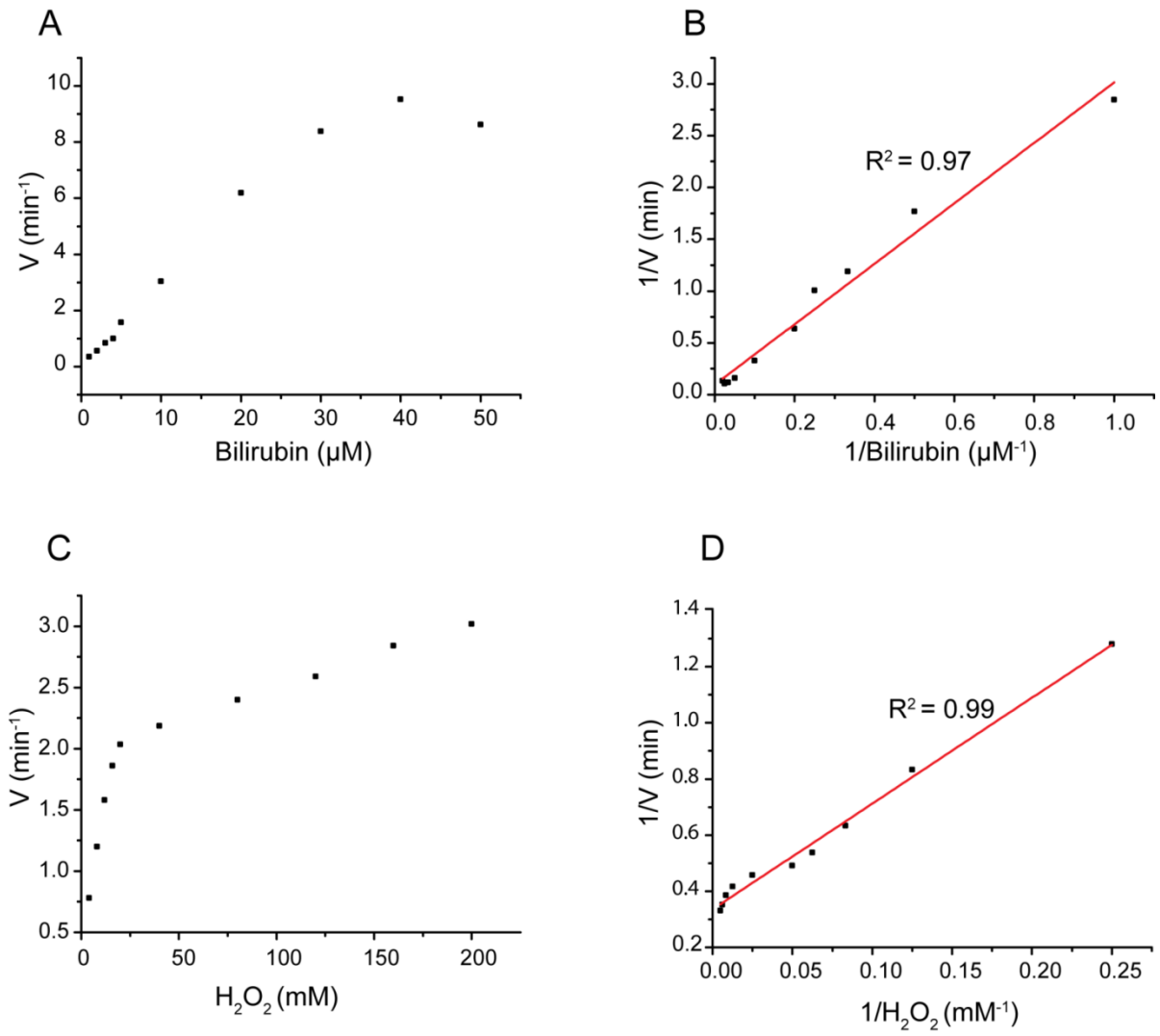

Fig. 3.6: Initial reaction velocity of the reactions measured using 0.5 ng of HRP at varying concentration of bilirubin (A) and H_2O_2 (C) while concentration of the other substrate was kept constant. (B) and (D) are double reciprocal plots corresponding to plot (A) and (C).

Chapter IV

HSA-stabilized gold nanocluster as electrochemical probe for detection of bilirubin

CHAPTER IV

HSA-stabilized gold nanocluster as electrochemical probe for detection of bilirubin

4.1. Overview

In the previous chapter, the concept of interaction of free bilirubin with its natural carrier HSA and the distinctive electronic nature of the nanoclusters were successfully implemented for detecting bilirubin using HSA-AuNC as optical detection probe in a laboratory setup. We would like to explore here the electrochemical properties of HSA-AuNC to understand the feasibility of using these nano-conjugates for quantitative detection of bilirubin. Notably, the electrochemical transducer-based platforms have been widely exploited for developing commercial biosensors due to their high sensitivity, simplicity and scope of reducing their sizes for portability and low-cost production (Ronkainen et al., 2010). In a few studies, the AuNCs were utilized in electrochemical sensing of ascorbic acid, uric acid, dopamine (Kumar et al., 2011) and glucose (Kwak et al., 2014). However, the electrochemical properties of AuNCs for detection of bilirubin are not exploited yet. Here, we

used HSA stabilized AuNCs as biorecognition element for free bilirubin in an amperometric transducer based biosensor platform. The HSA-AuNC was covalently immobilized over Indium tin oxide (ITO) electrodes. The electrochemical investigation showed interesting behavior of the HSA-AuNC on the electrode surface for redox conversion of bilirubin and the phenomena was exploited for the sensitive detection of free bilirubin in serum samples.

4.2. Experimental Approaches

4.2.1. Reagents

Bilirubin, Human serum albumin (HSA), Indium tin oxide coated glass plates (ITO) (200~250 Ω cm^{-2}), (3-Aminopropyl)triethoxysilane (APTES), *N*-(3-Dimethylaminopropyl)-*N*′-ethylcarbodiimide hydrochloride (EDC), N-Hydroxysuccinimide (NHS) and auryl chloride ($HAuCl_4$) were obtained from Sigma-Aldrich (USA). All other reagents were of analytical reagent grade and used without further purification. Nanopure water (18.2 MΩ: Millipore Co., USA) was used throughout the experiment.

4.2.2. Synthesis and purification of HSA-stabilized nanocluster

The HSA-stabilized nanoclusters were synthesized by microwave-assisted method as described under the section 2.2.2. Purification of synthesized HSA-AuNC was done by following Zn^{2+} assisted precipitation method as described under the section 2.2.3.

4.2.3. Preparation of HSA-AuNC modified ITO electrode

The ITO plates were cut into 1 cm x 2.54 cm rectangular pieces and cleaned with acetone, ethanol, and a copious amount of deionized water. The cleaned plates were immersed in a solution of H_2O_2 / NH_4OH / H_2O (1:1:5, v/v) for 30 min at 80 °C for hydrolysis to obtain a uniform distribution of OH groups over the ITO surface. Then, they

were rinsed thoroughly with deionized water and dried. The hydroxylated ITO plates were immersed in a 1 % (v/v) solution of APTES in toluene overnight at room temperature (RT) for silanization (Arya et al., 2007). Following the coupling reaction, the electrodes were rinsed with toluene and water to remove the physically absorbed silane from the surface. The modified electrodes were then dried under a stream of nitrogen. A total of 10 µl of HSA-AuNC (5 mg ml^{-1} in PBS, pH 7.4) was diluted to 50 µl with distilled water containing 0.2 M EDC and 0.05 M NHS (Saxena et al., 2011). Ten microliters of the above solution was poured onto the silanized ITO plate and dried overnight at RT to allow covalent attachment of the HSA-AuNC to the modified ITO plates (Scheme 4.1). The electrodes were washed thoroughly with PBS (pH 7.4) containing 0.9 % NaCl and 0.05 % Tween 20 to remove the unbound molecules. The control electrodes were synthesized with HSA using a similar procedure. For the reproducibility studies, five different HSA-AuNC-modified ITO electrodes were prepared using this mentioned procedure. To study the lifetime and repeatability, the bioelectrode was washed with 0.1 M NaOH after each of the successive measurements.

4.2.4. Characterization of modified electrodes

The fabricated electrodes were characterized by atomic force microscopy (AFM), cyclic voltammetry (CV), electrochemical impedance spectroscopy (EIS) and Energy-dispersive X-ray spectroscopy (EDX). AFM was performed using an ambient air scanning probe microscope (Agilent Technologies 5500, USA), and the images were recorded in a non-contact mode using Picoscan 5 software. CV and EIS were performed with an Autolab PGSTAT 1212 (Eco Chemie, Netherlands). A three-electrode system was used, with a platinum rod as the counter electrode, Ag/AgCl (saturated KCl) as the reference electrode, and ITO or modified ITO as the working electrode. The CV data were acquired using the

potential window of -0.5 V to 0.75 V at 50 mV sec^{-1}. The EIS measurements were performed in a background solution of 5 mM $K_3Fe(CN)_6$ / $K_4Fe(CN)_6$ (1:1) and 0.1 M KCl in PBS within the frequency range of 0.05 Hz to 10 kHz. The amplitude of the alternate voltage was 5 mV. All of the electrochemical experiments were performed in triplicate.

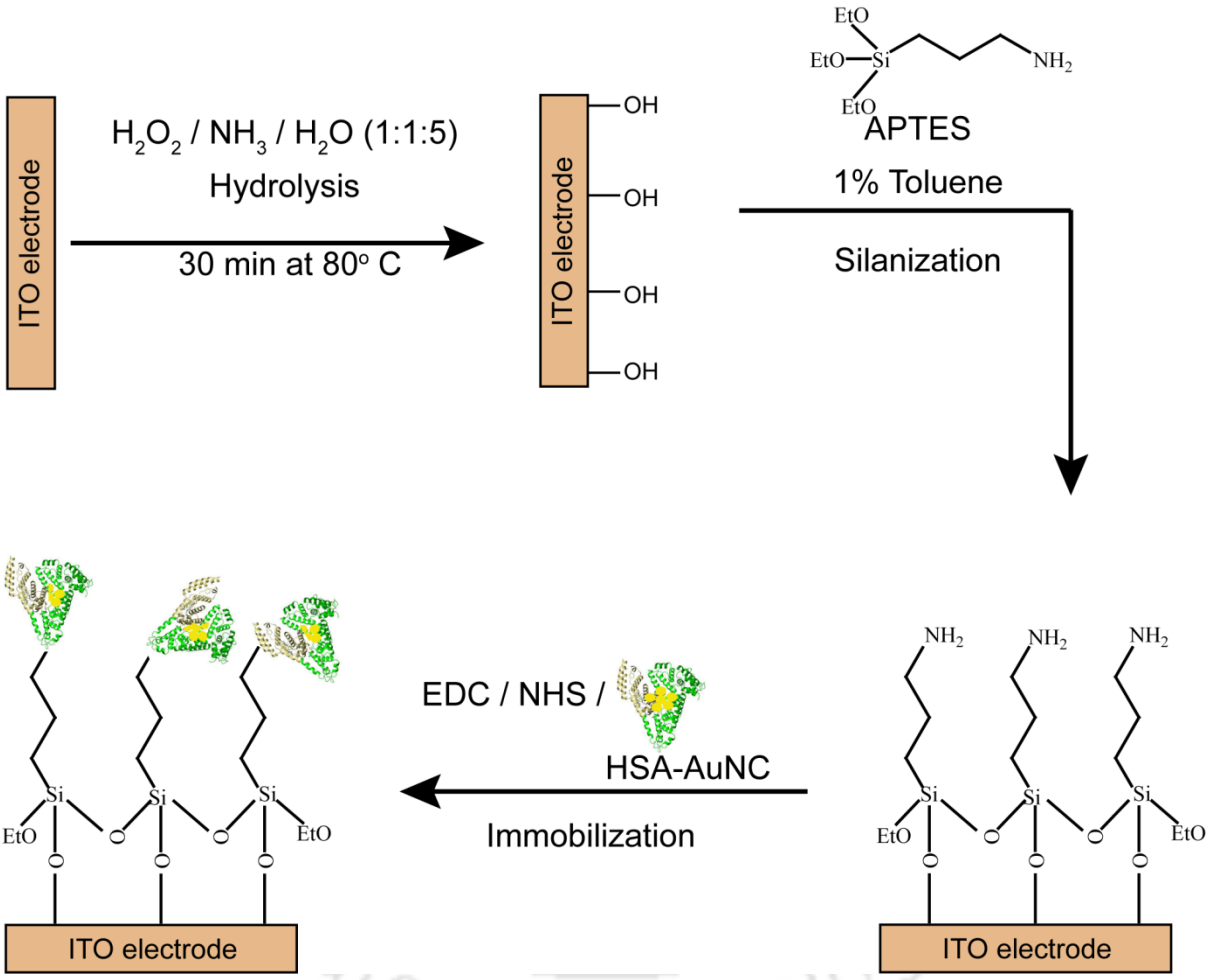

Scheme 4.1: Schematic representation on the covalent immobilization of HSA-AuNC on the ITO plates.

4.2.5. Docking studies

The initial coordinates for HSA were obtained from the protein databank (PDB entry 2VUE). The coordinates for $Au_{18}NC$ were obtained from the Cambridge cluster

database (Elliott et al., 2009). The HSA protein was docked with Au_{18}NC using the online PatchDock software. It predicts the possible binding pocket for Au_{18}NC in HSA through a blind docking approach. The results obtained by the docking study were further refined with FireDock tools (Mudedla et al., 2015). The five best docked structures were selected for further analysis based on their scores. The molecular visualization program PyMOL (DeLano, 2002) was used to view the 3D structures and measure the inter molecular distance between the nanocluster cores of the different models and bilirubin in the HSA-bound bilirubin structure.

4.3. Result and discussion

4.3.1 Surface characterization of modified electrodes

AFM images were recorded to study the morphological changes of the electrode surface obtained after each major step of electrode fabrication. The AFM images indicate that the bare ITO surface (Fig. 4.1A) was relatively smooth, whereas the APTES/ITO electrode shows homogeneously distributed APTES molecules with an increased roughness height (Fig. 4.1B). Once the HSA-AuNC were covalently immobilized onto APTES/ITO, the electrode surface transformed into a heterogeneous globular-like structure (Fig. 4.1C), with an increase in thickness, indicating successful immobilization of the latter onto APTES/ITO. The RMS roughness values of bare ITO, APTES-ITO, and HSA-AuNC-modified ITO were 2.16 ± 0.98, 11.54 ± 3.66 and 46.53 ± 8.15, respectively (Fig. 4.2). The ITO (Fig.4.1D), APTES-modified ITO electrode (Fig. 4.1E) and HSA-AuNC-modified APTES/ITO (Fig.4.1F) had extra elements, namely, Si, O and N for the APTES-modified electrode and Si, O, N and Au for the HSA-AuNC-modified electrode, confirming that the layers shown in scheme 4.1 are formed.

4.3.2 Electrochemical characterization of modified electrodes

The EIS spectra, presented as Nyquist plots, were employed to examine the charge transfer process occurring at the electrode interface (Fig. 4.3A). The electron-transfer resistance (R_{ct}) estimated from the diameters of the semi-circle were 321.5 ± 9.4 Ω for bare ITO and 37.6 ± 1.3 Ω for APTES-modified ITO. The decrease in R_{ct} is attributed to the positive charges formed on the electrode surface due to the polarization of the terminal NH_2 group in the APTES layer, which facilitates the transport of negatively charged $FeCN_6^{(-3/-4)}$ to the electrode. Moreover, at pH 7.4, the amino groups in the APTES moiety [(pK_a ~10.6 (Bini et al., 2012)] acquire positive charge, thus assisting in the diffusion of the negatively charged redox probe. A similar decrease in charge transfer resistance after the formation of the APTES layer has been reported (Canbaz and Sezgintürk, 2014; Şimşek et al., 2014). The R_{ct} of the HSA- and HSA-AuNC-modified APTES/ITO plates was increased compared with that of APTES/ITO, indicating the insulating role of the protein in charge transfer. However, the R_{ct} value of HSA-AuNC/APTES/ITO (85.2 ± 2.1 Ω) was less than that of HSA/APTES/ITO (115.2 ± 3.1 Ω), indicating the positive role of the AuNCs in the ability of the HSA protein to facilitate the charge transfer on the electrode interface. The R_{ct} of the HSA-AuNC-modified ITO in the presence of bilirubin (5 µM) increased from 85.2 ± 2.1 Ω to 123.4 ± 3.2 Ω (Fig. 4.4), indicating that the binding of bilirubin to HSA inhibits the diffusion of the redox probes.

The CV spectrum was featureless in the absence of bilirubin (Fig. 4.3B). The ITO electrode (Fig. 4.5B) showed distinct oxidation peaks at + 0.25 V, + 0.37 V and + 0.50 V (vs. Ag/AgCl) in the presence of bilirubin. The absence of a reduction peak in the spectra indicates the irreversible nature of the reactions. The three oxidation peaks were attributed to the sequential oxidation of bilirubin to biliverdin (peak I), biliverdin

to purpurine (peak II), and purpurine to choletelin (peak III) (Scheme 4.2) (Taurino et al., 2014, 2013).

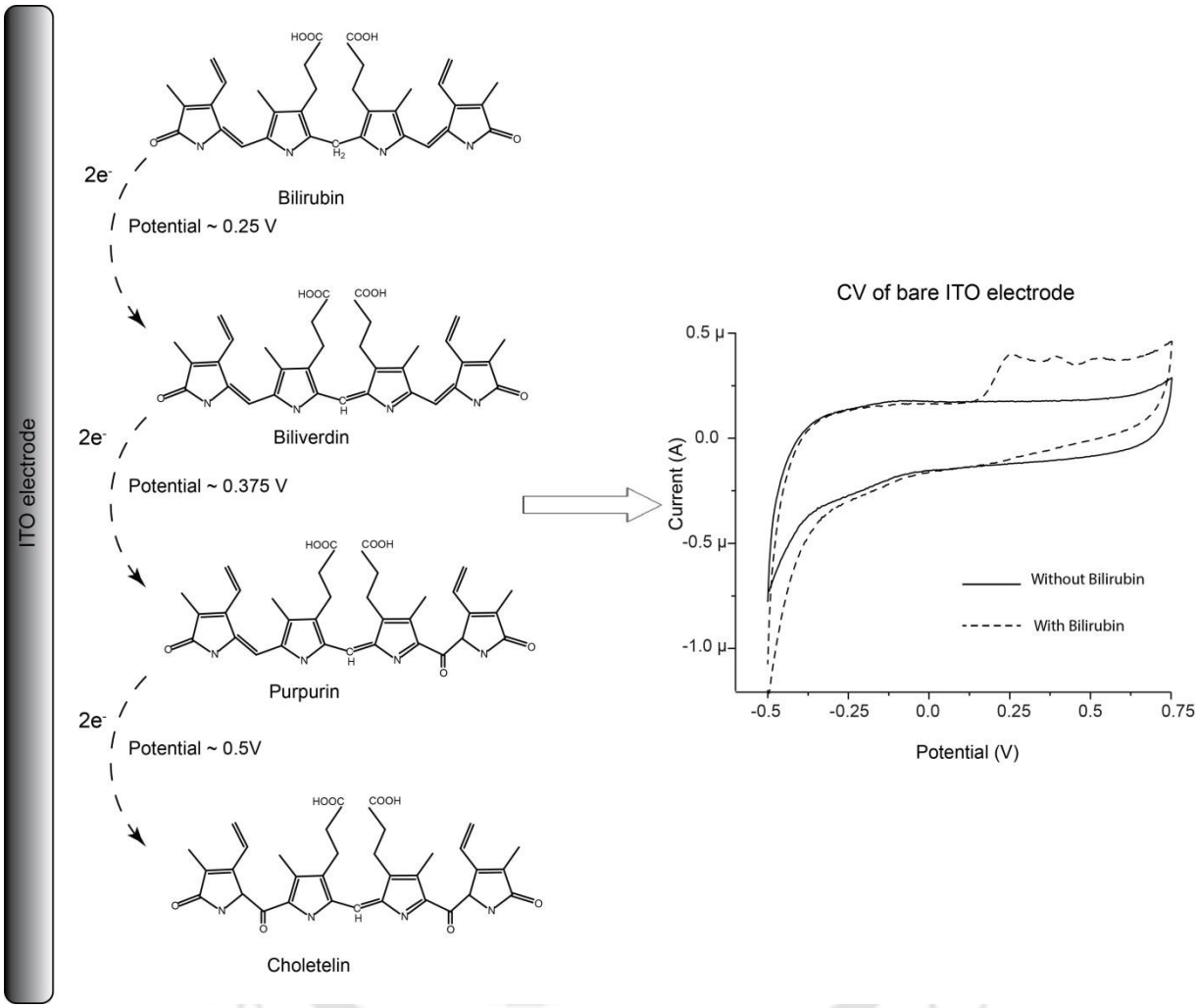

Scheme 4.2: Reaction occurring at the bare ITO electrode in presence of bilirubin.

The positions of the oxidation peaks were slightly different from the reported results which can be attributed to the changes in the experimental conditions, as well as the presence/absence of an additional layer over the electrode. Meanwhile, the HSA-AuNC-immobilized ITO electrode showed a well-defined redox peak, with oxidation at + 0.3 V and reduction at + 0.25 V (vs. Ag/AgCl), instead of the three sequential oxidation peaks. However, the ITO electrode with HSA alone did not

produce any peak in the presence of bilirubin, indicating the insulating behavior of the HSA protein. The results infer that the embedded AuNCs in the protein matrix provide an electronic bridge between the redox functional group of bilirubin and the ITO electrode for electron exchange. Moreover, the appearance of a single pair of redox peaks at the formal potential of + 0.27 V (vs. Ag/AgCl) implies site-specific binding of bilirubin on the HSA surface that only allowed the oxidation of the dipyrromethane moiety to dipyrromethene and its reversion (Scheme 4.3). The electrocatalytic oxidations of the other functional sites in bilirubin are forbidden, probably due to the steric hindrance caused by its specific binding to HSA. The increase in the bilirubin concentration increased both the anodic and cathodic peak currents (Fig. 4.5A). However, the magnitude of the anodic peak current was higher than the cathodic peak current, indicating that the oxidation of bilirubin is more favorable than the reduction of the oxidized product attached to the bioelectrode. Moreover, the magnitude of the bilirubin oxidation peak at + 0.3 V (vs. Ag/AgCl) on bioelectrode was ~ 3.5-fold higher than that of the bare ITO electrode (Fig. 4.5A and 4.5B). The reason for this difference may be attributed to the increase in the electroactive surface area of the electrode after immobilization of HSA-AuNC, as well as the rapid sequestration of the bilirubin substrate onto the bioelectrode surface due to its natural affinity to bind with HSA. This resulted in higher electrocatalytic oxidation of the substrate on the bioelectrode, leading to an increase in peak height compared to the bare ITO electrode. The electrochemical surface area of the ITO and modified ITO electrodes was measured in an electrolyte solution containing 0.1 M KCl and 1 mM K_3FeCN_6. The Randles-Sevcik equation (1) (Bard and Faulkner, 2000), was employed to measure the electrochemical surface area (A) using D, the diffusion coefficient of the K_3FeCN_6 in solution (6.70×10^{-6} cm^2 sec^{-1}), n, the number of electrons (n=1), γ, the scan rate (V

sec^{-1}), and C, the concentration of the probe.

$$I_p = 2.69 \times 10^5 \times A \times D^{1/2} \times n^{3/2} \times \gamma^{1/2} \times C \text{.....(1)}$$

The calculated surface areas of the electrodes were 0.13±0.05 cm^2 and 0.45±0.12 cm^2 for bare ITO and HSA-AuNC-modified ITO, respectively. Thus, the immobilization of HSA-AuNC onto silanized ITO increased the overall electroactive surface area of the electrode, indicating that the 3-D nanocluster-embedded protein was layered on the electrode surface.

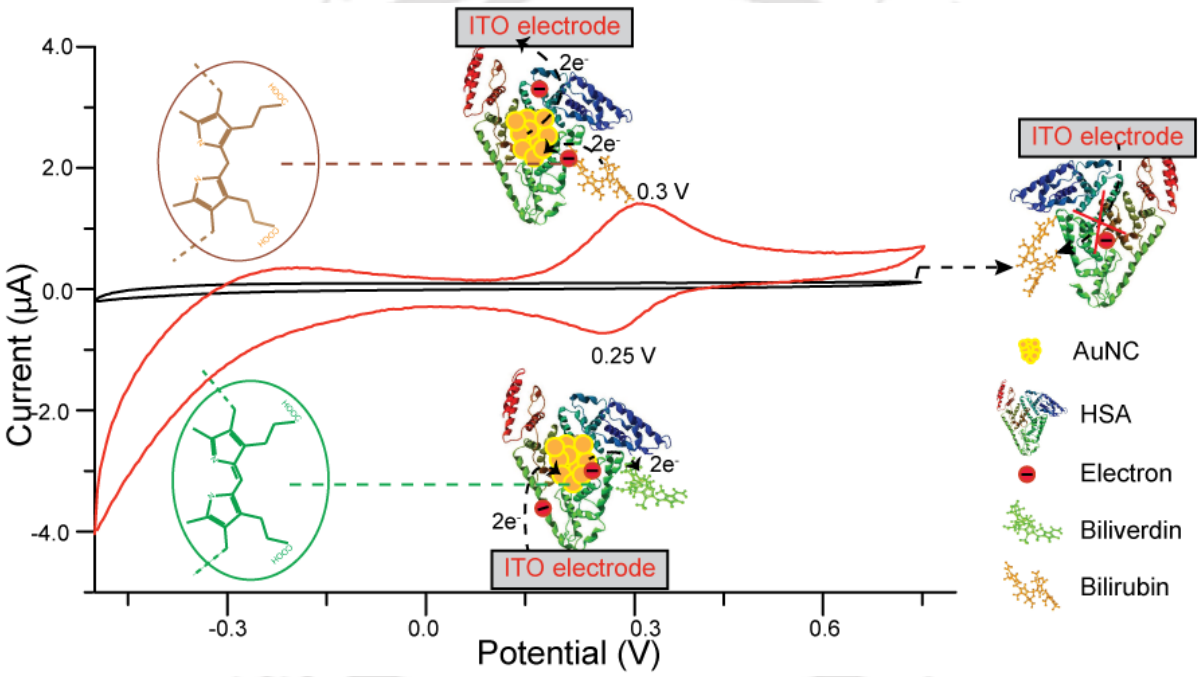

Scheme 4.3: Reaction occurring at the HSA/ HSA-AuNC modified ITO electrode in presence of bilirubin.

The crystallographic data for HSA and the bilirubin complex indicate that bilirubin binds to the L-shaped hydrophobic pocket in subdomain IB of HSA (Zunszain et al., 2008). The superimposed structure of HSA with the Au_{18}-docked models and HSA-bound bilirubin are shown in Fig. 4.6A and 4.6B. The five best

docked Au_{18} nanoclusters were centered on the IA (3 models), IIA (1 model) and IIIA (1 model) domains of HSA. The average distance between C1 of bilirubin and the different models is 19.1 Å, which is shorter than the other two carbon atoms (C2 and C3) (Table 4.1). Thus, the orientation of the C1 carbon atom near the AuNCs might be the reason for the observed site-specific oxidation of bilirubin.

To obtain the kinetic parameters of the modified electrodes with respect to bilirubin oxidation, CV was performed at different scan rates ranging from 0.05 to 0.9 V s^{-1} (Fig. 4.7). Both the anodic (I_{pa}) and cathodic peak current (I_{pc}) vs. scan rate plots (Fig. 4.7B) exhibited linearity with regression coefficients (R^2) of 0.97 and 0.98, respectively, as expected for a surface-confined redox process. The peak to peak separation is approximately 50 mV at scan rates of less than 0.1 V s^{-1}, suggesting a reversible redox reaction and facile charge transfer kinetics over this range of sweep rates. The anodic and the cathodic peak potentials were plotted against the square roots of the scan rates (γ) (Fig. 4.7C) to obtain various electron transfer parameters of the bioelectrode (Das et al., 2014). The charge transfer coefficient (α) was determined using the slope from linear plots of E_{Pa} and E_{Pc} vs. log (γ) using the equation $\alpha = \frac{\delta_{pa}}{\delta_{pa}-\delta_{pc}}$, where δ_{pa} and δ_{pc} are the anodic and the cathodic slopes, respectively, of the linear region of the graph in Fig. 4.7C. From the slopes of δ_{pa}, the number of electrons (n) involved in the reaction can be calculated using the following equation, $\delta_{pa} = \frac{2.3\,RT}{(1-\alpha)nF}$, where R is the universal gas constant, T is the temperature, and F is the Faraday constant. From these equations, α and n were calculated as 0.54 and 2, respectively. The electron transfer rate constant (K_s) was 1.38 s^{-1}, which signifies efficient electron transfer on the electrode surface. Thus, the redox reaction of bilirubin over the HSA-AuNC/APTES-ITO film interface involves two electron

transfer processes, which corroborates a previous report (Cheng et al., 1994). Additionally, the effect of pH on the potential response of the bioelectrode for bilirubin oxidation was studied. The oxidation potential of bilirubin shifted positively as the pH increased from 6.4 to 8.4 (Fig. 4.8). The slope ($\frac{\delta_E}{\delta_{pH}}$) discerned from the data using the anodic peak potentials was 63 mV pH^{-1}. Using the relation, $\frac{\delta_E}{\delta_{pH}} = 0.059\frac{m}{n}$, the number of hydrogen ion (m) involved in the reaction was ~2, which conforms to a previous report of bilirubin oxidation. In this study, the maximum current response was obtained at pH 7.4, which might be because physiological pH favors the HSA-bilirubin interaction (Bae et al., 1995; Slifstein and Ariel, 1977).

Table 4.1: Table showing the distance between different models of nanocluster and bilirubin.

Bilirubin	Au_{18} Nanocluster	Distance (A)	Average distance (A)
C1	Model 1	10.5	
	Model 2	19.5	19.1
	Model 3	26.1	
	Model 4	17.1	
	Model 5	22.3	
C2	Model 1	12.4	
	Model 2	23	20.8
	Model 3	25.9	
	Model 4	19.6	
	Model 5	23.1	
C3	Model 1	14.7	
	Model 2	21.4	20.4
	Model 3	27.1	
	Model 4	14.2	
	Model 5	24.8	

AuNCs in this size range are reported to mediate the electrocatalytic reduction of oxygen and oxidation of CO (Chen and Chen, 2009; Herzing et al., 2008).

However, the featureless CV spectrum (Fig 4.3B, brown trace) with the HSA-AuNC electrode indicated the lack of a catalytic role for the HSA-stabilized AuNCs. It is likely that the surface coordination of the AuNCs is saturated by the amino acid moieties in the HSA protein matrix, thus blocking the diffusion of soluble oxygen to the cluster surface. One of the new findings reported here is the electrical bridging effect of the AuNCs in the protein matrix, as shown in the CV and impedance data. The charge conductive nature of the NCs may be explained by the size-dependent surface potential of the different sizes of AuNCs (Zheng et al., 2007). The potential of the Au_{18} clusters is likely to behave as a Wood-Saxon potential, which is midway between the spherical harmonic potential and Square Well potential, thus supporting both the fluorescence and conducting properties of the cluster. We have already demonstrated the fluorescence properties of these HSA-stabilized AuNC in the previous chapter.

4.3.3. Response of HSA-AuNC/APTES/ITO electrodes to the detection of bilirubin

The response of the bioelectrode was investigated with a fresh loading of 66 ± 7.4 µg cm^{-2} (0.94 nM) of HSA-AuNC on the electrode. The chronoamperometric analysis at 0.3 V (vs. Ag/AgCl*)* (Fig. 4.9) produced a linear response in the bilirubin concentration range of 0.2 µM to 7 µM, yielding a calibration equation I(µA) = (2.09 ± 0.13) + (0.34 ± 0.04) [C] µM (Fig. 4.9 Inset). The sensitivity of 0.34 µA $µM^{-1}$ and limit of detection [LOD = (3*SD of Blank)/(Slope of calibration curve)] of 86.32 nM at S/N 3 were discerned from the analyses. The fouling (yellowing) of the bioelectrode caused by the accumulation of bilirubin could be neutralized by washing the absorbed bilirubin with 0.1 M NaOH for 5 min (Fig. 4.10).

4.3.4. Reproducibility, stability, interference and real sample analysis

The effect of some common interfering substances, such as ascorbic acid, glucose, lactic acid and uric acid, on the measurement of bilirubin levels by HSA-AuNC/APTES/ITO electrode was investigated. For this study, 5 µM of bilirubin was measured in the absence and presence of 5 µM of each of the potential interfering agents. The selectivity coefficient (SC) of the bioelectrode for each of the compounds was calculated using the formula, $SC=I_{c+i}/I_c$, where I_{c+i} and I_c are the amperometric response at 0.3 V (vs. Ag/AgCl**)** for bilirubin (5 µM) in the presence and the absence of the tested compound, respectively. The calculated SC was found to be within ± 5% of the control, indicating that the response of the bioelectrode towards bilirubin is not significantly altered in the presence of these compounds. The results infer that the presence of HSA-AuNC on the electrode provides a selective barrier that allows only bilirubin to bind and oxidize at the electrode surface (Fig. 4.11). The reproducibility of five HSA-AuNC-modified ITO electrodes in detecting bilirubin (5 µM) in 0.1 M PBS (pH7.4) buffer was examined. The RSD of the bioelectrode response was ~ 4 %. The operational stability of the electrode was examined by subjecting a freshly prepared HSA-AuNC-modified ITO electrode to 5 µM bilirubin in PBS buffer (pH 7.4) and assessed its response in 15 successive measurements over a period of 4 h. After each measurement, the bioelectrode was washed with a 0.1 M NaOH solution to remove the adsorbed bilirubin. The results (Fig. 4.12A) indicate that the bioelectrode maintained ~75 % of its initial activity at the end of the 15 measurements. The storage stability of the HSA-AuNC-modified ITO electrode was assessed periodically at 1-day intervals for 7 days. The bioelectrode was washed and stored at 4 °C under dry conditions when not in use. It was observed that the bioelectrode retained ~ 80 % of its activity at the end of the 7 days of storage time (Fig. 4.12B).

The amperometric measurement of bilirubin-spiked serum samples was performed to examine the potential of using the developed sensor to analyze real samples. The blood samples collected from healthy volunteers were processed, and the deproteinized serum sample was prepared according to a previously reported method (Chen et al., 2012). The serum samples were diluted 1:10 in 50 mM PBS, pH 7.4 and spiked with known concentrations of bilirubin, and then, the free bilirubin concentration in the sample was measured at 0.3 V (vs. Ag/AgCl). The results were compared with the standard peroxidase method (Table 4.2). The present method exhibited a recovery of 97-98 %, with comparable RSD values to the standard peroxidase method. Notably, under hyperbilirubinemic conditions, the total serum bilirubin concentrations can reach up to 35 mg dl^{-1} or 0.599 mM. At this concentration, the level of free bilirubin is in the range of 0.3 µM to 2.8 µM (Daood et al., 2009). Thus, the HSA-AuNC-modified electrode can detect free bilirubin within this level in the diseased conditions.

Table 4.2: Detection of bilirubin in serum sample by proposed electrochemical method and comparison with standard peroxidase method.

Samples	HSA-AuNC/ITO electrochemical method		Peroxidase Method		Recovery (%)
	Amount Detected (µM) [a]	RSD(%) [b]	Amount detected (µM) [a]	RSD (%) [b]	
Serum + 1µM of bilirubin	1.10 ± 0.06	5.9	1.12 ± 0.07	6.5	98.2
Serum + 5µM of bilirubin	5.12 ± 0.42	8.3	5.24 ± 0.16	3.2	97.7

[a] Value = mean ± S.D. (n=5), [b]RSD=Root mean square deviation.

4.4. Conclusion

This is the first report on the use of HSA-AuNCs as a bio-recognition element for the sensitive amperometric detection of unbound bilirubin in deproteinized serum samples. The dynamic range of the response covered the free bilirubin level that is normally present in hyperbilirubinemic conditions. The AuNCs in the protein matrix acted as an electronic bridge by contacting a specific redox active moiety of the HSA-attached bilirubin molecule and the polarized electrode. The HSA in the HSA-AuNC contains a specific binding site for bilirubin and allows selective oxidation at a particular moiety of the molecules, as indicated by the docking studies. Thus, the fabricated bioelectrode has potential as a biosensor for sensitive detection of the free bilirubin levels in serum samples.

Figures

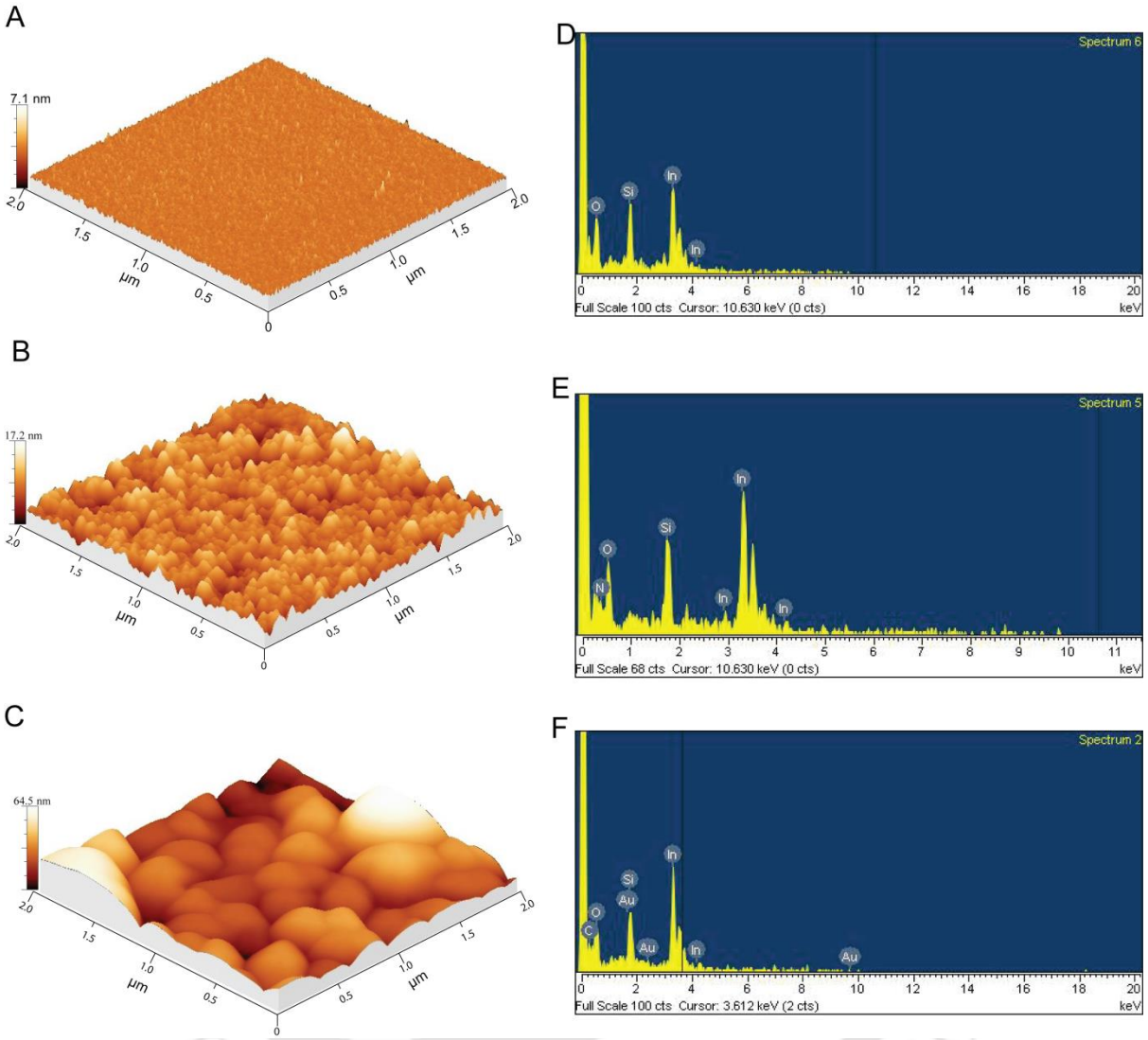

Fig. 4.1: 3-D AFM images of bare ITO (A), APTES-modified ITO (B) and HSA-AuNC-modified silanized ITO (C). EDX spectra of bare ITO (D), APTES-modified ITO (E) and HSA-AuNC modified APTES-ITO (F).

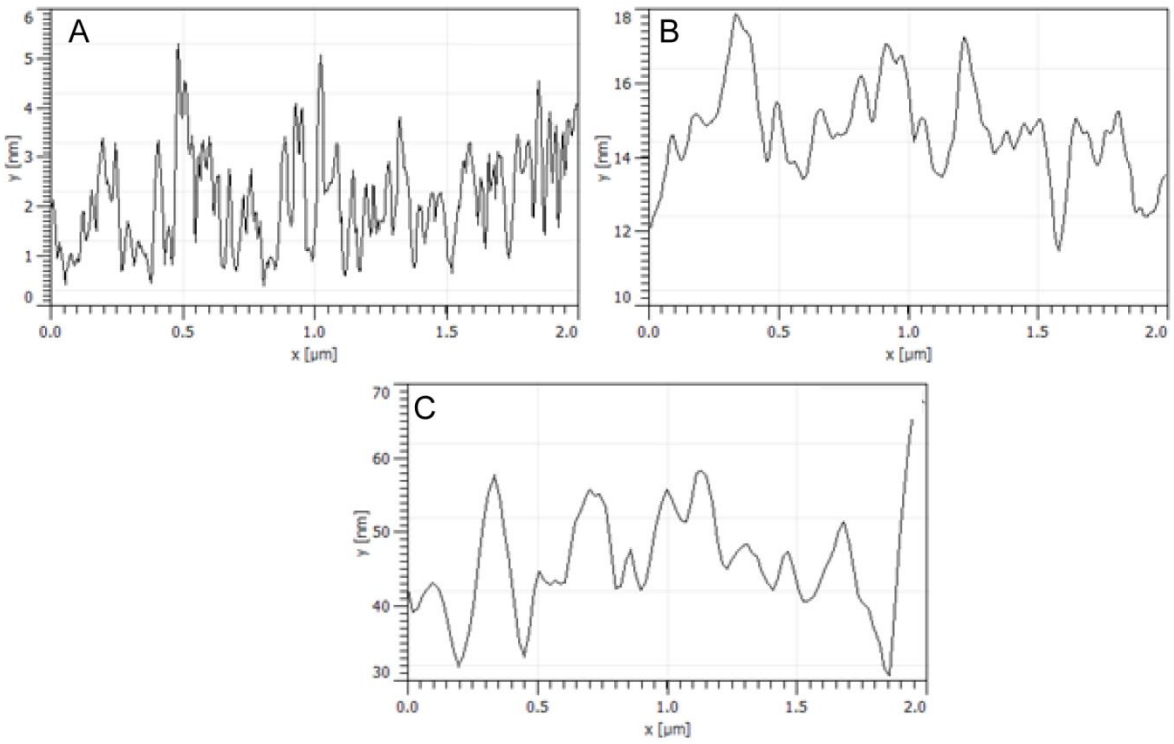

Fig. 4.2: AFM Roughness profile of bare ITO (A), APTES modified ITO (B) and HSA-AuNC modified ITO (C). RMS roughness of bare ITO, APTES ITO and HSA-AuNC modified ITO were 2.16 ± 0.98, 11.54 ± 3.66 and 46.53 ± 8.15, respectively.

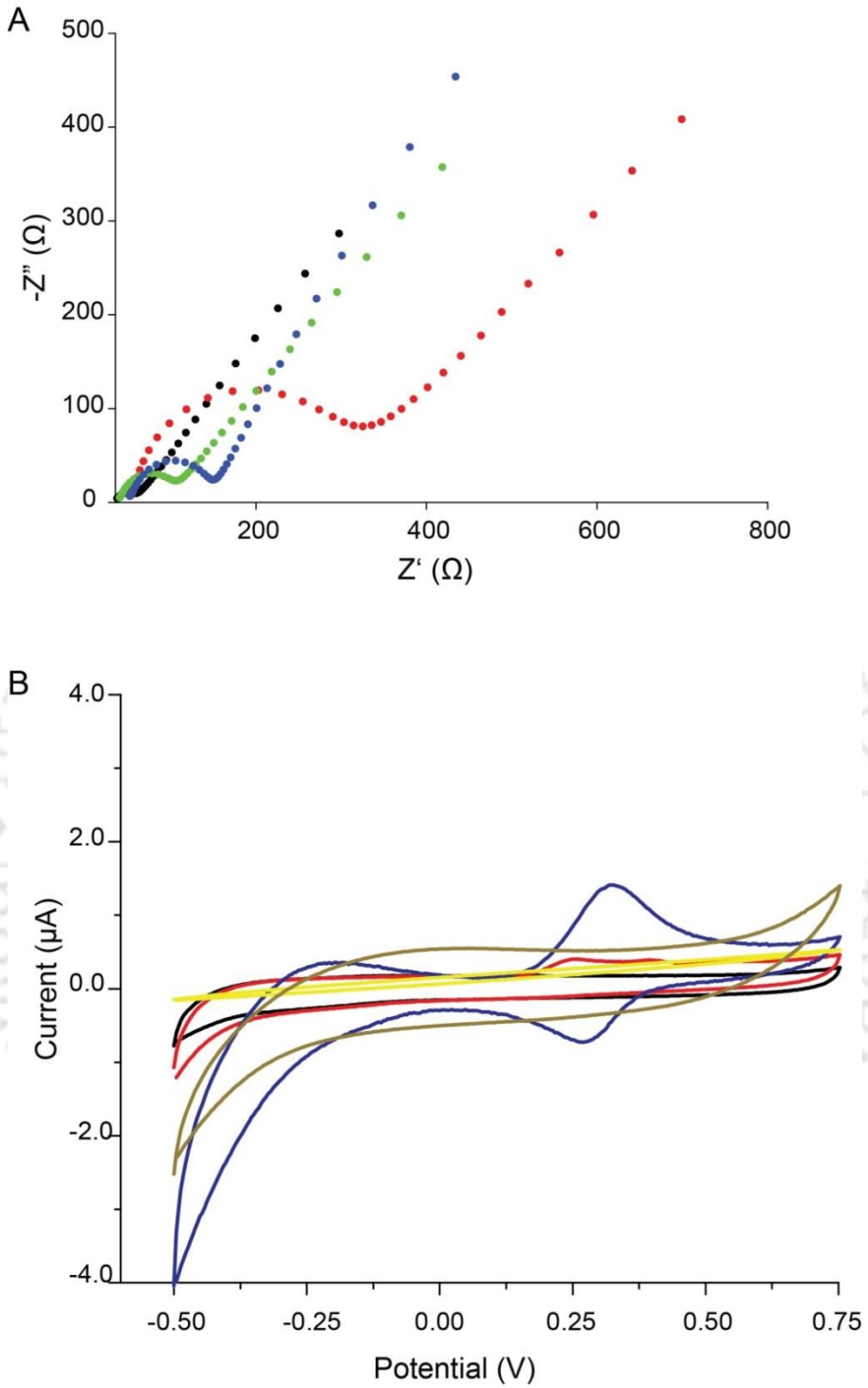

Fig. 4.3: A) EIS spectra of bare ITO (red), APTES-ITO (black), HSA-AuNC/APTES-ITO (green) and HSA/APTES-ITO (blue) in 5 mM $K_3Fe(CN)_6/K_4Fe(CN)_6$ (1:1) and 0.1 M KCl. B) CV of bare ITO (black trace) with bilirubin (red trace), HSA-AuNC/APTES-ITO (brown trace) with bilirubin (blue trace), and HSA/APTES ITO with bilirubin (yellow trace) in PBS buffer (pH 7.4).

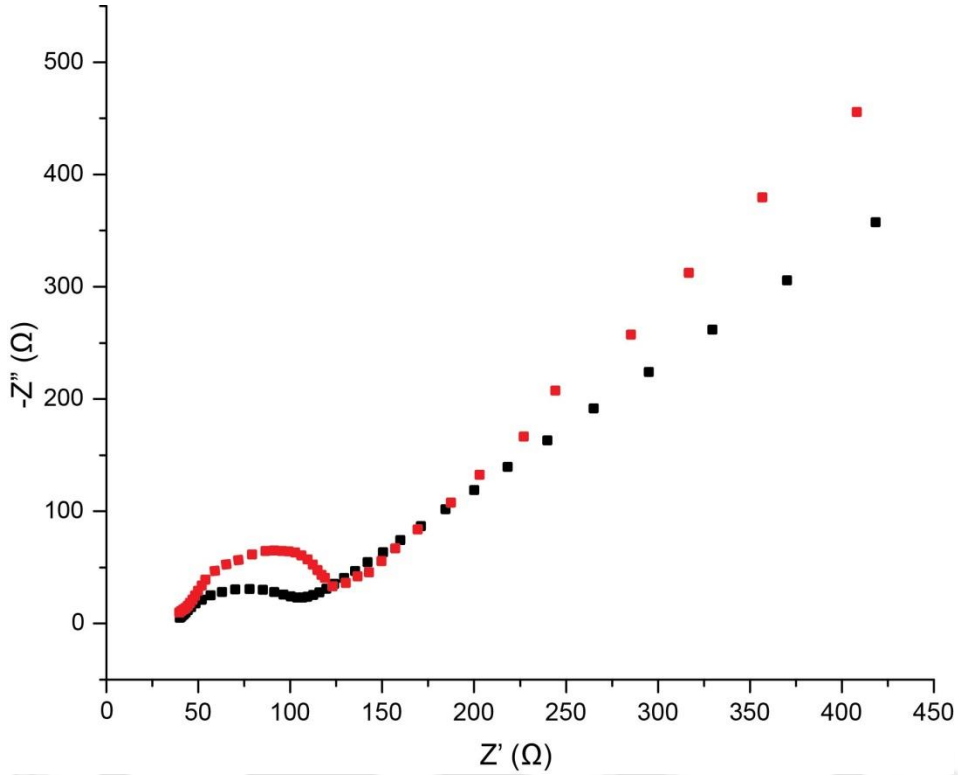

Fig. 4.4: EIS spectra of HSA-AuNC modified ITO electrode in the presence (red dot) and absence (black dot) of bilirubin. Supporting electrolyte contains 5 mM $K_3Fe(CN)_6$ /$K_4Fe(CN)_6$ (1:1) and 0.1 M KCl.

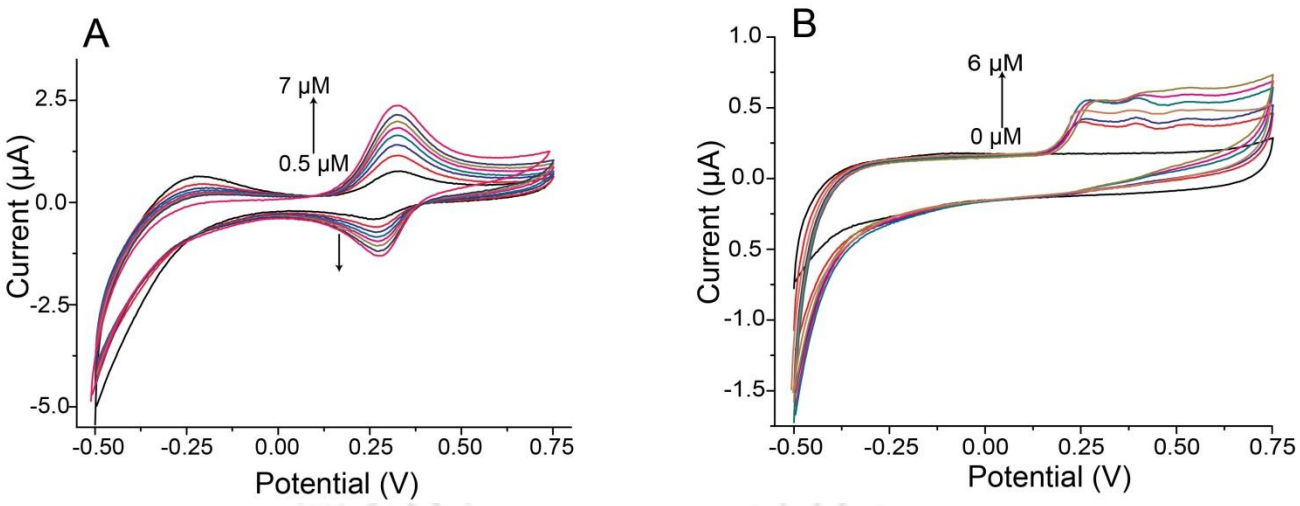

Fig. 4.5: CV plot of HSA-AuNC/APTES/ITO (A) and bare ITO (B) at different bilirubin concentration.

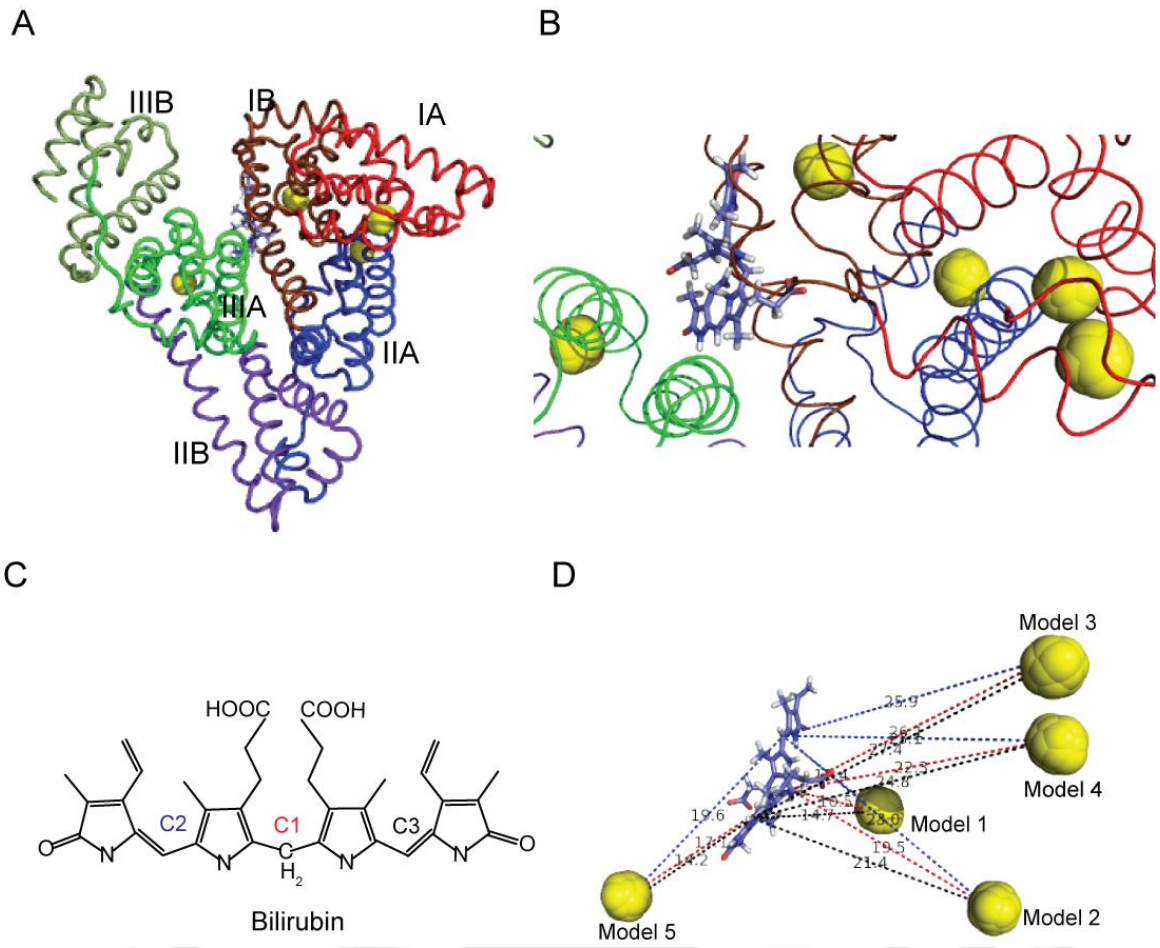

Fig. 4.6: Schematic representation of the structure of HSA (the different colors indicate the different subdomains) containing docked Au_{18} NCs and bound bilirubin (A). B) Expanded view of the HSA-bilirubin binding pocket, along with docked nanocluster models. C) Structure of bilirubin and (D) the measured inter molecular distance between the C1 (red), C2 (blue) and C3 (black) atoms of bilirubin and the AuNC.

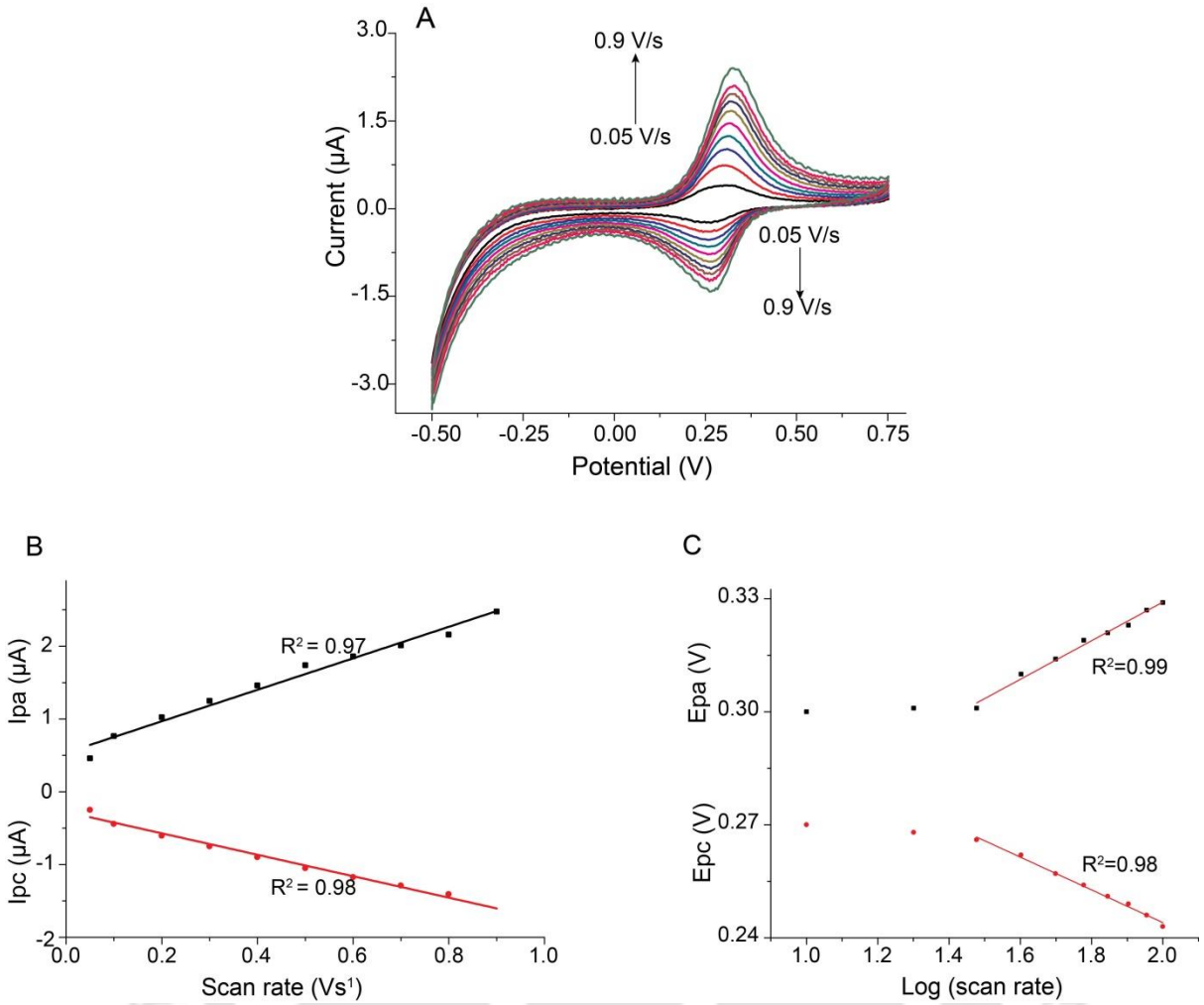

Fig. 4.7: A) CV of HSA-AuNC/APTES/ITO at different scan rate (0.05 to 0.9 V sec^{-1}) in PBS buffer pH 7.4 containing 5 µM of bilirubin, B) Plot of peak current vs. scan rate and C) Plot of anodic and cathodic peak potential vs. log (scan rate).

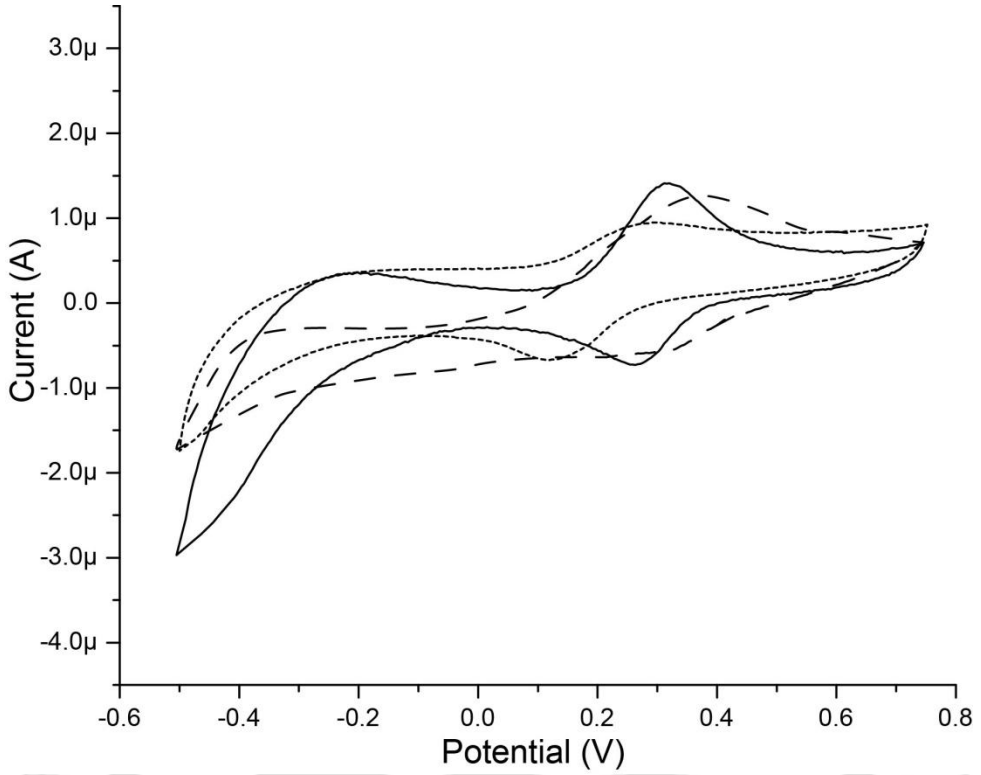

Fig. 4.8: CV plot of HSA-AuNC/APTES/ITO against 3 μM bilirubin in pH 6.4 (dot), pH 7.4 (solid) and pH 8.4 (dash) buffers.

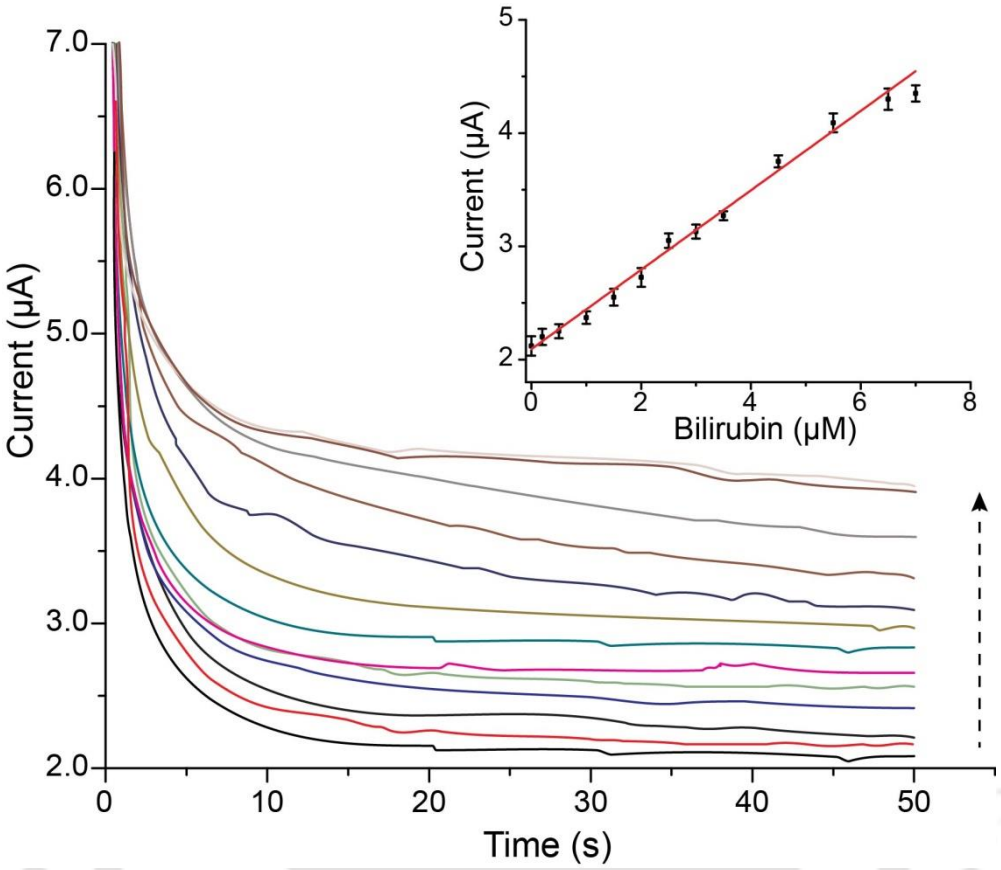

Fig. 4.9: Chronoamperometric response of the HSA-AuNC/APTES-ITO electrode to different concentrations of bilirubin at a potential of 0.3 V (vs. Ag/AgCl). Inset: calibration plot of the current vs. bilirubin concentration. A linear regression line for the present data is represented by the equation y = 0.34 *[c] + 2.09, with an R^2 = 0.98. The error bars represent the SD (n = 3).

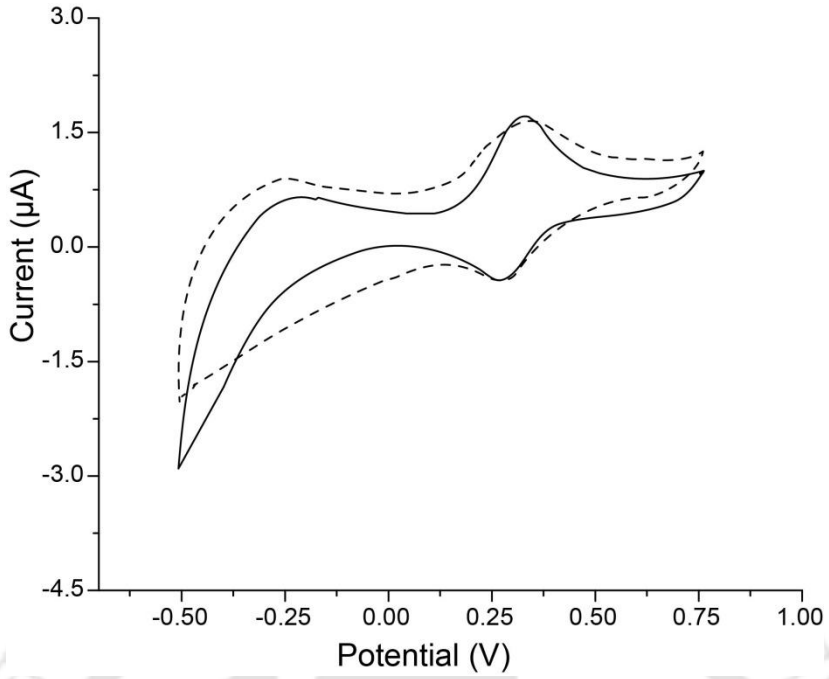

Fig. 4.10: CV plot of freshly prepared HSA-AuNC/APTES/ITO (solid) and NaOH washed (dash) HSA-AuNC/APTES/ITO electrode against the same bilirubin concentration (3 µM).

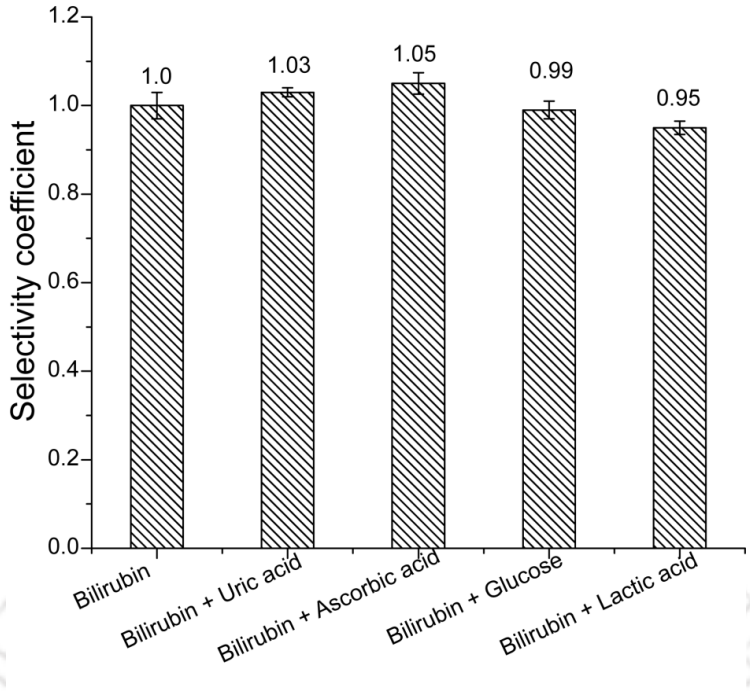

Fig. 4.11: Interference study of HSA-AuNC/APTES/ITO for bilirubin detection in presence of different potential interfering agents.

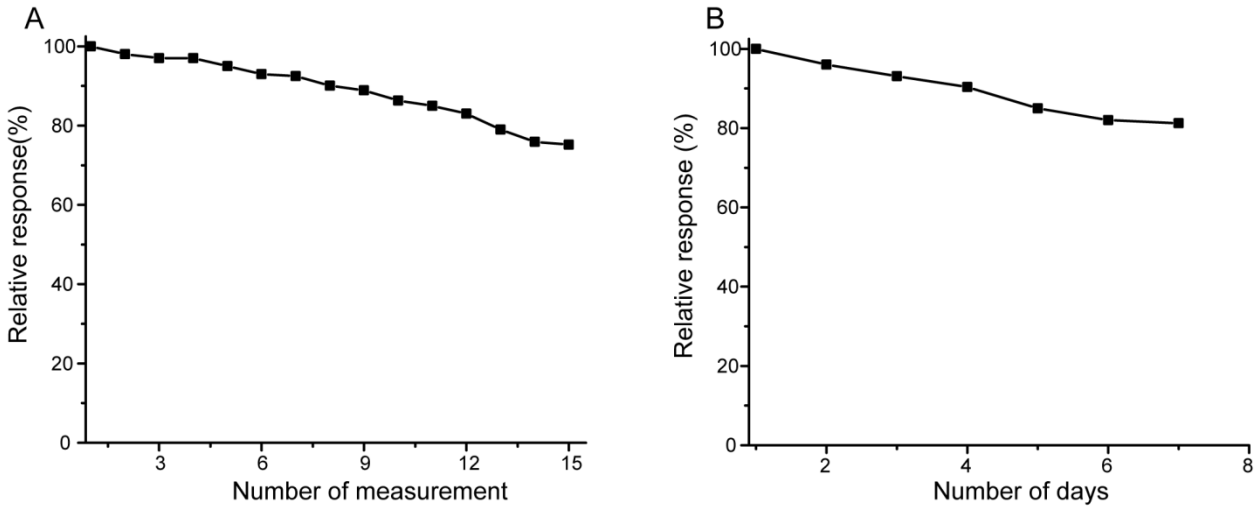

Fig. 4.12: Operational (A) and storage (B) stability of HSA-AuNC modified ITO electrode for detection of bilirubin.

Chapter V

HSA-stabilized gold nanocluster in microfluidic paper based platform for electrochemical detection of bilirubin

CHAPTER V

HSA-stabilized gold nanocluster in microfluidic paper based platform for electrochemical detection of bilirubin

5.1. Overview

In the previous chapter, the electronic bridging effect of AuNC in the HSA-AuNC conjugate on the ITO electrode responsible for the electrochemical detection of bilirubin was established. The method offers sensitive and selective detection of bilirubin in a laboratory based analytical setup. In order to carry forward the concept for application in a resource limiting and point-of-care (POC) setup, we propose to use a biosensing platform that complies the 'ASSURED' mandate of World health organization (WHO) for their application in under-developed and developing nations (Peeling et al., 2006). The word 'ASSURED' implies affordable, selective, sensitive, user- friendly, robust, equipment- free and deliverable. In this regard paper was identified as a right choice (Li et al., 2012) due to the following advantages: (i) inexpensive, portable, and easily accessible, (ii) compatible with biological samples (iii) transports liquids using capillary forces without the assistance of

external forces and (iv) can be easily modified to immobilize different biomolecules like protein, DNA, small molecules, etc., (Kakoti et al., 2015). Further, we would like to utilize the concept of microfluidics for developing the paper-based platform. Microfluidic paper-based analytical devices (μPADs) have gained high attention as a promising technology for point-of-care testing due to its short response time, simplicity, ease of miniaturization, simple fabrication and operation (Desmet et al., 2016; Dungchai et al., 2009; Martinez et al., 2008; Nie et al., 2010; Noiphung et al., 2013).

In this chapter microfluidics paper-based electrochemical device (μPED) has been reported for the detection of bilirubin by using the HSA-AuNC as electrochemical probe. For creating micro- channels, hydrophobic patterns over chromatographic paper was performed by using ink jet printing with a modified cartridge containing AKD (alkyl ketene dimer) in a suitable solvent. AKD is hydrophobic in nature and acts as a barrier to fluid flow. Further, to enhance the surface area over the electrode zinc oxide nanorods (ZnO-NRs) were directly synthesized over the working electrode *vi*a a solvothermal method. ZnO nanostructures are promising functional materials with distinctive features such as, high surface area, non-toxic, biocompatible, chemically stable, shows biomimetic and high electron communication (Wang et al., 2006; Weintraub et al., 2010). Moreover, high isoelectric point (*pI* ~ 9.5) of ZnO nanostructures makes the immobilization of low *pI* biomolecules more practical (Zhao et al., 2009). Later, by utilizing electrostatic interaction, the HSA-AuNC (*pI*, 5.7) was immobilized over ZnO-NRs which were grown over working electrode. The electrochemical and response characteristics of HSA-AuNC/ZnO-NR modified μPED were evaluated and presented here.

5.2. Experimental Approaches

5.2.1. Reagents

Zinc acetate, zinc nitrate hexahydrate, hexamethyl tetraamine (HMT), polyethylene glycol (PEG), chitosan of high purity (99 %) and bilirubin were purchased from Sigma-Aldrich (USA). Alkyl ketene dimer (AKD 1840) was purchased from Flourish paper and chemicals Limited (Mumbai, India) All other chemicals namely, potassium hydroxide, ethanol, methanol, disodium hydrogen phosphate, sodium dihydrogen phosphate and hydrochloric acid etc. were of analytical grade and purchased from Merck (India). Whatman chromatographic papers grade1 (20 cm x 20 cm) were procured from GE Lifesciences (India). Silk fibroin and sericin were extracted from *Bombyx mori* cocoons following a reported method (Rockwood et al., 2011).

5.2.2. Fabrication of paper-based electrochemical device

The shapes of the hydrophilic working zones for paper were designed with Adobe illustrator CS6. Hydrophobic patterns of AKD–heptane solution (5 %, v/v) was printed on hydrophilic chromatographic papers using a reconstructed commercial digital ink jet printer (HP Deskjet 1000). The modification of the printer involved replacing the ink in cartridge with the AKD–heptane solution. The printed chromatographic paper samples were then heated in an oven at 100 ^{0}C for 8 min to cure AKD onto the cellulose fibers (Li et al., 2010).

5.2.3. Preparation of conductive graphite ink

Biocompatible conductive inks were prepared by using graphite powder dispersed in biocompatible polymers, PEG, chitosan, silk fibroin and sericin. Briefly, 30 % (weight) of graphite powder was dispersed in 60 % (weight) PEG solution containing either 1 % (weight) of chitosan, silk fibroin or silk sericin. The obtained pastes were dispersed homogeneously

by the application of ultra-sonication. Later the conductive pastes were characterized for conductivity and surface modification. Finally, the paste with a better conductivity was chosen for the fabrication of electrode. The working electrode was hand-painted with graphite paste on paper strip-1. Similarly, graphite paste and silver paste were hand-painted on a paper strip-2 as the counter electrode and the reference electrode, respectively with particular dimension as shown in scheme 5.1. The prepared electrodes were allowed to dry for 30 min and later polished with tissue paper to obtain a smooth surface.

5.2.4. Synthesis of ZnO nanorods over paper substrate

ZnO nanorods were grown over hardened ZnO seed layer by solvothermal method (Manekkathodi et al., 2010). Seed layer of ZnO nanoparticles was prepared by dropwise mixing of 30 mM of potassium hydroxide with 10 mM zinc acetate in methanol at 60 °C for 2 h. Around 5 µl of seed layer (ZnO nanoparticle) was dropped over the fabricated working electrode and heated at 180 °C for 30 min to harden the seed layer. In the meanwhile, equimolar ratio of zinc nitrate hexahydrate and HMT were mixed in distilled water for 30 min at RT. The ZnO nanoparticle seeded paper substrate was dipped vertically in the solution and was heated for 5 h at 85 °C. Finally, the paper substrate withdrawn was rinsed with distilled water to remove any residues and dried.

5.2.5. Synthesis and immobilization of HSA-stabilized nanocluster

The HSA-stabilized nanoclusters were synthesized by microwave assisted method as described under the section 2.2.2. Purification of synthesized HSA-AuNC was done by following Zn^{2+}-assisted precipitation method described under the section 2.2.3. Around 5 µl of purified HSA-AuNC (10 mg ml^{-1}) was drop casted over ZnO-NR grown paper electrode and dried at RT for overnight.

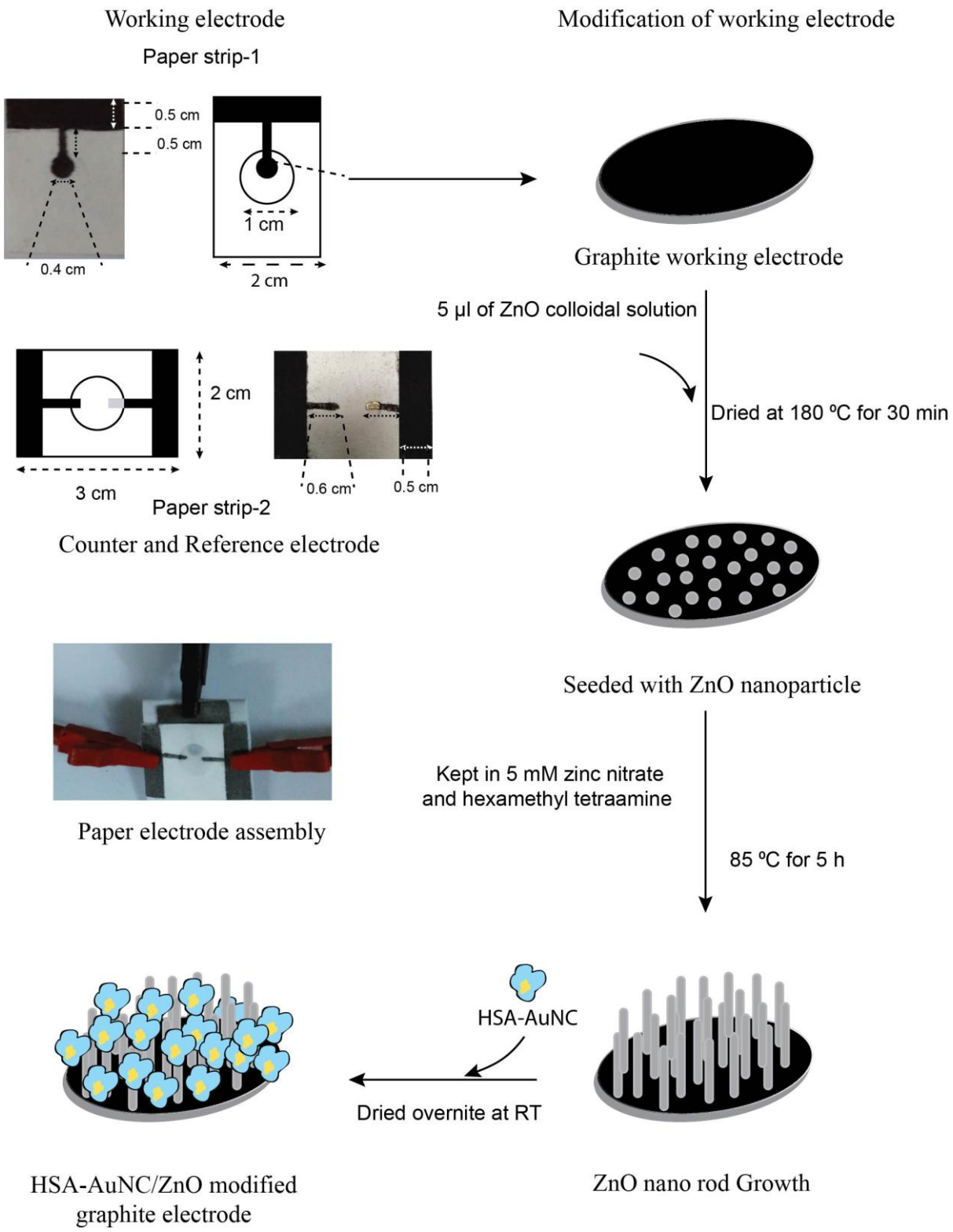

Scheme 5.1: Scheme of immobilization of HSA-AuNC over *in-situ* grown ZnO nanorods on paper-based graphite electrode.

5.2.6. Apparatus and measurements

Biocompatible conductive inks were characterized for resistance by using two electrode data acquisition system (Agilent 34972A LXI). Thermal stability of the conductive inks was monitored by thermo-gravimetric analysis (TGA) and differential scanning calorimetry (DSC) analysis which were performed simultaneously in thermal analyzer (NETZSCH STA-449 F3 Jupiter®) from RT to 400 °C at a rate of 10 °C min^{-1} under dry nitrogen.

The degree of crystallinity of conductive pastes were analyzed by using an X-ray powder diffractometer (Rigaku X-Ray Diffractometer TTRAX III, Japan) equipped with Cu Kα radiation (λ, 1.54178 Å) in a continuous scanning mode. The morphological characterization of patterned paper and different modified electrodes were performed by a field emission scanning electron micro-scope (FESEM) (Zeiss, Germany), with EHT 1.00 kV. CV and differential pulse voltammetry (DPV) were performed with an Autolab PGSTAT 1212 (Eco Chemie, Netherlands).

5.2.7. Detection procedure of the electrochemical device

The three-electrode system was employed for electrochemical measurements. The paper based electrochemical device consisted of two rectangular paper. First strip (strip-1) containing the working electrode was kept below the second paper strip (strip-2) which contained reference and counter electrodes. Both paper strips (1 and 2) were clamped together by using paper clip. Strip-1 containing graphite paste and *in-situ* grown ZnO-NR over graphite was served as control, while HSA-AuNC immobilized over *in-situ* grown ZnO-NRs acted as bioelectrode for bilirubin detection. Effect of buffer volume, time of incubation and pH on the response of paper electrochemical device were carried out by measuring current response at 0.25 V at different condition by using 5 µM of potassium ferricyanide

(K_3FeCN_6) in phosphate buffer as electrochemical probe.

5.3. Results and discussion

5.3.1. Characterizations of the patterned paper and conductive ink

5.3.1.1. Spectroscopic and thermal characterization of the ink

Different conductive graphite inks were prepared by combining various biocompatible polymers and then characterized by measuring resistance using two electrode systems. The Fig. 5.1A shows the plot of resistance of different conductive pastes over the course of time. Among the different graphite paste, the paste containing sericin displayed better conductivity with resistance 0.7 ± 0.11 KΩ cm^{-2}. Whereas, the graphite paste with chitosan and silk fibroin displayed resistance of 2.2 ± 0.15 KΩ cm^{-2} and 2.6 ± 0.21 KΩ cm^{-2}, respectively which were almost three to four fold higher in the resistance than the sericin-graphite paste. The electrical transduction properties of some hydrogels were reported to be enhanced when they doped with sericin. Sericin is a charged molecule. It is suggested that higher ordered conducting chains formed throughout the hydrogel network improve the charge transfer property of the hydrogel (Cheong et al., 2014).

Initial observation on the drawing traces of graphite paste with only PEG showed that after incubation with buffer, the traces were dissolved easily. This is due to the high aqueous solubility of PEG. On the other hand traces made by the graphite paste containing mixture of PEG and sericin were stable during incubation in the buffer. The reason may be attributed to the glue like property of sericin rendering less solubility of the paste in the presence of PEG. Solubility of sericin in water decreases when the sericin molecules are transformed from random coil into the *β*-sheet structure. The introduction of PEG into the sericin solution known to induce changes of secondary structural conformation from the random coils to *β*-sheets (Cho et al., 2003).

The stability of the graphite ink was studied using DSC and TGA techniques. Fig. 5.1B (black trace) showed the TGA plot for graphite ink containing PEG and sericin. A reduction in mass by 25 % was observed at ~ 100 ^{0}C, which could be due to evaporation of residual water from the graphite ink. Absence of any major drastic changes in the mass of the sample during heat treatment up to 320 ^{0}C indicates that the polymer binders do not degrade into small subunits within this temperature range. DSC measurement of the graphite paste containing PEG and sericin is shown in fig. 5.1B (blue trace), which indicates the presence of doublet endothermic peaks one at 91.5 ^{0}C and the other shoulder peak at 62.5 ^{0}C. These peaks can be attributed to the melting of PEG binder (Pielichowski and Flejtuch, 2002). The appearance of another endothermic broad peak at ~ 275 ^{0}C was suggested to be caused by the melting of sericin in sericin–PEG graphite paste (Zhang et al., 2011).

Fig. 5.2 (A and B) shows the XRD patterns of the graphite, PEG, sericin powder and their composites graphite-PEG, graphite-sericin and graphite-PEG-sericin powder. The XRD pattern in fig. 5.2A at the reported 2θ range is dominated by peaks at 26.54^0 correspond to graphite (Wojtoniszak et al., 2012) while sericin exhibit two weak intensity peaks at 23.26^0 and 19.06^0. Upon interaction of graphite with sericin, the peak intensity corresponds to graphite crystallinity increases, which infers that the addition of sericin causes the graphite crystalline. Fig. 5.2B shows the XRD pattern of PEG, PEG-graphite, and PEG-graphite-sericin. PEG exhibit distinct two peaks at 23.29^0 and 19.12^0 (Wang et al., 2012). The crystallinity of both PEG and graphite decreases in the respective composite mixture, as evident from the decrease in intensity of the peak corresponds to PEG and graphite. While incorporation of sericin to the PEG-graphite composite increases the intensity of graphite peak at 26.5^0.

5.3.1.2. Morphological characterization of μPED by FESEM

The surface morphology of the unmodified and AKD modified paper substrate were analyzed by FESEM technique. Fig. 5.3A shows the FESEM image of the blank Whatman chromatography paper, where the porous structure of the paper is revealed as expected. Whereas, the AKD printed paper showed less porous morphology (Fig. 5.3B) indicating that the AKD penetrated deeply into the chromatographic paper. The surface characteristics of chromatographic paper after applying graphite conductive paste was also studied through FESEM which revealed the smooth uniform morphology (Fig. 5.3C and 5.3D). The ZnO nanorods grown over graphite drawn paper showed regular lawn of rod like structures with hexagonal face as clearly visible from Fig.5.4B. The magnified images (Fig. 5.4C) showed vertically aligned hexagonal shaped nanorods with diameter ~ 200 nm. The morphology of the HSA-AuNC immobilized electrode showed the disappearance of the rod like structure of ZnO after the deposition of HSA-AuNC, transforming the electrode surface to a uniform layer.

5.3.2. Electrochemical characterization of the fabricated electrodes

5.3.2.1. Parameters optimization

The effect of incubation time and the buffer volume on the current response of HSA-AuNC/ ZnO-NR modified μPEDs was studied by measuring the DPV signal at 0.25 V using phosphate buffer containing 5 μM of K_3FeCN_6 as a probe. DPV response increased with increasing incubation time and stabilized after 120 s (Fig. 5.5A). The optimal incubation time of 120 s was selected for the subsequent experiments. The optimum analyte volume for the μPED was found to be 10 μl (Fig 5.5B). The electrochemical studies were performed at pH 7.4 which was an optimized value detected from our previous work with HSA-AuNC modified ITO electrode.

5.3.2.2. Cyclic voltammetry

CV analysis of paper electrode assembly was performed by connecting the three electrodes terminals with the potentiostat equipment. The modified electrodes assemblies were first characterized in the absence of bilirubin. Both ZnO-NR grown electrode assembly and the HSA-AuNC/ZnO-NR modified electrode assembly did not furnish any redox peaks in the potential window at -0.5 V to 0.75 V (Fig. 5.6 black and green trace). The CV of HSA-AuNC/ZnO-NR modified electrode assembly showed increase in peak less back ground current density compared to ZnO-NR grown electrode assembly. This was due to the conducting role of nanocluster within the protein matrix which facilitated the facile movement of the electrons. While in the presence of bilirubin, ZnO-NR grown electrode assembly showed increase in oxidation current at potential ~ 0.25 V to 0.50 V, indicating oxidation of bilirubin at the electrode. The absence of any reduction peak in the CV spectra indicates irreversibility of the oxidation reactions. The appearance of oxidation peaks are attributed to electroactive nature of bilirubin. In fact, similar appearance of oxidation peak for bilirubin at this potential over different electrode systems has been previously observed (Avan et al., 2015; Taurino et al., 2014).

In the presence of bilirubin, the HSA-AuNC/ZnO-NR electrode assembly showed an increase in current density at the forward as well as reverse scan of the CV (Fig 5.6 blue trace). The appearance of a pair of redox peaks with oxidation at ~ 0.3 V and reduction at ~ 0.25 V was attributed to the redox conversion of bilirubin at the electrode surface. The nanocluster present in the HSA protein matrix promoted specific redox conversion of the bilirubin. From our previous studies it has been observed that, when bilirubin binds to its natural carrier HSA in a specific way, the nanocluster present within the protein matrix assisted the specific redox conversion of bilirubin. The appearance of single pair of redox

peak implies site-specific binding of bilirubin on the HSA surface allowing oxidation at a specific site. Moreover, with the increase in the bilirubin concentration both anodic and cathodic peak current increased as shown in Fig 5.6B. These results further prove the observed CV peaks corresponds to the electrochemical conversion of bilirubin bound to HSA over the polarized HSA-AuNC/ZnO-NR electrode in μPED.

5.3.3. Response characteristics of bioelectrode towards bilirubin

The analytical performance of this method was verified by measuring DPV response at 0.3 V of the 10 µl of PBS containing various bilirubin concentrations under the optimized condition. The DPV response of paper electrode assembly in the absence and presence of various concentration of bilirubin in PBS was observed at 0.3 V (Fig. 5.7A). The fig. 5.6B shows linear current response against the concentration of bilirubin in the range of 0.5 µM to 35 µM (R^2 = 0.994). The sensitivity of the method was found to be 0.019 µA μM^{-1}. LOD calculated from the equation, $LOD = \frac{3*SD\ of\ Blank}{Slope\ of\ calibration\ curve}$, was found to be 57.3 nM at a signal to noise ratio of 3. Saturation in the peak current was noticed beyond 35 µM of bilirubin indicating saturation of the HSA-AuNC binding sites with bilirubin above this concentration.

5.3.4. Reproducibility and interference test

The device-to-device reproducibility of the present method for the determination of bilirubin was evaluated by analyzing DPV response generated by five different HSA-AuNC/ZnO-NR μPED assemblies fabricated by following similar protocol after the addition of bilirubin (20 µM) under the optimized condition. The relative standard deviation (RSD) value was found to be ~7.8 % indicating good repeatability of the electrode for the detection of bilirubin. The selectivity of the assay was evaluated by measuring the DPV response of the

*μ*PED in presence of bilirubin and different potential interfering substances (10 μM each). Increase in DPV response was obtained in case of bilirubin (Fig 5.8) which indicates that the paper based bioelectrode assembly was selective to bilirubin. This infers that the presence of layer of HSA allowed bilirubin to selectively bind and oxidize at the HSA-AuNC/ZnO-NR interface.

5.4. Conclusion

In summary, we have demonstrated here a simple *μ*PED for the ultra-sensitive detection of free bilirubin. A highly conductive, stable graphite ink was prepared by using silk sericin as binder and used the ink in preparing microelectrode for the device. The working electrode surface was modified with *in-situ* synthesized ZnO-NR over which HSA-AuNC was immobilized through electrostatic interaction. The device exhibits an improved dynamic bilirubin detection range of 0.5 μM to 35 μM, compared to the detection range of 0.2 μM to 7 μM obtained from HSA-AuNC/ITO bioelectrode platform that void ZnO-NR. Introduction of HSA-AuNC accelerated the electron transfer in the redox conversion of bilirubin at the electrode surface. The constructed *μ*PED could sensitively detect bilirubin in micro-molar range (10 μM) without challenge from the tested potential interferents present in the sample. Thus, the constructed device has great potential to develop as a simple, low-cost and sensitive sensor for rapid and reliable detection of free bilirubin in real sample.

Figures

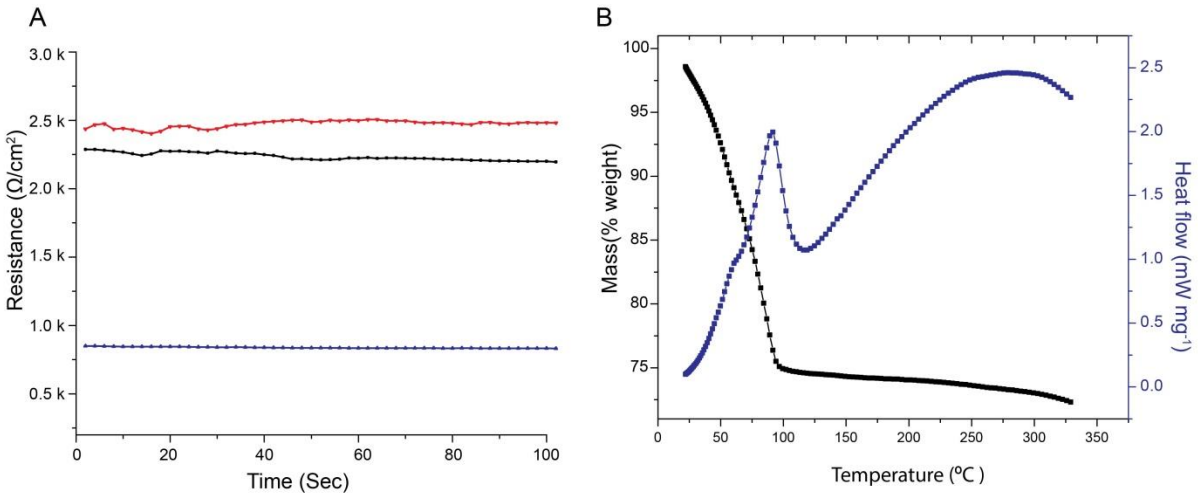

Fig. 5.1: A) The plot of resistance vs. time of graphite-PEG-sericin (blue trace), graphite-PEG-chitosan (black trace), and graphite-PEG-fibroin (red trace) pastes. B) DSC (green trace) and TGA (black trace) of graphite paste containing silk sericin (1% weight).

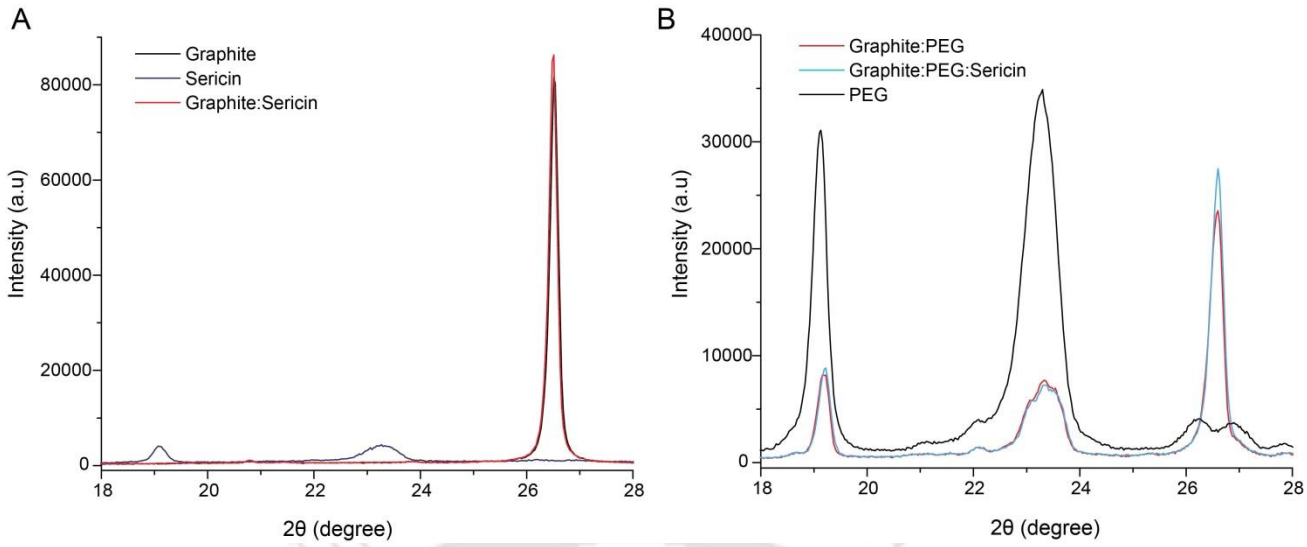

Fig. 5.2: XRD pattern of graphite, sericin and graphite-sericin composite powder (A) and PEG, graphite-PEG and graphite-PEG-sericin composite powder (B).

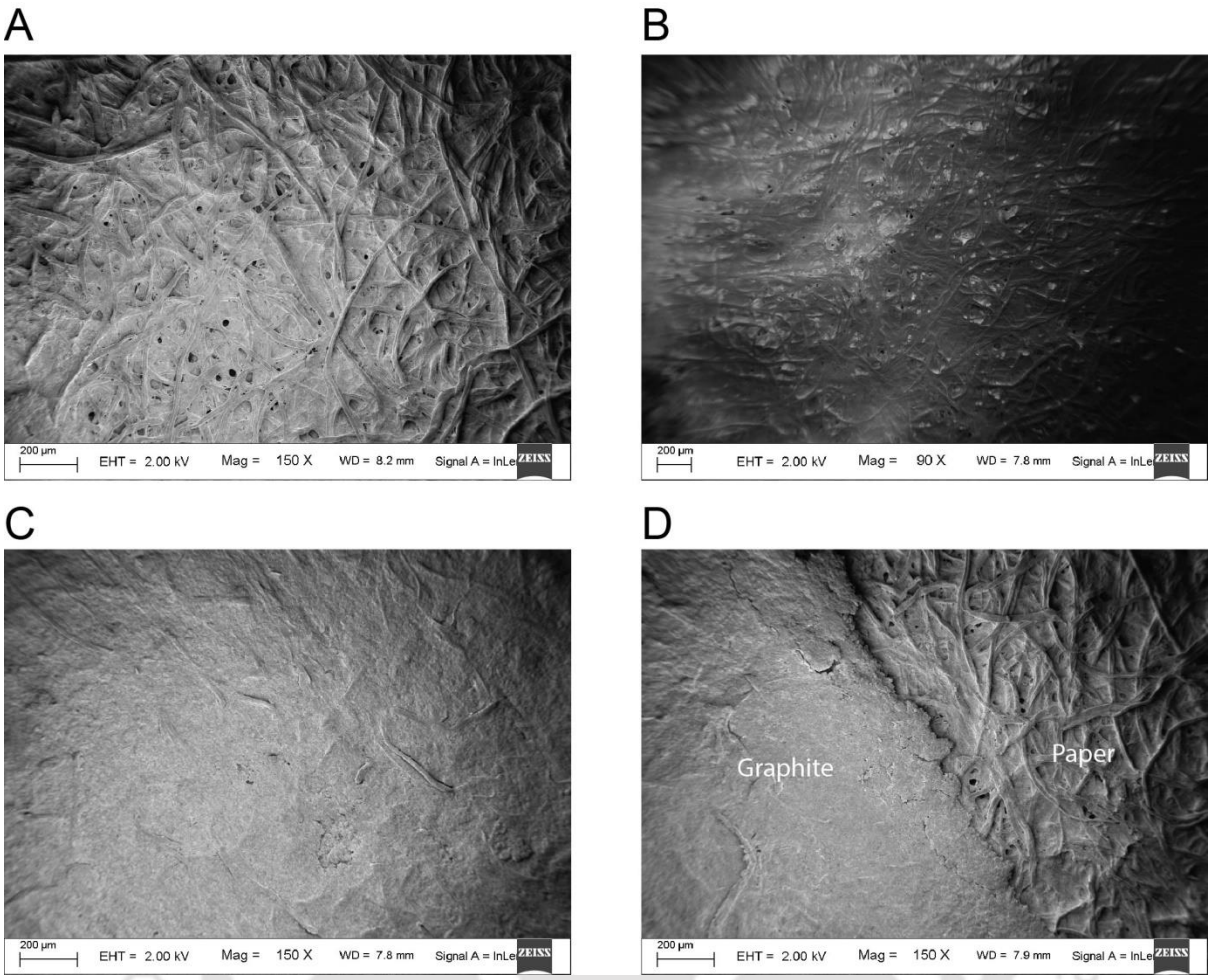

Fig. 5.3: FESEM images of chromatographic grade paper (A), AKD patterned paper (B), graphite dawn patterned paper (C), and Interface between graphite and paper (D).

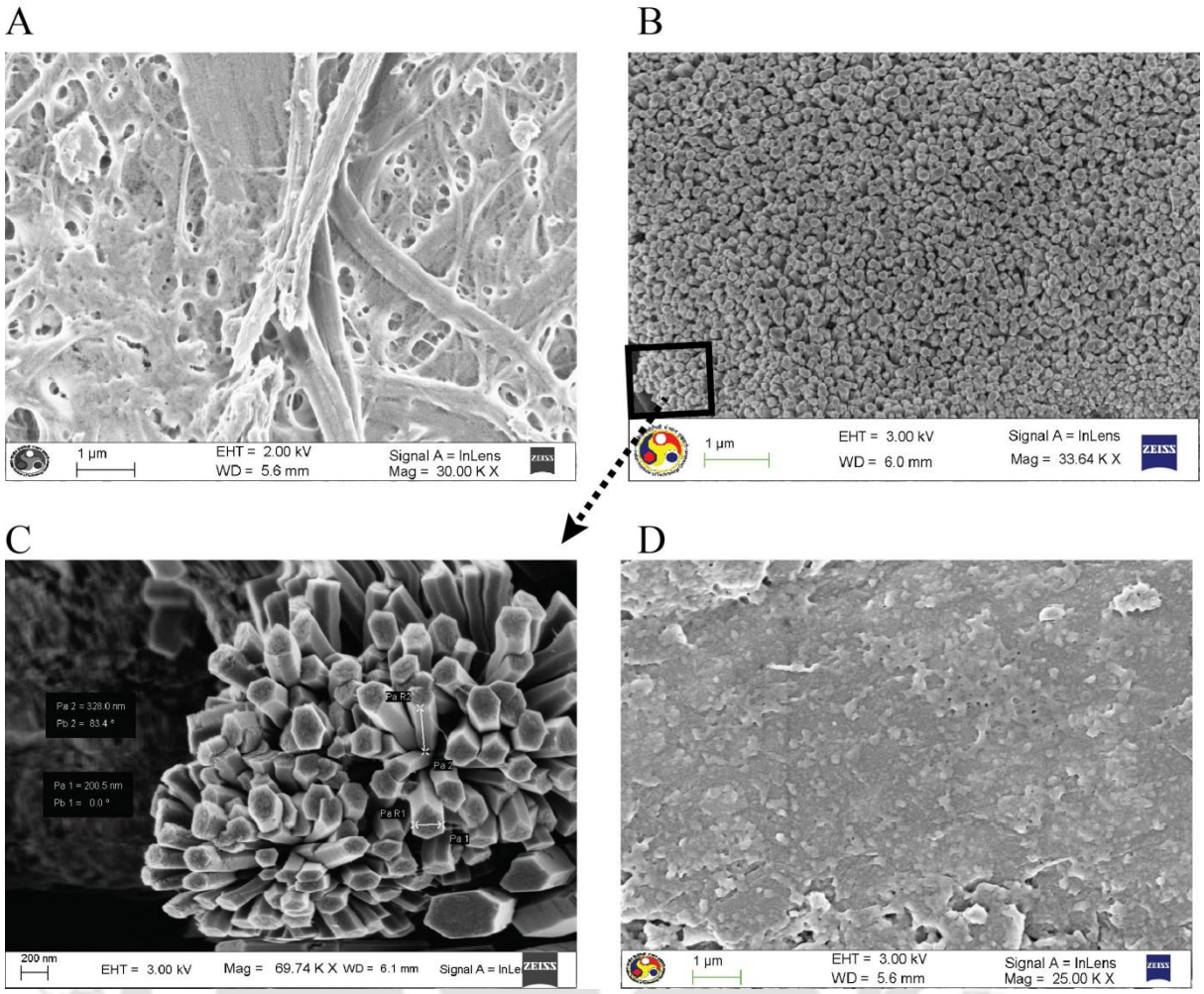

Fig. 5.4: FESEM images of unmodified chromatographic paper (A), paper modified with *in-situ* grown ZnO-NRs (B), magnified image (C) and HSA-AuNC/ZnO-NRs modified paper substrate (D).

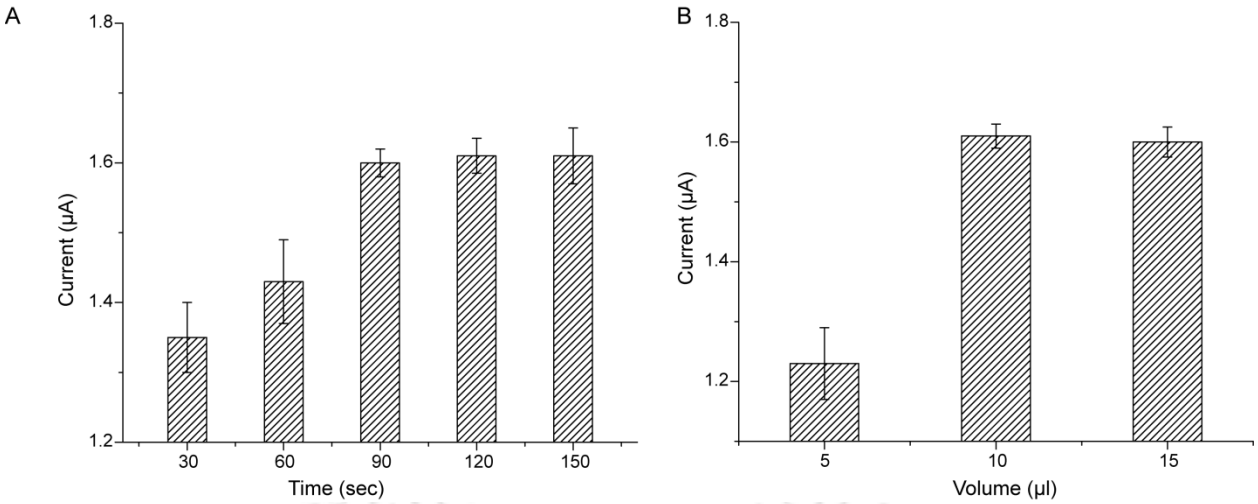

Fig. 5.5: Effect of incubation time (A) and sample volume (B) on the current response of *µ*PED at 0.25 V.

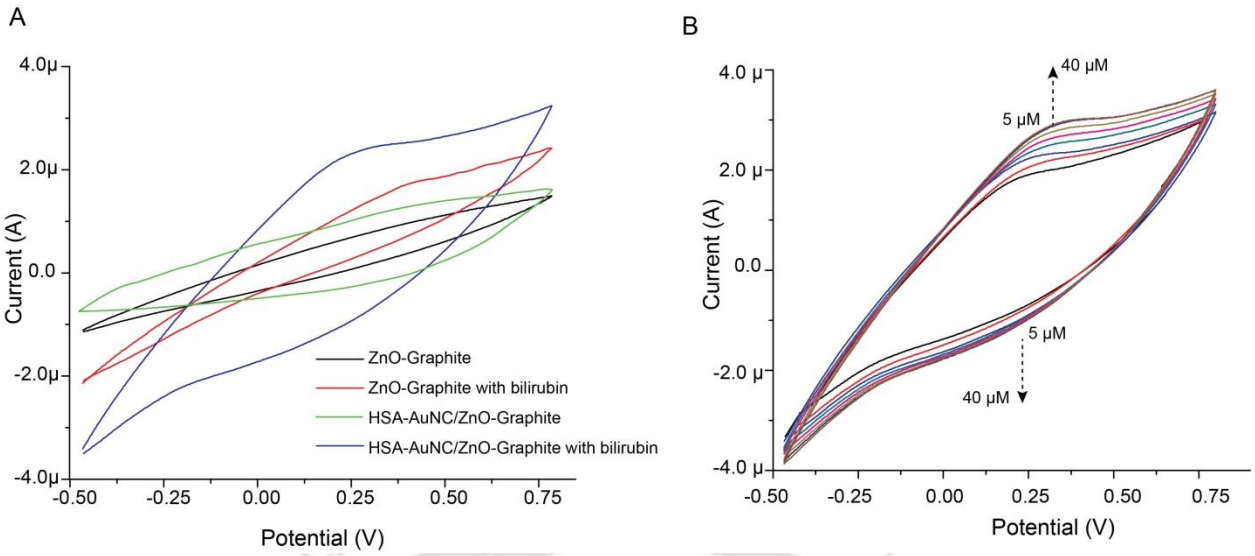

Fig. 5.6: A) CV plot of modified *µ*PED electrode assemblies. B) CV plot of HSA-AuNC/ZnO-NRs modified *µ*PED electrode assembly in presence of increasing bilirubin concentration.

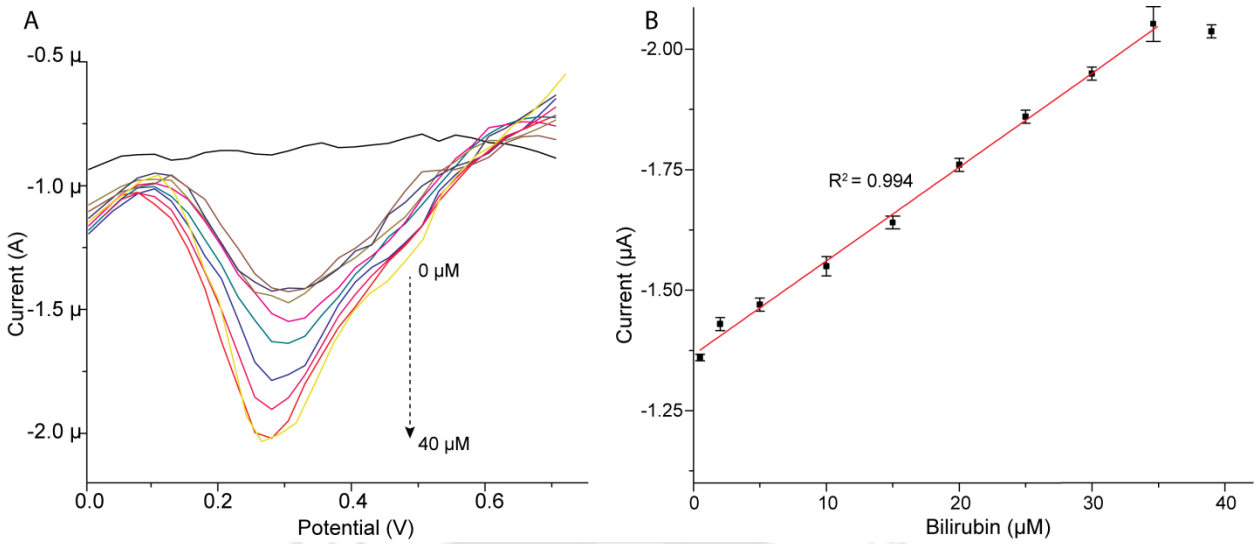

Fig. 5.7: A) DPV plot of HSA-AuNC/ZnO-NRs modified electrode assembly in presence of bilirubin. B) Response plot of current vs. bilirubin concentration.

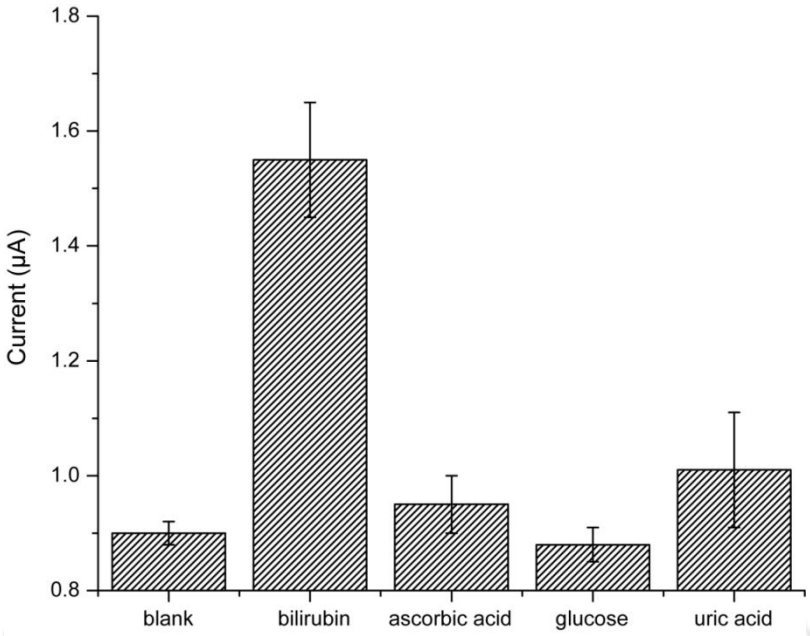

Fig. 5.8: The current response of HSA-AuNC/ZnO-NRs modified *µ*PED in presence of common interfering agents present in serum. Concentration of each analyte was 10 µM in a loaded volume of 10 µl of PBS (pH 7.4).

Conclusion and scope for future work

Conclusions and scope for future work

Conclusions

The present investigation was intended to develop different biosensing platform for the detection of free bilirubin in serum sample. We explored HSA stabilized gold nanocluster as optical and electrochemical probe and natural binding affinity of the HSA protein for selective detection of bilirubin in serum samples. The nanocluster emits bright red fluorescent with the maximum emission centered on 640 nm. The TEM and MALDI studies revealed that the *in-situ* formed nanocluster has size around ~ 2.5 nm and comprises 18 Au atoms. The formation of nanocluster within the protein matrix changes secondary structure marginally and increases charge density of the protein. Bilirubin binds strongly with the HSA-AuNC as revealed from the binding constant of 0.55×10^6 L $mole^{-1}$. We have demonstrated for the first time two novel sensitive methods for the selective detection of free bilirubin in human serum using HSA- stabilized gold nanoclusters, one utilizes fluorescence behavior while other exploits the color-based optical phenomena. The fluorescence-based method relies on the fluorescence quenching through static interaction between HSA-AuNC and bilirubin. This method relies on the natural carrier (HSA) of bilirubin in blood serum where bilirubin binds specifically and avidly. Further, the response obtained from the fluorometric method was practically unaltered in a wide pH and temperature ranges, thus the method offers to analyze samples under considerably compromised physiological conditions. In the colorimetric method the free bilirubin is oxidized to a colorless compound as a result of the peroxidative catalytic action of HSA-AuNC. The use of HSA-AuNC as a electrochemical probe for the sensitive amperometric detection of bilirubin is also reported here for the first time. The dynamic range of the response covered the free bilirubin level that is normally present

in hyperbilirubinemia conditions. The AuNCs in the protein matrix acted as an electronic bridge by contacting a specific redox active moiety of the HSA-attached bilirubin molecule and the polarized electrode. The HSA in the HSA-AuNC contains a specific binding site for bilirubin which allows selective oxidation at a particular moiety of the molecules, as also validated by the docking studies. The bioelectrode exhibits potential as a biosensor for sensitive detection of the free bilirubin levels in serum samples. Lastly, we have demonstrated a simple paper-based μPED for the detection of bilirubin. The highly conductive, stable graphite ink for the device was prepared by using silk sericin as binder. The working electrode surface modified with *in-situ* synthesized ZnO-NR which provided increased surface for the non-covalent immobilization HSA-AuNC through electrostatic interaction. The dynamic detection range of the sensor covers the concentration of free bilirubin usually present in the blood serum of clinical samples.

A comparative analysis on the performance of the biosensors constructed through this investigation with various prominent non-enzymatic bilirubin sensors reported over the last decade was carried out as shown in table A. The detection limit of the constructed biosensors were sensible for practical utility and a comparable dynamic range to that of previously reported sensors was obtained. Notably, under hyperbilirubinemic conditions, the total serum bilirubin concentrations can reach up to 35 mg dl^{-1} or 0.599 mM. At this concentration, the level of free bilirubin is in the range of 0.3 µM to 2.8 µM (Daood et al., 2009), thus validates the application potential of the constructed device for developing a commercially viable biosensor.

Table A: Comparison on performances of various non enzyme-based bilirubin biosensors

Detection technique	**Detection platform**	**Detection Limit (µM)**	**Linear Range (µM)**	**Sensitivity ($\mu A\ \mu M^{-1}$)**	**Reference**
CAM	Electrochemical (Ferrocene carboximide modified MWCNT/GNP/GCE)	0.12	1-100	0.1336	Wang et al., (2009)
CV	Electrochemical (Nanographite based micro electrode)	NA	Up to 56	0.015	Taurino et al., (2014)
CAM	Electrochemical (GO/Polystyrene sulfonate composite/GCE)	2	Up to 450	0.16	Balamurugan and Berchmans, (2015)
CV	Electrochemical (MWCNT based Screen printed electrode)	4.2	200-500	0.086	Taurino et al., (2013)
SWV	Electrochemical (NF/ER-GO/GCE)	0.84	2-20	NA	Avan et al., (2015)
SWV	Electrochemical (NF/MWCNTs/GCE)	0.014	0.8-10	NA	Filik et al., (2015)
Fluorometric	Fluorescence (Fluorescence quenching of polyfluorene)	0.15	25-50	NA	Senthilkumar and Asha, (2015)
Fluorometric and colorimetric	**Fluorescence (Fluorescence quenching of HSA-AuNC)**	**0.25**	**1-50**	**---**	**Santhosh et al., (2014)**
	Optical (Peroxidase like catalytic activity of HSA-AuNC)	**0.2**	**0.25-2**	**---**	
CA	**Electrochemical (Covalent immobilization of HSA-AuNC on ITO)**	**0.086**	**0.2-7**	**0.34**	**Santhosh et al., (2016)**
DPV	**Electrochemical (HSA-AuNC/ZnO- NR/*µ*PED)**	**0.057**	**0.5 - 35**	**0.019**	**Communicated**

* Few values were normalized for making the units uniform for better comparison. CAM: Chronoamperometric, CV: Cyclic voltammetry, SWV: Square wave voltammetry, DPV: Differential pulse voltammetry, MWCNT: Multi walled carbon nanotube, NF: Nafion, ER-GO: Electrochemically reduced graphene oxide, GCE: Glassy carbon electrode, HSA-AuNC: Human serum albumin stabilized gold nanocluster, ITO: Indium tin oxide, ZnO-NR: Zinc oxide nano rods.

Scope for future work

Following points have been identified as major gap areas from the studies included in this thesis that warrant further investigations for augmenting the concept to develop bilirubin biosensor for practical utility. The detailed molecular mechanism involved in the formation of metal NCs inside protein matrix needs to be elucidated. The developed detection methods need to be improved for the analysis of unaltered serum samples, preferably in a lab-on-chip device, which has potential to clarify the proteinaceous materials and there by support the interference-free detection of free bilirubin. The strategies for preparation of AuNCs in the presence of a small amount of protein needs to be developed. The catalytic role of HSA-AuNC needs further investigation to understand the mechanism being involved. The microfluidic platform design needs further optimization for the sensitive and interference free detection of bilirubin directly in the blood serum.

Bibliography

Bibliography

Ahlfors, C.E., 2000. Measurement of plasma unbound unconjugated bilirubin. Anal. Biochem. 279, 130–135.

Ahlfors, C.E., Vreman, H.J., Wong, R.J., Bender, G.J., Oh, W., Morris, B.H., Stevenson, D.K., 2007. Effects of sample dilution, peroxidase concentration and chloride ion on the measurement of unbound bilirubin in premature newborns. Clin. Biochem. 40, 261–267.

Amazon, K., Soloni, F., Rywlin, A.M., 1981. Separation of bilirubin from hemoglobin by recording derivative spectrophotometry. Am. J. Clin. Pathol. 75, 519–523.

American Academy of Pediatrics Subcommittee on Hyperbilirubinemia., 2004. Management of hyperbilirubinemia in the newborn infants: 35 or more weeks of gestation. Pediatrics. 297–316.

Andreu, Y., Galbán, J., de Marcos, S., Castillo, J.R., 2000. Determination of direct-bilirubin by a fluorimetric-enzymatic method based on bilirubin oxidase. Fresenius. J. Anal. Chem. 368, 516–521.

Andreu, Y., Ostra, M., Ubide, C., Galbán, J., De Marcos, S., Castillo, J.R., 2002. Study of a fluorometric-enzymatic method for bilirubin based on chemically modified bilirubin-oxidase and multivariate calibration. Talanta 57, 343–353.

Arya, S.K., Prusty, A.K., Singh, S.P., Solanki, P.R., Pandey, M.K., Datta, M., Malhotra, B.D., 2007. Cholesterol biosensor based on N-(2-aminoethyl)-3-aminopropyl-trimethoxysilane self-assembled monolayer. Anal. Biochem. 363, 210–218.

Asefa, T., Duncan, C,T., Sharma, K,K., 2009. Recent advances in nanostructured chemosensors and biosensors. Analyst 134 (10), 1980-1990.

Athar, H., Ahmad, N., Tayyab, S., Qasim, M. A, 1999. Use of fluorescence enhancement technique to study bilirubin-albumin interaction. Int. J. Biol. Macromol. 25, 353–358.

Au, L., Lim, B., Colletti, P., Jun, Y.S., Xia, Y., 2010. Synthesis of gold microplates using bovine serum albumin as a reductant and a stabilizer. Chem. - An Asian J. 5, 123–129.

Avan, A., Aydar, S., Filik, H., 2015. Voltammetric sensing of bilirubin based on nafion /electrochemically reduced graphene oxide composite modified glassy carbon electrode. Curr. Anal. Chem. 11, 96–103.

Bae, Z.U., Lee, H.L., Park, T.M., Seo, M.L., 1995. Amperometric determination of bilirubin with flow injection analysis system. Anal. Lett. 28, 1775–1783.

Balamurugan, T., Berchmans, S., 2015. Non-enzymatic detection of bilirubin based on a graphene–polystyrene sulfonate composite. RSC Adv. 5, 50470–50477.

Bard, A. J., Faulkner, L.R., 2000. Electrochemical methods: Fundamentals and applications, John Willey and Sons New York.

Batra, B., Lata, S., Sunny, Rana, J.S., Pundir, C.S., 2013. Construction of an

amperometric bilirubin biosensor based on covalent immobilization of bilirubin oxidase onto zirconia coated silica nanoparticles/chitosan hybrid film. Biosens. Bioelectron. 44, 64–69.

Baydemir, G., Bereli, N., Andaç, M., Say, R., Galaev, I.Y., Denizli, A., 2009. Bilirubin recognition via molecularly imprinted supermacroporous cryogels. Colloids Surfaces B Biointerfaces 68, 33–38.

Bhargava, S.K., Booth, J.M., Agrawal, S., Coloe, P., Kar, G., 2005. Gold nanoparticle formation during bromoaurate reduction by amino acids. Langmuir 21, 5949–5956.

Bhutani, V.K., Gourley, G.R., Adler, S., Kreamer, B., Dalin, C., Johnson, L.H., 2000. Noninvasive measurement of total serum bilirubin in a multiracial predischarge newborn population to assess the risk of severe hyperbilirubinemia. Pediatrics 106, E17.

Bian, W., Zhang, N., Jiang, C., 2011. Spectrofluorimetric determination of bilirubin in serum samples. Luminescence 26, 54–58.

Bian, W., Zhang, N., Wang, L., 2010. Spectrofluorometric determination of total bilirubin in human serum samples using tetracycline-Eu^{3+}. Anal. Sci. 26, 785–789.

Bian, W.W., 2014. Spectrofluorimetric Determination of bilirubin using enoxacine-terbium probe. Appl. Mech. Mater. 556-562, 421–424.

Bijster, P., Vader, H.L., Vink, C.L., 1981. On the standardisation of the direct spectrophotometric bilirubin determination. Influence of the albumin source and the molar bilirubin: albumin ratio. Ann. Clin. Biochem. 18 (2), 102–105.

Bini, R.A., Marques, R.F.C., Santos, F.J., Chaker, J.A., Jafelicci, M., 2012. Synthesis and functionalization of magnetite nanoparticles with different amino-functional alkoxysilanes. J. Magn. Magn. Mater. 324, 534–539.

Blaha, G., Siam, M., Lehner, H., 1997. A circular dichroism (CD) study of the consecutive binding of serum albumin to bilirubin: Possible implications for the bilirubin level. J. Chem. Soc. - Perkin Trans. 2, 2119–2124.

Bonnett, R., Davies, J.E., Hursthouse, M.B., 1976. Structure of bilirubin. Nature 262, 326–328.

Burt, J.L., Gutierrrez-Wing, C., Miki-Yoshida, M., Jose-Yacaman, M., 2004. Noble-metal nanoparticles directly conjugated to globular proteins. Langmuir 20, 11778–11783.

Canbaz, M.Ç., Sezgintürk, M.K., 2014. Fabrication of a highly sensitive disposable immunosensor based on indium tin oxide substrates for cancer biomarker detection. Anal. Biochem. 446, 9–18.

Charbonneau, D., Beauregard, M., Tajmir-Riahi, H.-A., 2009. Structural analysis of human serum albumin complexes with cationic lipids. J. Phys. Chem. B 113, 1777–1784.

Chaudhari, K., Xavier, P.L., Pradeep, T., 2011. Understanding the evolution of luminescent gold quantum clusters in protein templates. ACS Nano 5, 8816–8827.

Chen, L., Wang, C., Yuan, Z., Chang, H., 2015. Fluorescent gold nanoclusters: Recent advances in sensing and imaging. Anal. Chem. 87, 216–229.

Chen, P.C., Chiang, C.K., Chang, H.T., 2013. Synthesis of fluorescent BSA-Au NCs for the detection of Hg^{2+} ions. J. Nanoparticle Res. 15(1), 1-10.

Chen, W., Chen, S., 2009. Oxygen electroreduction catalyzed by gold nanoclusters: Strong core size effects. Angew. Chemie - Int. Ed. 48, 4386–4389.

Chen, Z., Qian, S., Chen, X., Gao, W., Lin, Y., 2012. Protein-templated gold nanoclusters as fluorescence probes for the detection of methotrexate. Analyst 137, 4356–4361.

Cheng, G., Yang, Y., Dong, S., 1994. *In-situ* UV-visible spectroelectrochemical and circular dichroic electrochemical study of bilirubin and bilirubin + human serum albumin complex. Bioelectrochemistry Bioenerg. 34, 141–147.

Cheong, M.G.L., Lim, K.S., Jakubowicz, A., Martens, P.J., Poole-Warren, L.A., Green, R.A., 2014. Conductive hydrogels with tailored bioactivity for implantable electrode coatings. Acta Biomater. 10, 1216–1226.

Chinnadayyala, S.R., Santhosh, M., Singh, N.K., Goswami, P., 2015. Alcohol oxidase protein mediated *in-situ* synthesized and stabilized gold nanoparticles for developing amperometric alcohol biosensor. Biosens. Bioelectron. 69, 151–161.

Cho, K.Y., Moon, J.Y., Lee, Y.W., Lee, K.G., Yeo, J.H., Kweon, H.Y., Kim, K.H., Cho, C.S., 2003. Preparation of self-assembled silk sericin nanoparticles. Int. J. Biol. Macromol. 32, 36–42.

Chou, S.-K., Syu, M.-J., 2009. Via zinc(II) protoporphyrin to the synthesis of poly(ZnPP-MAA-EGDMA) for the imprinting and selective binding of bilirubin. Biomaterials 30, 1255–1262.

Cui, M.L., Liu, J.M., Wang, X.X., Lin, L.P., Jiao, L., Zheng, Z.Y., Zhang, L.H., Jiang, S.L., 2013. A promising gold nanocluster fluorescent sensor for the highly sensitive and selective detection of S^{2-}. Sensors Actuators, B Chem. 188, 53–58

Daka, N.J., Sipehia, R., Chang, T.M.S., 1989. Enhanced oxidation of bilirubin by an immobilized tri-enzyme system of glucose oxidase, bilirubin oxidase and horseradish peroxidase. Biochim. Biophys. Acta 991, 487–489.

Daniel, M.C., Astruc, D., 2004. Gold Nanoparticles: Assembly, supramolecular chemistry, quantum-size-related properties and applications toward biology, catalysis and nanotechnology. Chem. Rev. 104 (1), 293-246.

Daood, M.J., McDonagh, A.F., Watchko, J.F., 2009. Calculated free bilirubin levels and neurotoxicity. J. Perinatol. 29, S14–S19.

Das, P., Barbora, L., Das, M., Goswami, P., 2014. Highly sensitive and stable laccase based amperometric biosensor developed on nano-composite matrix for detecting

pyrocatechol in environmental samples. Sensors Actuators B Chem. 192, 737–744.

De, M., Ghosh, P.S., Rotello, V.M., 2008. Applications of nanoparticles in biology. Adv. Mater. 20, 4225–4241.

DeLano, W.L., 2002. The PyMOL molecular graphics system, version 1.1. Schrödinger LLC http://www.pymol.org.

Desmet, C., Marquette, C.A., Blum, L.J., Doumèche, B., 2016. Paper electrodes for bioelectrochemistry: Biosensors and biofuel cells. Biosens. Bioelectron. 76, 145–63.

Dickerson, M.B., Sandhage, K.H., Naik, R.R., 2008. Protein- and peptide-directed syntheses of inorganic materials. Chem. Rev. 108, 4935–4978.

Doumas, B.T., 1986. Bilirubin assay. US patent no. 4,563,429.

Doumas, B.T., Perry, B., Jendrzejczak, B., Davis, L., 1987. Measurement of direct bilirubin by use of bilirubin oxidase. Clin. Chem. 33, 1349–1353.

Doumas, B.T., Poon Pat K-C, Perry, B.W., JendrzeJczak, B., McComb, R.B., Schaffer, R., Hause, L.L., 1985. Candidate reference method for determination of total bilirubin in serum: Development and validation. Clin. Chem. 31, 1779–1789.

Dungchai, W., Chailapakul, O., Henry, C.S., 2009. Electrochemical detection for paper-based microfluidics. Anal. Chem. 81, 5821–5826.

Eftink, M. R., Ghiron, C. A., 1976. Fluorescence techniques for studying protein structure. Biochemistry 15, 672–680.

Elliott, J.A., Shibuta, Y., Wales, D.J., 2009. Global minima of transition metal clusters described by Finnis–Sinclair potentials: A comparison with semi-empirical molecular orbital theory. Philos. Mag. 89, 3311-3332.

Feng, Q., Du, Y., Zhang, C., Zheng, Z., Hu, F., Wang, Z., Wang, C., 2013. Synthesis of the multi-walled carbon nanotubes-COOH/graphene/gold nanoparticles nanocomposite for simple determination of bilirubin in human blood serum. Sensors Actuators B Chem. 185, 337–344.

Filik, H., Avan, A., Aydar, S., 2015. Nafion/multi-wall carbon nanotubes composite modified glassy carbon electrode for sensitive determination of bilirubin. Curr. Nanosci. 11, 784–791.

Fortuney, A., Guilhault, G.G., 1996. Enzyme electrode for the determination of bilirubin. Electroanalysis 8, 3–6.

Fowweather, F.S., 1932. Bilirubin and the van den Bergh reaction. Biochem. J. 26, 165–182.

Geddes, C.D., 2014. Metal enhanced fluorescence- based sensing methods. US patent no. 8,759,110 B2.

Goldfinch, E.M., Maguire, A.G., 1988. Investigation of the use of bilirubin oxidase to measure the apparent unbound bilirubin concentration in human plasma. Ann. Clin. Biochem. 25, 73–77.

Goncharova, I., Orlov, S., Urbanová, M., 2013. The location of the high- and low-affinity bilirubin-binding sites on serum albumin : Ligand-competition analysis investigated by circular dichroism. Biophys. Chem. 180-181, 55–65.

Gordon, E.R., Goresky, C.A., 1982. A rapid and quantitative high performance liquid chromatographic method for assaying bilirubin and its conjugates in bile. Can. J. Biochem. 60, 1050–1057.

Goresky, C.A., Gordon, E.R., 1990. High-performance liquid chromatographic separation of bilirubin conjugates : The effects of change in molarity and pH. J. Chromatogr. 528, 123–141.

Greenfield, N., 2007. Using circular dichroism spectra to estimate protein secondary structure. Nat. Protoc. 1, 2876–2890.

Grohmann, K., Roser, M., Rolinski, B., Kadow, I., Muller, C., Goerlach-Graw, A., Nauck, M., Kuster, H., 2006. Bilirubin measurement for neonates: Comparison of 9 frequently used methods. Pediatrics 117, 1174–1183.

Guan, G., Zhang, S.-Y., Cai, Y., Liu, S., Bharathi, M.S., Low, M., Yu, Y., Xie, J., Zheng, Y., Zhang, Y.-W., Han, M.-Y., 2014. Convenient purification of gold clusters by co-precipitation for improved sensing of hydrogen peroxide, mercury ions and pesticides. Chem. Commun. 50, 5703–5705.

Heinemann, B.G., Vogt, W., 1988. The determination of bilirubin with a new enzymatic method (Dri-STAT ® Bilirubin) using the Hitachi 704 selective analyzer. J. Clin. Chem. Clin. Biochem. 26, 391–397.

Hertz, H., Dybkær, R., Lauritzen, M., 1974. Direct spectrometric determination of the concentration of bilirubins in serum. Scand. J. Clin. Lab. Invest. 33, 215–230.

Herzing, A.A., Kiely, C.J., Carley, A.F., Landon, P., Hutchings, G.J., 2008. Identification of active gold nanoclusters on iron oxide supports for CO oxidation. Science 321, 1331–1335.

Hladilkova, J., Callisen, T.H., Lund, M., 2016. Lateral protein interactions at hydrophobic and charged surfaces as a function of pH and salt concentration. J. Phys. Chem. B 120 (13), 3303–3310.

Holtrop, P., Maisels, M., 1996. Hyperbilirubinemia. In: Spitzer A.R, editor. Intensive care of the fetus and neonate. St Louis: Mosby , 888–898.

Homsher, R., Chu, J.-W., 1983. A spectrophotometric study on the interaction of hemoglobin in a diazo coupling reaction of neonatal bilirubin. Microchem. J. 28, 250–262.

Hu, L., Han, S., Parveen, S., Yuan, Y., Zhang, L., Xu, G., 2012. Highly sensitive fluorescent detection of trypsin based on BSA-stabilized gold nanoclusters. Biosens. Bioelectron. 32, 297–299.

Huang, C.Y., Syu, M.J., Chang, Y.S., Chang, C.H., Chou, T.C., Liu, B.D., 2007. A portable potentiostat for the bilirubin-specific sensor prepared from molecular

imprinting. Biosens. Bioelectron. 22, 1694–1699.

Huber, A.H., Zhu, B., Kwan, T., Kampf, J.P., Hegyi, T., Kleinfeld, A.M., 2012. Fluorescence sensor for the quantification of unbound bilirubin concentrations. Clin. Chem. 58, 869–876.

Ihara, H., Aoki, Y., Aoki, T., Yoshida, M., 1990. Light has a greater effect on direct bilirubin measured by the bilirubin oxidase method than by the diazo method. Clin. Chem. 36, 895–897.

Itoh, S., Kawada, K., Kusaka, T., Yasuda, S., Okada, H., Imai, T., Isobe, K., 2002. Influence of glucuronosyl bilirubin and (EZ) -cyclobilirubin on determination of serum unbound bilirubin by UB-analyser. Assos. Clin. Biochem. 39, 583–588.

Jacobsen, J., Brodersen, R., 1983. Albumin-bilirubin binding mechanism. J. Biol. Chem. 258, 6319–6326.

Jacobsen, J., Wennberg, R.P., 1974. Determination of unbound bilirubin in the serum of newborns. Clin. Chem. 20, 783–789.

Jendrassik, L., Grof, P., 1938. Vereinfachte photometrische methoden zur bestimmung des bilirubins. Biochem. Z. 297, 81-89.

Jin, L., Shang, L., Guo, S., Fang, Y., Wen, D., Wang, L., Yin, J., Dong, S., 2011. Biomolecule-stabilized Au nanoclusters as a fluorescence probe for sensitive detection of glucose. Biosens. Bioelectron. 26, 1965–1969.

Jin, W., Zhao, X., Ding, C., Wang, F., Gao, Z., 1992. Investigation in bioanalytical chemistry: Differential pulse adsorption voltammetry of bilirubin. Anal. Chim. Acta 268, 185–188.

Kakoti, A., Siddiqui, M.F., Goswami, P., 2015. A low cost design and fabrication method for developing a leak proof paper based microfluidic device with customized test zone. Biomicrofluidics 9, 1-10.

Kamruzzaman, M., Alam, A.M., Hak Lee, S., Ho Kim, Y., Kim, G.M., Hyub Oh, S., 2012. Spectrofluorimetric quantification of bilirubin using yttrium-norfloxacin complex as a fluorescence probe in serum samples. J. Lumin. 132, 3053–3057.

Kang, J., Liu, Y., Xie, M.-X., Li, S., Jiang, M., Wang, Y.-D., 2004. Interactions of human serum albumin with chlorogenic acid and ferulic acid. Biochim. Biophys. Acta 1674, 205–214.

Kannan, P., Chen, H., Lee, V.T.W., Kim, D.H., 2011. Highly sensitive amperometric detection of bilirubin using enzyme and gold nanoparticles on sol-gel film modified electrode. Talanta 86, 400–407.

Kerman, K., Saito, M., Yamamura, S., Takamura, Y., Tamiya, E., 2008. Nanomaterial-based electrochemical biosensor for medical applications. Tr. Anal. Chem. 27(7). 585-592.

Khan, M.A., Kumar, Y., Tayyab, S., 2002. Bilirubin binding properties of pigeon serum

albumin and its comparison with human serum albumin. Int. J. Biol. Macromol. 30, 171–178.

Kitsommart, R., Pornladnun, P., Chomchai, C., Urujchutchairut, P., Paes, B., 2013. Accuracy and precision of transcutaneous bilirubinometry in postdischarge Asian neonates. Eur. J. Pediatr. 172, 781–786.

Klemm, J., Prodromidis, M.I., Karayannis, M.I., 2000. An Enzymic Method for the Determination of Bilirubin Using an Oxygen Electrode. Electroanalysis 12, 292–295.

Koch, T.R., Aklngbe, O., 1981. Feasibility of measuring free and total bilirubin electrochemically in serum. Clin. Chem. 27 (7), 1295–1299.

Kohashi, K., Date, Y., Morita, M., Tsuruta, Y., 1998. Fluorescence reaction of bilirubin with zinc ion in dimethyl sulfoxide and its application to assay of total bilirubin in serum. Anal. Chim. Acta 365, 177–182.

Kosaka, A., Yamamoto, C., Morishita, Y., Nakane, K., 1987. Enzymatic determination of bilirubin fractions in serum. Clin. Biochem. 20, 451–458.

Kumar, S.S., Kwak, K., Lee, D., 2011. Electrochemical sensing using quantum-sized gold nanoparticles. Anal. Chem. 83, 3244–3247.

Kurosaka, K., Senba, S., Tsubota, H., Kondo, H., 1998. A new enzymatic assay for selectively measuring conjugated bilirubin concentration in serum with use of bilirubin oxidase. Clin. Chim. Acta 269, 125–136.

Kwak, K., Kumar, S.S., Pyo, K., Lee, D., 2014. Ionic liquid of a gold nanocluster: A versatile matrix for electrochemical biosensors. ACS Nano 8, 671–679.

Lamola, A.A., Eisinger, J., Blumberg, W.E., Patel, S.C., Flores, J., 1979. Fluorometric study of the partition of bilirubin among blood components: Basis for rapid microassays of bilirubin and bilirubin binding capacity in whole blood. Anal. Biochem. 100, 25–42.

Lan, G.-Y., Chen, W.-Y., Chang, H.-T., 2011. One-pot synthesis of fluorescent oligonucleotide Ag nanoclusters for specific and sensitive detection of DNA. Biosens. Bioelectron. 26, 2431–2435.

Lauff, J.J., Kasper, M.E., Ambrose, R.T., 1983. Quantitative liquid-chromatographic estimation of bilirubin species in pathological serum. Clin. Chem. 29, 800–805.

Lauff, J.J., Kasper, M.E., Ambrose, R.T., 1981. Separation of bilirubin species in serum and bile by high- performance reversed-phase liquid chromatography. J.Chromatogr. 226, 391–402.

Lee, D., Donkers, R.L., Wang, G., Harper, A.S., Murray, R.W., 2004. Electrochemistry and optical absorbance and luminescence of molecule-like Au_{38} nanoparticles. J. Am. Chem. Soc. 126, 6193–6199.

Lee, S.H., Karim, M.M., Seikh, A.M., Sang, L.H., 2007. Quantitative determination of bilirubin by inhibition of chemiluminescence from lucigenin. Luminescence 22, 331–

337.

Levine, R,L., 1977. Fluorescence-quenching studies of the binding of bilirubin to albumin. Clin. Chem. 23, 2292-2301.

Li, F., Lim, K., Peters, T., 1986. Reverse phase HPLC of conjugated and unconjugated bilirubins in body fluids. J. Chromatogr. 353, 19–26.

Li, P.H., Lin, J.Y., Chen, C.T., Ciou, W.R., Chan, P.H., Luo, L., Hsu, H.Y., Diau, E.W.G., Chen, Y.C., 2012. Using gold nanoclusters as selective luminescent probes for phosphate-containing metabolites. Anal. Chem. 84, 5484–5488.

Li, X., Ballerini, D.R., Shen, W., 2012. A perspective on paper-based microfluidics: Current status and future trends. Biomicrofluidics 6, 12–14.

Li, X., Fortuney, A., Guilbault, G.G., Suleiman, A.A., 1996. Determination of bilirubin by fiberoptic biosensor. Anal. Lett. 29, 171–180.

Li, X., Rosenzweig, Z., 1997. A fiber optic sensor for rapid analysis of bilirubin in serum. Anal. Chim. Acta 353, 263–273.

Li, X., Tian, J., Garnier, G., Shen, W., 2010. Fabrication of paper-based microfluidic sensors by printing. Colloids Surfaces B Biointerfaces 76, 564–570.

Liang, L., Tajmir-Riahi, H. A, Subirade, M., 2008. Interaction of β-lactoglobulin with resveratrol and its biological implications. Biomacromolecules 9, 50–56.

Lightner, D. A., 2013. Bilirubin: Jekyll and Hyde Pigment of Life. Springer-Verlag Wein

Lim, C.K., 1979. The separation of conjugated and unconjugated bilirubin in bile by high-performance liquid chromatography. J. Liq. Chromatogr. 2, 37–43.

Lim, C.K., Bull, R.V.A., Rideout, J.M., 1981. High-performance liquid chromatography of bile pigments. J. Chromatogr. A 204, 219–223.

Lin, J.P., Vitek, L., Schwertner, H. A., 2010. Serum bilirubin and genes controlling bilirubin concentrations as biomarkers for cardiovascular disease. Clin. Chem. 56, 1535–1543.

Longhi, P., Mussini, T., Rondinini, S., Dada, G., Paolo, M., Diego, M., 1987. A study of the elctrochemical reduction of bilirubin and its derivatives. Bioelectrochemistry Bioenerg. 17, 101–104.

Lopez-Acevedo, O., Kacprzak, K.A., Akola, J., Häkkinen, H., 2010. Quantum size effects in ambient CO oxidation catalysed by ligand-protected gold clusters. Nat. Chem. 2, 329–334.

Lu, D., Liu, L., Li, F., Shuang, S., Li, Y., Choi, M.M.F., Dong, C., 2014. Lysozyme-stabilized gold nanoclusters as a novel fluorescence probe for cyanide recognition. Spectrochim. Acta - Part A Mol. Biomol. Spectrosc. 121, 77–80.

Malloy, H.T., Evelyn, K., 1936. The determination of bilirubin with the photoelectric colorimeter. J. Biol. Chem. 119, 481–490.

Manekkathodi, A., Lu, M.Y., Wang, C.W., Chen, L.J., 2010. Direct growth of aligned zinc oxide nanorods on paper substrates for low-cost flexible electronics. Adv. Mater. 22, 4059–4063.

Martelanc, M., Žiberna, L., Passamonti, S., Franko, M., 2014. Direct determination of free bilirubin in serum at sub-nanomolar levels. Anal. Chim. Acta 809, 174–182.

Martinez, A., Phillips, S., Wiley, B., Gupta, M., Whitesides, G., 2008. FLASH: A rapid method for prototyping paper-based microfluidic devices. Lab Chip 9, 2477–2483.

Matui, Y., Yoshihara, Y., Yaniguti, T., 1985. Japanese Kokai Tokyo Koho 60, 110290.

Min, J., Meng-Xia, X., Dong, Z., Yuan, L., Xiao-Yu, L., Xing, C., 2004. Spectroscopic studies on the interaction of cinnamic acid and its hydroxyl derivatives with human serum albumin. J. Mol. Struct. 692, 71–80.

Minomo, A., Ishima, Y., Kragh-hansen, U., Chuang, V.T.G., Uchida, M., 2011. Biological characteristics of two lysines on human serum albumin in the high-affinity binding of 4Z, 15Z -bilirubin-IX a revealed by phage display. FEBS J. 278, 4100–4111.

Monacelli, F., Storace, D., D'Arrigo, C., Sanguineti, R., Borghi, R., Pacini, D., Furfaro, A.L., Pronzato, M.A., Odetti, P., Traverso, N., 2013. Structural alterations of human serum albumin caused by glycative and oxidative stressors revealed by circular dichroism analysis. Int. J. Mol. Sci. 14, 10694–10709.

Moosavi-Movahedi, Z., Bahrami, H., Zahedi, M., Mahnam, K., Chamani, J., Safarian, S., Saboury, A. A., Moosavi-Movahedi, A. A., 2007. A theoretical elucidation of bilirubin interaction with HSA's lysines: First electrostatic binding site in IIA subdomain. Biophys. Chem. 125, 375–387.

Mudedla, S.K., Singam, E.R.A., Sundar, J.V., Pedersen, M.N., Murugan, N.A., Kongsted, J., Ågren, H., Subramanian, V., 2015. Enhancement of internal motions of lysozyme through interaction with gold nanoclusters and its optical imaging. J. Phys. Chem. C 119, 653–664.

Mullon, C.J.P., Langer, R., 1987. Determination of conjugated and total bilirubin in serum of neonates, with use of bilirubin oxidase. Clin. Chem. 33, 1822–1825.

Muraca, M., Blanckaert, N., 1983. Liquid-chromatographic assay and identification of mono- and diester conjugates of bilirubin in normal serum. Clin. Chem. 29, 1767–1771.

Murao, S., Tanaka, N., 1981. A new enzyme " Bilirubin Oxidase " produced by *Myrothecium verrucaria*. Agric. Biol. Chem. 45, 2383–2384.

Na, S.-I., Kim, S.-S., Jo, J., Kim, D.-Y., 2008. Efficient and flexible ITO-free organic solar cells using highly conductive polymer anodes. Adv. Mater. 20, 4061–4067

Nagaoka, S., Cowger, M., 1979. Method to determine total and free serum bilirubin. Anal. Biochem. 96, 364–377.

Nakayama, K., 1995. Differences between enzymatic and diazo methods for measuring direct Bilirubin. Clin. Chem. Lab. Med. 33, 513–518.

Nie, Z., Nijhuis, C.A., Gong, J., Chen, X., Kumachev, A., Martinez, A.W., Narovlyansky, M., Whitesides, G.M., 2010. Electrochemical sensing in paper-based microfluidic devices. Lab Chip 10, 477–83.

Noh, H.-B., Won, M.-S., Shim, Y.-B., 2014. Selective nonenzymatic bilirubin detection in blood samples using a Nafion/Mn–Cu sensor. Biosens. Bioelectron. 61, 554–561.

Noiphung, J., Songjaroen, T., Dungchai, W., Henry, C.S., Chailapakul, O., Laiwattanapaisal, W., 2013. Electrochemical detection of glucose from whole blood using paper-based microfluidic devices. Anal. Chim. Acta 788, 39–45.

Oh, W., Stevenson, D.K., Tyson, J.E., Morris, B.H., Ahlfors, C.E., Bender, G.J., Wong, R.J., Perritt, R., Vohr, B.R., van Meurs, K.P., Vreman, H.J., Das, A., Phelps, D.L., O'Shea, T.M., Higgins, R.D., 2010. Influence of clinical status on the association between plasma total and unbound bilirubin and death or adverse neuro-developmental outcomes in extremely low birth weight infants. Acta Paediatr. 99, 673- 678.

Onks, D., Silverman, L., Robertson, A., 1993. Effect of melanin, oxyhemoglobin and bilirubin on transcutaneous bilirubinometry. Acta Paediatr. 82, 19–21.

Orlov, S., Goncharova, I., Urbanová, M., 2014. Circular dichroism study of the interaction between mutagens and bilirubin bound to different binding sites of serum albumins. Spectrochim. Acta - Part A Mol. Biomol. Spectrosc. 126, 68–75.

Osawa, S., Sugo, S., Yoshida, T., Yamaoka, T., Nomura, F., 2006. An assay for separating and quantifying four bilirubin fractions in untreated human serum using isocratic HPLC. Clin. Chim. Acta 366, 146–155.

Otsuji, S., Mizuno, K., Ito, S., Kawahara, S., Kai, M., 1988. A new enzymatic approach for estimating total and direct bilirubin. Clin. Biochem. 21, 33–38.

Palilis, L.P., Calokerinos, A.C., Grekas, N., 1996. Chemiluminescence arising from the oxidation of bilirubin in aqueous media. Anal. Chim. Acta 333, 267–275.

Peeling, R., Holmes, K., Mabey, D., Ronald, A., 2006. Rapid tests for sexually transmitted infections (STIs): the way forward. Sex. Transm. Infect 82, 1–6.

Petersen, C.E., Ha, C.E., Harohalli, K., Feix, J.B., Bhagavan, N. V, 2000. A dynamic model for bilirubin binding to human serum albumin. J. Biol. Chem. 275, 20985–20995.

Plavskii, V.Y., Mostovnikov, V.A., Mostovnikova, G.R., Tretyakova, A.I., 2007. Spectral fluorescence and polarization characteristics of Z,Z-bilirubin IXα. J. Appl. Spectrosc. 74, 120–132.

Pielichowski, K., Flejtuch, K., 2002. Differential scanning calorimetry studies on poly(ethylene glycol) with different molecular weights for thermal energy storage materials. Polym. Adv. Technol. 13, 690–696.

Priya, C., Sivasankari, G., Sriman Narayanan, S., 2012. Electrochemical behavior of azure A/gold nanoclusters modified electrode and its application as non-enzymatic hydrogen peroxide sensor. Colloids Surfaces B Biointerfaces 97, 90–96.

Rahman, M., Laurent, S., Tawil, N., Yahia, L.H., 2013. Protein- nanoparticle interactions. Martinac, B. editor, Springer.

Rahman, M.A., Lee, K.S., Park, D.S., Won, M.S., Shim, Y.B., 2008. An amperometric bilirubin biosensor based on a conductive poly-terthiophene-Mn(II) complex. Biosens. Bioelectron. 23, 857–864.

Rana, S., Yeh, Y.-C., Rotello, V.M., 2010. Engineering the nanoparticle–protein interface: Applications and possibilities. Curr. Opin. Chem. Biol. 14, 828–834.

Rangnekar, A., Sarma, T.K., Singh, A.K., Deka, J., Ramesh, A., Chattopadhyay, A., 2007. Retention of enzymatic activity of α-amylase in the reductive synthesis of gold nanoparticles. Langmuir 23, 5700–5706.

Robertson, A., Kazmierczak, S., Vos, P., 2002. Improved transcutaneous bilirubinometry: comparison of SpectR_X Bili*Check* and Minolta jaundice meter JM-102 for estimating total serum bilirubin in a normal newborn population. J. Perinatol. 22, 12.

Rockwood, D.N., Preda, R.C., Yucel, T., Wang, X., Lovett, M.L., Kaplan, D.L., 2011. Materials fabrication from *Bombyx mori* silk fibroin. Nat. Protoc. 6, 1612–1631.

Roca, L., Calligaris, S., Wennberg, R.P., Ahlfors, C.E., Malik, S.G., Ostrow, J.D., Tiribelli, C., 2006. Factors affecting the binding of bilirubin to serum albumins: Validation and application of the peroxidase method. Pediatr. Res. 60, 724–728.

Ronkainen, N.J., Halsall, H.B., Heineman, W.R., 2010. Electrochemical biosensors. Chem. Soc. Rev. 39, 1747–1763.

Roy-Chowdhury, N., Lu, Y., Roy-Chowdhury, J., 2004. Bilirubin in medical history: Formation and sources of bilirubin. Biochem. J. 5, 165–174.

Santhosh, M., Chinnadayyala, S.R., Kakoti, A., Goswami, P., 2014. Selective and sensitive detection of free bilirubin in blood serum using human serum albumin stabilized gold nanoclusters as fluorometric and colorimetric probe. Biosens. Bioelectron. 59, 370–376.

Santhosh, M., Chinnadayyala, S.R., Singh, N.K., Goswami, P., 2016. Human serum albumin-stabilized gold nanoclusters act as an electron transfer bridge supporting specific electrocatalysis of bilirubin useful for biosensing applications. Bioelectrochemistry 111, 7–14.

Sato, H., Honore, B., Brodersen, R., 1988. Multiple binding of bilirubin to human serum albumin and co-binding with laurate. Arch. Biochem. Biophys. 260, 811–821.

Saxena, U., Chakraborty, M., Goswami, P., 2011. Covalent immobilization of cholesterol oxidase on self-assembled gold nanoparticles for highly sensitive amperometric detection of cholesterol in real samples. Biosens. Bioelectron. 26, 3037–3043.

Scharschmidt, B.., Blanckaert, N., Farina, F.., Kabra, P.., Stafford, B.., Weisiger, R.., 1982. Measurement of serum bilirubin and its mono- and diconjugates : application to patients with hepatobiliary disease . Gut 23, 643–649.

Senthilkumar, T., Asha, S.K., 2015. Selective and sensitive sensing of free bilirubin in human serum using water-soluble polyfluorene as fluorescent probe. Macromolecules 48, 3449–3461.

Senthilkumar, T., Asha, S.K., 2013. Self-assembly in tailor-made polyfluorenes: Synergistic effect of porous spherical morphology and FRET for visual sensing of bilirubin. Macromolecules 46, 2159–2171.

Shao, Y., Jin, Y., Dong, S., 2004. Synthesis of gold nanoplates by aspartate reduction of gold chloride. Chem. Commun. 1104–1105.

Shang, L., Yang, L., Stockmar, F., Popescu, R., Trouillet, V., Bruns, M., Gerthsen, D., Nienhaus, G.U., 2012. Microwave-assisted rapid synthesis of luminescent gold nanoclusters for sensing Hg^{2+} in living cells using fluorescence imaging. Nanoscale 4, 4155-4160.

Sheldon, R. A, 2007. Enzyme immobilization: The quest for optimum performance. Adv. Synth. Catal. 349, 1289–1307.

Shoham, B., Migron, Y., Riklin, A., Willner, I., Tartakovsky, B., 1995. A bilirubin biosensor based on a multilayer network enzyme electrode. Biosens. Bioelectron. 10, 341–352.

Şimşek, Ç.S., Teke, M., Sezgintürk, M.K., 2014. An ITO based disposable biosensor for ultrasensitive analysis of retinol binding protein. Electroanalysis 26, 328–339.

Singh, J., Bowers, L., 1985. Quantitative fractionation of serum bilirubin species by reversed-phase high-performance liquid chromatography. J. Biol. Chem. 380, 321–330.

Slifstein, C., Ariel, M., 1977. pH eefects on the reduction of bilirubin in aqueous media. J. Electroanal. Chem. 75, 551–564.

Slusher, T.M., Zipursky, A., Bhutani, V.K., 2011. A global need for affordable neonatal jaundice technologies. Semin. Perinatol. 35, 185–191.

Song, M.J., Yun, D.H., Min, N.K., Hong, S.I., 2007. Electrochemical biosensor array for liver diagnosis using a silanization technique on nano-porous silicon electrode. J. Biosci. Bioeng. 103, 32–37.

Spivak, W., Careyt, M.C., 1985. Reverse-phase HPLC separation, quantification and preparation of bilirubin and its conjugates from native bile. Biochem. J. 225, 787–805.

Sticova, E., Jirsa, M., 2013. New insights in bilirubin metabolism and their clinical implications. World J. Gastroenterol. 19, 6398–407.

Stocker, R., Yamamoto, Y., McDonagh, A.F., Glazer, A.N., Ames, B.N., 1987. Bilirubin

is an antioxidant of possible physiological importance. Science 235, 1043–1046.

Sung, C., Lavin, A., Klibanov, A.M., Langer, R., 1986. An immobilized enzyme reactor for the detoxification of bilirubin. Biotechnol. Bioeng. 28, 1531–1539.

Syu, M.-J., Deng, J.-H., Nian, Y.-M., Chiu, T.-C., Wu, A.-H., 2005. Binding specificity of α-bilirubin-imprinted poly(methacrylic acid-co-ethylene glycol dimethylacrylate) toward α-bilirubin. Biomaterials 26, 4684–4692.

Syu, M.-J., Nian, Y.-M., Chang, Y.-S., Lin, X.-Z., Shiesh, S.-C., Chou, T.-C., 2006. Ionic effect on the binding of bilirubin to the imprinted poly(methacrylic acid-co-ethylene glycol dimethylacrylate). J. Chromatogr. A 1122, 54–62.

Taboada, P., Gutiérrez-Pichel, M., Mosquera, V., 2004. Effects of the molecular structure of two amphiphilic antidepressant drugs on the formation of complexes with human serum albumin. Biomacromolecules 5, 1116–1123.

Taurino, I., Van Hoof, V., Arnaud, M., Laszlo, F., De Micheli, G., Carrara, S., 2014. Efficient voltammetric discrimination of free bilirubin from uric acid and ascorbic acid by a CVD nanographite-based microelectrode. Talanta 130, 423–426.

Taurino, I., Van Hoof, V., De Micheli, G., Carrara, S., 2013. Superior sensing performance of multi-walled carbon nanotube-based electrodes to detect unconjugated bilirubin. Thin Solid Films 548, 546–550.

Tenhunen, R., Marver, H.S., Schmid, R., 1969. Microsomal heme oxygenase. Characterization of the enzyme. J. Biol. Chem. 244, 6388–6394.

Tenhunen, R., Ross, M.E., Marver, H.S., Schmid, R., 1970. Reduced nicotinamide-adenine dinucleotide phosphate dependent biliverdin reductase: Partial purification and characterization. Biochemistry 9, 298–303.

Thévenot, D.R., Toth, K., Durst, R.A., Wilson, G.S., 2001. Electrochemical biosensors: Recommended definitions and classification. Biosens. Bioelectron. 16, 121–131.

Uesugi, T., Adachi, S., Kamisaka, K., 1983. Separation of bilirubin isomers and their conjugates by high- performance reversed-phase liquid chromatography. J.Chromatogr. 277, 308–313.

Valeur, B., 2001. Molecular fluorescence: Principles and applications. Wiley-VCH Verlag GmbH.

Van Norman, J.D., Szentirmay, R., 1974. Chemistry of bilirubin and biliverdin in N,N-dimethylformamide. Anal. Chem. 46, 1456–1464.

Vasapollo, G., Sole, R. Del, Mergola, L., Lazzoi, M.R., Scardino, A., Scorrano, S., Mele, G., 2011. Molecularly imprinted polymers: Present and future prospective. Int. J. Mol. Sci. 12, 5908–5945.

Wang, C., Feng, L., Li, W., Zheng, J., Tian, W., Li, X., 2012. Shape-stabilized phase change materials based on polyethylene glycol/porous carbon composite: The influence of the pore structure of the carbon materials. Sol. Energy Mater. Sol. Cells

105, 21–26.

Wang, C., Wang, G., Fang, B., 2009. Electrocatalytic oxidation of bilirubin at ferrocenecarboxamide modified MWCNT-gold nanocomposite electrodes. Microchim. Acta 164, 113–118.

Wang, X.X., Wu, Q., Shan, Z., Huang, Q.M., 2011. BSA-stabilized Au clusters as peroxidase mimetics for use in xanthine detection. Biosens. Bioelectron. 26, 3614–3619.

Wang, G.L., Jin, L.Y., Dong, Y.M., Wu, X.M., Li, Z.J., 2015. Intrinsic enzyme mimicking activity of gold nanoclusters upon visible light triggering and its application for colorimetric trypsin detection. Biosens. Bioelectron. 64, 523–529.

Wang, J., Luo, D.., Farias, P.A.., 1985. Determination of bilirubin by adsorptive stripping voltammetry.. J. Electroanal. Chem 185, 61–71.

Wang, J., Ozsoz, M.M., 1990. A polishable amperometric biosensor for bilirubin. Electroanalysis 2, 647–650.

Wang, Y.Q., Zhao, T., He, X.W., Li, W.Y., Zhang, Y.K., 2014. A novel core-satellite CdTe/Silica/Au NCs hybrid sphere as dual-emission ratiometric fluorescent probe for Cu^{2+}. Biosens. Bioelectron. 51, 40–46.

Wang, J.X., Sun, X.W., Wei, A., Lei, Y., Cai, X.P., Li, C.M., Dong, Z.L., 2006. Zinc oxide nanocomb biosensor for glucose detection. Appl. Phys. Lett. 88, 4–7.

Watson, D., 1961. Analytic methods for bilirubin in blood plasma. Clin. Chem. 7, 603–625.

Weintraub, B., Zhou, Z., Li, Y., Deng, Y., 2010. Solution synthesis of one-dimensional ZnO nanomaterials and their applications. Nanoscale 2, 1573–1587.

Wells, R., Drew, J.H., Hammond, K.B., 1981. Bilirubin binding capacity and free bilirubin concentration: fluorescence quenching compared with peroxidase oxidation and Sephadex column elution techniques. Clin. Chim. Acta 116, 69–79.

Wen, F., Dong, Y., Feng, L., Wang, S., Zhang, S., Zhang, X., 2011. Horseradish peroxidase functionalized fluorescent gold nanoclusters for hydrogen peroxide sensing. Anal. Chem. 83, 1193–1196.

Wennberg, R.P., Ahlfors, C.E., Aravkin, A.Y., 2009. Intervention guidelines for neonatal hyperbilirubinemia: an evidence based quagmire. Curr. Pharm. Des. 15. 2939-2945.

Wojtoniszak, M., Chen, X., Kalenczuk, R.J., Wajda, A., Łapczuk, J., Kurzewski, M., Drozdzik, M., Chu, P.K., Borowiak-Palen, E., 2012. Synthesis, dispersion, and cytocompatibility of graphene oxide and reduced graphene oxide. Colloids Surfaces B Biointerfaces 89, 79–85.

Xavier, P.L., Chaudhari, K., Verma, P.K., Pal, S.K., Pradeep, T., 2010. Luminescent quantum clusters of gold in transferrin family protein, lactoferrin exhibiting FRET. Nanoscale 2, 2769–2776.

Xie, J., Zheng, Y., Ying, J.Y., 2009. Protein-directed synthesis of highly fluorescent gold

nanoclusters. J. Am. Chem. Soc. 131, 888–889.

Yamashita, M., Adachi, Y., Yamamoto, T., 1986. Analysis of bilirubin conjugates in human bile by column liquid chromatography. J. Chromatogr. 375, 386–391.

Yan, L., Cai, Y., Zheng, B., Yuan, H., Guo, Y., Xiao, D., Choi, M.M.F., 2012. Microwave-assisted synthesis of BSA-stabilized and HSA-protected gold nanoclusters with red emission. J. Mater. Chem. 22, 1000-1005.

Yang, Y., Long, Y., Cao, Q., Li, K., Liu, F., 2007. Molecularly imprinted polymer using β-cyclodextrin as functional monomer for the efficient recognition of bilirubin. Anal. Chim. Acta 6, 92–97.

Yang, G.-H., Shi, J.-J., Wang, S., Xiong, W.-W., Jiang, L.-P., Burda, C., Zhu, J.-J., 2013a. Fabrication of a boron nitride-gold nanocluster composite and its versatile application for immunoassays. Chem. Commun. 49, 10757–10759.

Yang, X., Yang, L., Dou, Y., Zhu, S., 2013b. Synthesis of highly fluorescent lysine-stabilized Au nanoclusters for sensitive and selective detection of Cu^{2+} ion. J. Mater. Chem. 1, 6748–6751.

Yang, Z., Yan, J., Zhang, C., 2012. Piezoelectric detection of bilirubin based on bilirubin-imprinted titania film electrode. Anal. Biochem. 421, 37–42.

Yang, Z., Yan, J., Zhang, C., Luo, S., 2011. Enhanced removal of bilirubin on molecularly imprinted titania film. Colloids Surf. B. Biointerfaces 87, 187–91.

Yang, Z., Zhang, C., 2011. Molecularly imprinted hydroxyapatite thin film for bilirubin recognition. Biosens. Bioelectron. 29, 167–171.

Yue, Y., Liu, T.-Y., Li, H.-W., Liu, Z., Wu, Y., 2012. Microwave-assisted synthesis of BSA-protected small gold nanoclusters and their fluorescence-enhanced sensing of silver(i) ions. Nanoscale 4, 2251-2254.

Zelenka, J., Lenícek, M., Muchová, L., Jirsa, M., Kudla, M., Balaz, P., Zadinová, M., Ostrow, J.D., Wong, R.J., Vítek, L., 2008. Highly sensitive method for quantitative determination of bilirubin in biological fluids and tissues. J. Chromatogr. B. 867, 37–42.

Zhang, H., Deng, L., Yang, M., Min, S., Yang, L., Zhu, L., 2011. Enhancing effect of glycerol on the tensile properties of bombyx mori cocoon sericin films. Int. J. Mol. Sci. 12, 3170–3181.

Zhao, J., Wu, D., Zhi, J., 2009. A novel tyrosinase biosensor based on biofunctional ZnO nanorod microarrays on the nanocrystalline diamond electrode for detection of phenolic compounds. Bioelectrochemistry 75, 44–49.

Zheng, J., Nicovich, P.R., Dickson, R.M., 2007. Highly fluorescent noble-metal quantum dots. Annu. Rev. Phys. Chem. 58, 409–431.

Zhou, Y., Chen, W., Itoh, H., Naka, K., Ni, Q., Yamane, H., Chujo, Y., 2001. Preparation of a novel core-shell nanostructured gold colloid-silk fibroin bioconjugate by the

protein in situ redox technique at room temperature. Chem. Commun. 23, 2518–2519.

Zietz, B., Macpherson, A.N., Gillbro, T., 2004. Resolution of ultrafast excited state kinetics of bilirubin in chloroform and bound to human serum albumin. Phys. Chem. Chem. Phys. 6, 4535-4537.

Zsila, F., 2011. Circular dichroism spectroscopy is a sensitive tool for investigation of bilirubin - enzyme interactions. Biomacromolecules 12, 221–227.

Zunszain, P.A., Ghuman, J., McDonagh, A.F., Curry, S., 2008. Crystallographic analysis of human serum albumin complexed with 4Z,15E-bilirubin-IXα J. Mol. Biol. 381, 394–406.

Publications

List of Publications

Publications in referred journals

Mallesh Santhosh, Somasekhar R. Chinnadayyala, Naveen Kumar Singh, Pranab Goswami*. Human serum albumin-stabilized gold nanocluster act as an electron transfer bridge supporting specific electrocatalysis of bilirubin useful for biosensing application. *Bioelectrochemistry* (2016) 111: 07-14.

Mallesh Santhosh, Somasekhar R. Chinnadayyala, Ankana Kakoti, Pranab Goswami*. Selective and sensitive detection of free bilirubin in blood serum using human serum albumin stabilized gold nanoclusters as fluorometric and colorimetric probe. *Biosens. Bioelectron*. (2014) 59:370-376.

Mallesh Santhosh, Priyanki Das, Babina Chakma, Pranab Goswami*. Human serum albumin-stabilized gold nanocluster immobilized over *in-situ* grown zinc oxide nanorods over paper electrode for electrochemical detection of bilirubin. (*Communicated*).

Somasekhar R. Chinnadayyala, **Mallesh Santhosh**, Naveen Kumar Singh, Pranab Goswami*. Alcohol oxidase protein mediated in-situ synthesized and stabilized gold nanoparticles for developing amperometric alcohol biosensor. *Biosens. Bioelectron*. (2015) 69:155-161.

Somasekhar R. Chinnadayyala, Ankana Kakoti, **Mallesh Santhosh**, Pranab Goswami*. A novel amperometric alcohol biosensor developed in a 3rd generation bioelectrode platform using peroxidase coupled ferrocene activated alcohol oxidase as biorecognition system. *Biosens. Bioelectron*. (2014) 55:120-126.

Somasekhar R. Chinnadayyala, **Mallesh Santhosh**, Pranab Goswami*. Microwave based reversible unfolding and refolding of alcohol oxidase protein probed by fluorescence and circular dichroism spectroscopy. *J. Biophys. Chem*. (2012) 3:317-323.

Sharbani Kaushik, Mrinal Sarma, Phurpa D Thungon, **Mallesh Santhosh**, Pranab Goswami*. Thin films of silk-fibroin and its blend with chitosan strongly promote biofilm growth of *Synechococcus sp*. BDU 140432. *J. Colloid and Interface Science* (2016) 479: 251–259.

Patent

Pranab Goswami, **Mallesh Santhosh**, Priyanki Das, Phurpa D Thungon. SILK SERICIN ENHANCES THE CONDUCTIVITY AND STABILITY OF GRAPHITE PASTE INK. (*Application no. 201631022633*).

Conference

Mallesh Santhosh, Somasekhar R. Chinnadayyala, Ankana Kakoti, Pranab Goswami*. Human serum albumin stabilized gold nanoclusters as a novel fluorescent and colorimetric probe for the detection of bilirubin-IX. 24th Anniversary World Congress on Biosensors 2014, Melbourne, Victoria, Australia, 27-30 May 2014. Abstract no: P2-148.

Mallesh Santhosh and Pranab Goswami* Studies on the electro-catalytic activity of HSA-stabilized gold nanocluster for bilirubin sensing. National conference in New Advances and Horizons in Nanoscience and Nanotechnology, 20-21st December (2014), held at IASST Guwahati, Assam, India. Abstract no: P-31.

Mallesh Santhosh and Pranab Goswami* Dual fluorometric/colorimetric assay-based on human serum albumin-stabilized gold nanoclusters for the sensitive detection of bilirubin. South Asian workshop on Optics and Photonics (SAWOP 2015) organized by UNESCO New Delhi held at IITG, Assam, India (Awarded 2nd best poster).

Mallesh Santhosh, Naveen K Singh, Pranab Goswami*. Human serum albumin-stabilized gold nanocluster act as an electron transfer bridge supporting specific electrocatalysis of bilirubin useful for biosensing application. Research Conclave, 23rd -24th March (2016), held at IITG, Assam, India.

Somasekhar R. Chinnadayyala, **Mallesh Santhosh**, Pranab Goswami***,** Bioengineering of alcohol oxidase by entrapping ferrocene in the protein matrix using microwave based

reversible refolding technique. World Congress on Biotechnology, 2012, Hyderabad, India, 4-6 May 2009. Abstract no: P-50.

Somasekhar R. Chinnadayyala, **Mallesh Santhosh**, Naveen K. Singh, Pranab Goswami*, Alcohol oxidase protein mediated *in-situ* synthesized and stabilized gold nanoparticles for developing amperometric alcohol biosensor. New Advances and Horizons in Nanoscience and Nanotechnology, 2014, Guwahati, Assam, India, 20-21 December 2014. Abstract no: P-32.